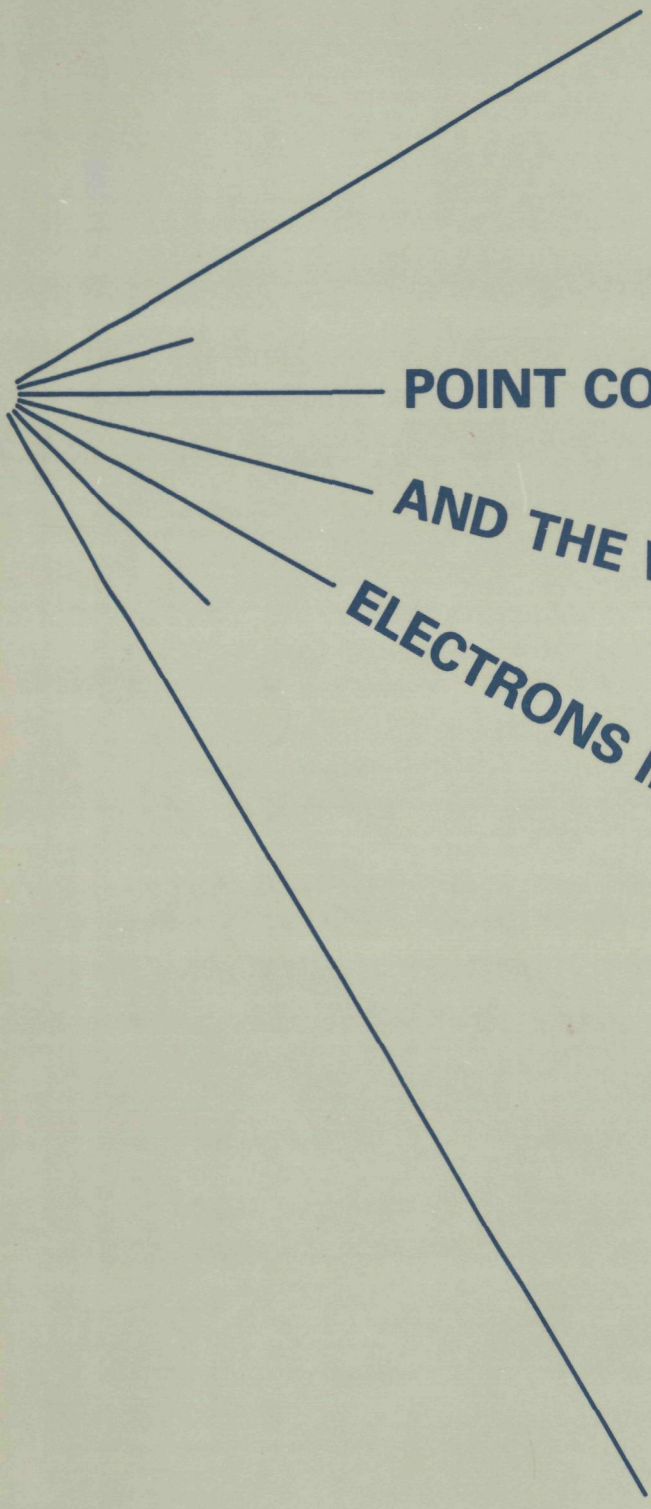

POINT CONTACTS AND THE WAYS OF ELECTRONS IN METALS

Peter van Son

POINT CONTACTS
AND THE WAYS OF ELECTRONS IN METALS

POINT CONTACTS
AND THE WAYS OF ELECTRONS IN METALS

PROEFSCHRIFT

TER VERKRIJGING VAN DE GRAAD VAN
DOCTOR IN DE WISKUNDE EN NATUURWETENSCHAPPEN
AAN DE KATHOLIEKE UNIVERSITEIT TE NIJMEGEN,
OP GEZAG VAN DE RECTOR MAGNIFICUS PROF. DR. B.M.F. VAN IERSEL
VOLGENS BESLUIT VAN HET COLLEGE VAN DECANEN
IN HET OPENBAAR TE VERDEDIGEN
OP DONDERDAG 15 OKTOBER 1987
DES NAMIDDAGS TE 3.30 UUR

door

PETER CORNELIS VAN SON
geboren te Dordrecht

1987
Druk: Krips Repro, Meppel

PROMOTORES

PROF. DR. P. WYDER
PROF. DR. H. VAN KEMPEN

Dit proefschrift had niet tot stand kunnen komen zonder de directe of indirecte medewerking van velen binnen en buiten de faculteit Bij deze, iedereen hartelijk bedankt daarvoor

Speciaal wil ik de mensen bedanken die de afgelopen jaren deel hebben uitgemaakt van de afdeling E N 4 en die hebben bijgedragen aan de prettige en stimulerende sfeer die ik er heb ervaren Die sfeer bevorderde niet alleen het wetenschappelijke onderzoek, maar uitte zich bijvoorbeeld ook in het afdelingsorkest, het Microcanoniek Ensemble, dat mij weer achter de toetsen kreeg

Buiten de afdeling heb ik mij de afgelopen vier jaar uit kunnen leven en indien nodig af kunnen reageren op een nabijgelegen sportveld Dat werd mogelijk gemaakt door een groepje mensen dat zich korfbalvereniging Noviomagum noemt en waarin ik mij steeds weer, en meestal met plezier, mengde

Ten slotte wil ik mijn ouders bedanken voor het feit dat ze me steeds hebben gestimuleerd om door te leren

We acknowledge the permission obtained from Physical Review Letters and from the Journal of Physics F Metal Physics to reprint previously published papers

This work was supported by the Stichting voor Fundamenteel Onderzoek der Materie (FOM), which is financially supported by the Nederlandse Organisatie voor Zuiver Wetenschappelijk Onderzoek (ZWO)

voor een ieder die het goede
met de natuurkunde voor (ogen) heeft

Contents

1. General Introduction 1

2. Transverse Electron Focusing 5
2.1 Introduction 6
2.2 Theory 10
2.3 Sample preparation and experimental set-up 19
References 20
2.4 New method to study the electron-phonon interaction in metals 22
References 25
2.5 Emitter current dependence of transverse electron focusing 26
References 30

3. Andreev reflection 31
3.1 Introduction 32
References 34
3.2 Andreev reflection and geometrical resonance effects for a gradual variation of the pair potential near the normal-metal-superconductor interface 35
I Introduction 36
II Bogoliubov equations 38
III Probability of Andreev reflection 42
IV Geometrical resonance effects 42
V Negative pair potential 45
VI Conclusion 46
Acknowledgment 47
Appendix 47
References 52
3.3 New method to study the proximity effect at the normal-metal-superconductor interface 53
References 59
3.4 Excess current of a point contact on a normal-metal single-crystal backed by a superconductor 60
References 71

4. Electron spin polarization 73
4.1 Introduction 74
References 75
4.2 New method to study the electron spin polarization at the Fermi level of a ferromagnetic metal 76
References 84
4.3 Current conversion at the ferromagnetic-nonferromagnetic metal interface 85
References 92

Summary 94

Samenvatting 96

Curriculum vitae 99

Chapter 1

GENERAL INTRODUCTION

The good electric conductivity of metals is due to the fact that the electrons in a metal are not bound to the metal ions but can move more or less free through the crystal If a voltage difference is applied to a metal, the current is not infinite because the electrons are scattered The scattering is due to imperfections of the lattice of the metal ions (such as impurity atoms, grain boundaries, or dislocations) or due to lattice vibrations (phonons) Viewed on a length scale that is large compared to the mean free path of the electrons, the energy distribution of the electrons is in equilibrium at every point, except that the electrons have a small drift velocity On this scale, there is a linear relation between voltage and current (Ohm's law)

However, to study the behavior of the conduction electrons in more detail, it is often convenient to look on a length scale that is of the order of the mean free path On that scale, the electrons move ballistically through the metal, their energy distribution is often a non-equilibrium one and then it is not a priori clear what a voltmeter measures This situation can be realized experimentally for instance by using a pure metal single-crystal and by doing the measurements at low temperatures In experiments of this kind, point contacts are convenient tools to fix the begin and end points of the electron trajectories They are made by gently pressing a metal wire with a sharp point onto the single-crystal surface If a current is sent through the point contact, electrons are injected into the crystal at a well-defined position Point contacts can also be used as detectors (with good spatial resolution) of electrons that arrive at the surface of the crystal Moreover, point contacts provide the possibility to control the energy with which the electrons are injected This means that effects that are usually studied by varying the temperature, can be studied directly as a function of the energy of the electrons Another important tool in these kinds of experiments is the magnetic field Electrons that move, feel a Lorentz force due to the applied field and their trajectories are bent The magnetic field can for instance be used to select specific trajectories of the electrons Then, the combination of single-crystals, point contacts, and the applied magnetic field makes it possible to study effects of anisotropy Because the injection and the detection of the electrons takes place at the surface of the crystal, the electrons do not get the opportunity to make many revolutions, so quantization in Landau states does not occur

In Chapter 2, transverse-electron-focusing experiments are described that were performed on very pure Ag single-crystals In these experiments, electrons that are injected at one point contact, are focused by an applied magnetic field onto a second point contact The orbits of the electrons depend on the direction of the magnetic field and on the position of the point contacts relative to the crystal axes The number of the electrons that arrive at the second point contact depends for instance on the probability for an electron to emit a phonon on its way through the crystal Thus, these experiments allow the determination of the electron-phonon interaction in metals as a function of the energy and of the wave vector of the electrons

The presence of a superconducting metal near a normal-metal point contact yields new possibilities for focusing experiments At an interface of a normal metal and a superconductor, Andreev reflection can take place, the incoming electron is then retroreflected as a hole A single point contact can be used to inject the electrons and to detect the holes The retroreflection process automatically yields a focusing effect, which can be disturbed for instance by an applied magnetic field In Chapter 3, two experiments that employ this geometry are described In a thin Ag single crystal backed by a Pb film, very small deviations from the ballistic electron orbits are found that are ascribed to the scattering of the electrons by dislocations In the even much thinner Ag-Pb bilayers, the focusing signal shows features that are due to the position dependence of the superconducting order parameter near the interface This experiment can therefore be used to study the proximity effect at the normal-metal-superconductor interface

Apart from an electric charge, an electron possesses an angular moment (spin) and, coupled to that, a magnetic moment This means that a magnetic field not only interacts with a moving electron through the Lorentz force but it also interacts with the magnetic moment of the electron In a magnetic field, the energy levels of spin-up and spin-down electrons shift in opposite directions (Zeeman shift), this effect gives rise to the Pauli spin paramagnetism of metals Because the Zeeman energy is much smaller than the Fermi energy, the effect is only small The situation is different in ferromagnetic metals Here, the inequivalence of spin-up and spin-down electrons is intrinsic and can be very large This is especially true for half-metallic ferromagnets, which are metals for one spin direction and semiconductors (or insulators) for the other spin direction It is clear that the spin asymmetry of the conduction electrons affects for instance the transport of electric current In Chapter 4, two effects are discussed that are related to that asymmetry

Most chapters of the thesis are presented in the form of published papers or of papers to be published

Chapter 2

TRANSVERSE ELECTRON FOCUSING

Chapter 2.1

INTRODUCTION

The concept of electron focusing in a metal single-crystal was introduced by Sharvin[1] and was realized by him and co-workers.[2,3] They placed point contacts on opposite sides of a thin Sn single-crystal slab. Electrons were injected at one point contact (the emitter, E) and were focused onto the second point contact (the collector, C) by means of a magnetic field directed along EC (Fig. 1). For specific values of the magnetic field, the voltage across the collector point contact showed peaks. Experimentally, it was very hard to align the direction of the magnetic field exactly with the line EC. Tsoi[4] introduced a different set-up of the focusing experiment in which this problem was avoided. The point contacts were placed on the same side of the crystal and the direction of the magnetic field was in the plane of the sample and perpendicular to the line EC (Fig. 2). Therefore, this set-up is referred to as Transverse Electron Focusing (TEF) while the original set-up is called Longitudinal Electron Focusing (LEF). Apart from the fact that there are less experimental difficulties, TEF has more advantages over LEF, so it has become the standard electron focusing technique. TEF has been employed successfully on various metals and semimetals: Bi,[4,5] Sb,[6] W,[7,8] Cu,[7,9] Ag,[10,11] Zn,[12] and Al.[13,14]

The origin of the focusing effect in a TEF experiment is made clear in Fig. 2 for the situation with the magnetic field directed exactly perpendicular to the line EC. The electrons are assumed to be free and the electron mean free path is much larger than the point-contact separation. At the emitter, electrons are injected into the crystal in all directions. The Lorentz force due to the applied magnetic field bends the electron orbits into circles in the plane perpendicular to the field. The velocity component of the electron parallel to the

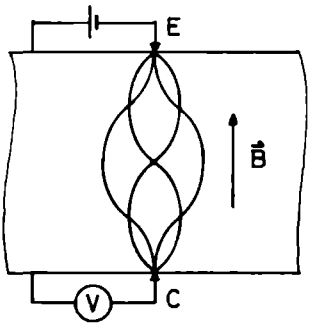

Fig. 1. Experimental arrangement for observing longitudinal electron focusing.

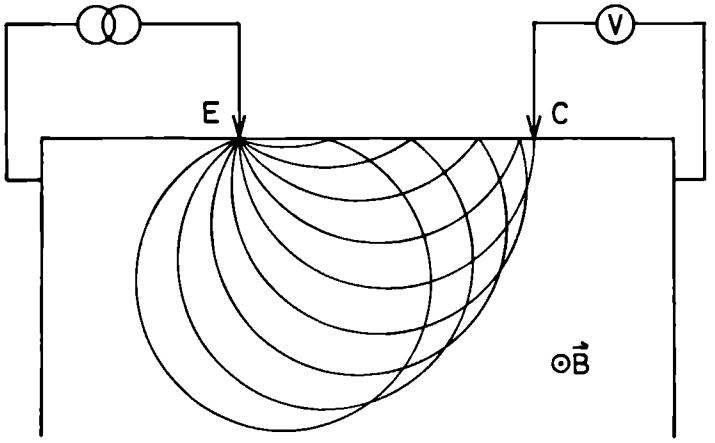

Fig. 2. Experimental arrangement for observing transverse electron focusing.

field is not influenced, so only electrons with no such velocity component are relevant in the geometry of Fig. 2. The electrons return to the crystal surface at a position that depends on the angle of injection. Electrons that are injected perpendicular to the surface obtain the largest separation from the emitter. As can be seen in Fig. 2, at this position also the density of electrons is largest, which results in a peak in the voltage across the collector point contact for a specific value of the magnetic field. By sweeping the magnetic field strength, the radius of the electron orbits is varied, so that with a fixed collector point contact, a line scan of the focusing signal is made. Typical TEF signals for Ag are shown in Fig. 3; the collector voltage shows a gradual build-up to a peak and a steep fall-off, in accordance with Fig. 2. As is also shown in Fig. 3, electron focusing is not limited to geometries in which the magnetic field is directed exactly perpendicular to EC. The situation is then more complicated because the velocity component of the electrons parallel to the field has to be taken explicitly into account, but in principle the focusing mechanism is the same.

If the point-contact separation is known, the focusing value of the magnetic field, B_0, yields information about the Fermi momentum of the electrons. However, the free-electron model can only be used if the electrons that contribute to the focusing signal move on a spherical part of the Fermi surface, as in Cu[7,9] and in Ag.[10,11] The first TEF experiments were performed by Tsoi on Bi,[4,5] in which the relevant part of the Fermi surface is almost cylindrical. The other (semi-) metals on which measurements of TEF have been done (see Refs. 6-8, 12-14) have more complicated Fermi surfaces. Then, the electron orbits in a magnetic field are no longer circular but reflect the shape of the Fermi surface. Focusing still

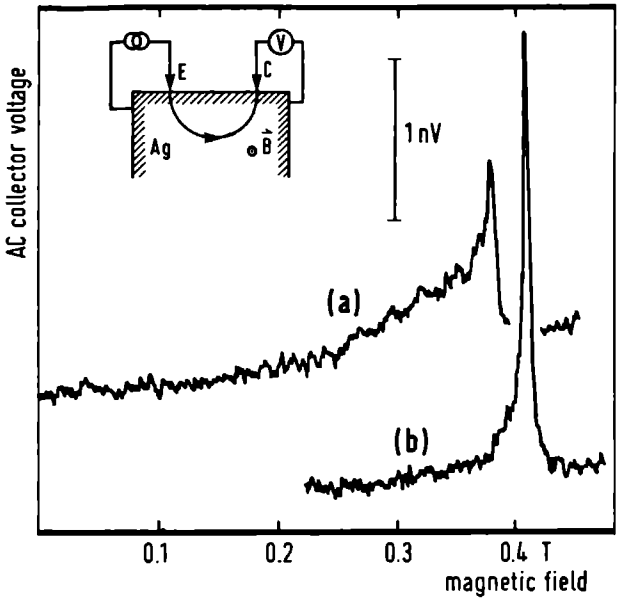

Fig. 3. Typical TEF signals for a Ag(100) sample. The point-contact separation is 42 μm. The magnetic field is directed perpendicular to the line EC for curve (a) while for curve (b) it is rotated over 35° in the plane of the sample surface.

occurs and the position and shape of the focusing peaks can be related to features of the Fermi surface of the crystal. Apart from the study of the Fermi surface, TEF is also used to measure specular reflection coefficients. If the electrons are specularly reflected at the crystal surface, the orbits in Fig. 2 can be continued accordingly. The result is that for multiples of the magnetic field strength B_0 also focusing peaks occur. From the heights of the higher order focusing peaks, the coefficient of specular reflection of a specific crystal surface can be determined.

An electron focusing experiment can still be used in another way. This application was pioneered by Sharvin and Bogatina[3] in a LEF experiment on a Sn single-crystal. They measured the temperature dependence of the focusing signal. The decrease of the signal with increasing temperature was interpreted as a decrease of the electron mean free path due to the electron-phonon interaction. In chapter 2.4, a TEF experiment on a Ag single-crystal is described in which also the electron-phonon interaction is studied. Here, directly the energy dependence of the electron mean free path is measured by injecting the electrons at the emitter with a specific energy above the Fermi energy. In a TEF experiment, various electron orbits can be selected, so also the anisotropy of the electron-phonon in-

teraction can be studied Sharvin and Bogatina[3] tried to measure the energy dependence but they found that the signal was dominated by the influence of the magnetic field of the injection current on the electron orbits This effect is also observed in the TEF measurements if the resistance of the emitter point contact is small In chapter 2 5, these results are discussed and a model calculation is given that qualitatively explains the observations Chapter 2 3 contains details of sample preparation and of the set-up of the experiments described in the chapters 2 4 and 2 5, while in chapter 2 2 several aspects of the theory of (transverse) electron focusing are discussed

Chapter 2.2

THEORY

The three main aspects of a TEF experiment will be discussed theoretically First, the injection of electrons at the emitter point contact is described with emphasis on the conditions for obtaining good energy resolution Then the detection of electrons at the collector point contact is discussed, especially how the measured signal arises Last but not least, a general theory developed by van Gelder[15] is given with which, for given magnetic field and for given Fermi surface, the fraction of the total number of injected electrons that reaches the collector can be calculated This theory will be illustrated by applying it to the simple case of a spherical Fermi surface

Both injection and detection of the electrons depend on the properties of the point contact To avoid smearing out of the focusing peak, the point-contact radius b has to be small compared to the point-contact separation There is however another important length scale the electron mean free path l For $l \ll b$, the electron transport through the contact is diffusive and Ohm's law is valid (i e the current density is proportional to the electric field) The resistance of a point contact in this regime has already been calculated by Maxwell [16] The point contact is modeled as a circular hole in an thin insulating screen that separates the two metals If the resistivity of the metal is ϱ, the Maxwell resistance R_M of a point contact is given by

$$R_M = \frac{\varrho}{2b} \tag{1}$$

The other regime, $l \gg b$, was first discussed by Sharvin [1] Now, the electrons pass the point contact ballistically As in the Maxwell regime, the voltage drop is located near the point contact For a Sharvin point contact, however, this means that the electrons that arrive at the point contact have the same equilibrium energy distribution as the electrons far from the contact As they cross the point contact without scattering, they are injected into the other metal with energies up to eV above the Fermi level there (V is the voltage drop over the point contact) The resistance R_S of a Sharvin point contact is

$$R_S = \frac{4(\varrho l)}{3\pi b^2} \tag{2}$$

The ϱl-product is a material parameter that does not depend on the mean free path because $\varrho \propto l^{-1}$ For simplicity, we will assume that the point-contact wires and the crystal are made of the same material

Sharvin point contacts can be used to study the energy dependence of the strength of scattering mechanisms of electrons because the energy of the injected electrons can be manipulated very easily For a review of this point-contact spectroscopy, see Ref 17 In a TEF experiment, the electron mean free path in the crystal is always much larger than b, so the properties of the point contact are determined by the mean free path in the point-contact wire For $l \ll b$ in the wire, the contact can be described as a half-Maxwell contact and a half-Sharvin contact in series The Maxwell resistance is much larger than the Sharvin resistance, so most of the voltage drop is located in the point-contact wire and the energies with which the electrons are injected are not well known For observing the focusing effect, this is no problem, but to study the dependence of the focusing signal on the electron energy properly, the emitter point contact should be fully in the Sharvin regime Another possibility is to use a small-area tunnel junction as the emitter If the transmission probability of the junction is low enough, the voltage drop will be mainly across the tunnel barrier and the electrons that tunnel through are injected with excess energies up to eV, just like with a Sharvin point contact A difference is that, with a Sharvin point contact, the electrons are injected in all directions while, with a tunnel junction, the injection will preferentially be perpendicular to the plane of the tunnel barrier

The second point of discussion is the dependence of the focusing signal that is measured on the properties of the collector point contact This effect was not recognized by Korzh,[18] he calculated the (electrostatic) potential distribution on the surface of the crystal due to the injected current and he implicitly assumed that this is the potential that is measured by the voltmeter connected to the collector point-contact wire A voltmeter, however, measures differences in electrochemical potential and not the electrostatic potential In a TEF experiment these are different things Within a mean free path away from the emitter, there exists no electrochemical potential because this is an equilibrium quantity and the energy distribution of the electrons is non-equilibrium and highly anisotropic To answer the question what the reading of the voltmeter will be, one should continue the description of the experiment until the electrons that arrive at the collector point contact have reached equilibrium, at that point, the electrochemical potential can be calculated This electrochemical potential in principle depends on the way in which the electrons reach equilibrium and therefore on the properties of the collector point contact

The situation is simplest for a Sharvin point contact Some of the electrons that are injected at the emitter penetrate the point-contact wire of the collector In the wire, they reach equilibrium on the scale of the mean free path, which is much larger than the point-contact diameter An electrochemical potential difference builds up between the wire and a reference contact on the crystal that is far away from the emitter and collector point contacts Due to this voltage, a current starts to flow back through the Sharvin contact (note that this is the only way for the current, as an ideal voltmeter draws no current) The voltage saturates at a value for which this current exactly compensates the current due to the electrons that are injected into the collector wire If J_{ce} is the density of the latter current

and ΔS_c is the area of the collector point contact, the collector voltage V_c is given by

$$V_c = R_S J_{ce} \Delta S_c = (4/3)(\varrho l) J_{ce} \tag{3}$$

For a collector point contact that is a half-Sharvin junction and a half-Maxwell junction, the situation is slightly more complicated The electrons again reach equilibrium on the scale of the mean free path l_c in the wire, which is now much smaller than the point-contact diameter If J_{ce} is constant over the area of the point contact, the problem is essentially one-dimensional At a distance l_c from the interface, a voltage builds up that again induces a current which eventually compensates J_{ce} This current "sees" the half-Sharvin resistance but only a very small part of the half Maxwell resistance, namely the resistance that corresponds to a length of order l_c Now, V_c is

$$V_c = (1/2) R_S J_{ce} \Delta S_c + \varrho_c l_c J_{ce} = (5/3)(\varrho l) J_{ce} \tag{4}$$

which is of the same order of magnitude as for a Sharvin point contact This is also the case if the collector is a tunnel junction because both J_{ce} and the compensating current are diminished due to the small transmission probability If this probability depends on the direction of the electrons, V_c will not be exactly the same as for a Sharvin point contact because J_{ce} and the compensating current have a different angular distribution and therefore their average transmission probability will be different

Instead of measuring the voltage across the collector point contact, it is also possible to measure directly the current $J_{ce} \Delta S_c$ This has been demonstrated experimentally by Payens[19] with the use of a SQUID In this set-up, the collector point-contact wire is connected with the reference contact on the crystal through superconducting wires instead of via a voltmeter At a distance from the point contact of the order of the mean free path, the electrons that are injected into the wire reach equilibrium The current can now follow two paths If the resistance of the external loop is smaller than the resistance of the way back through the point contact, the current will choose the external loop where it can be measured With a Sharvin point contact as the collector, this condition can easily be fulfilled

The third aspect that has to be discussed is the value of the collector current density J_{ce} for given emitter current, applied magnetic field, and Fermi surface In this, the theory by van Gelder[15] will be followed For a spherical Fermi surface, the focusing signal can also be calculated in a more direct way [20] Here, the general van Gelder theory will be illustrated by applying it to this simple case

Assuming that the emitter is a Sharvin point contact, the emitter current I_e can be written as an integral in momentum space over all electron states that contribute to the current, each weighed by the velocity component perpendicular to the interface

$$I_e = J_e \Delta S_e = 2e(2\pi)^{-3} \int \mathrm{d}k_x \int \mathrm{d}k_y \int \mathrm{d}k_z \, \frac{1}{\hbar} \frac{\partial \varepsilon}{\partial k_z} \Delta S_e \tag{5}$$

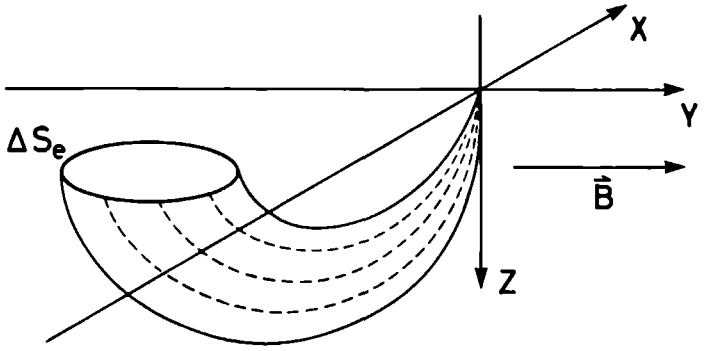

Fig. 4. The emitter point-contact area ΔS_e in the xy-plane defines a solid angle of velocity directions of electrons at the origin, where the collector point contact is located.

The emitter point-contact area ΔS_e lies in the xy-plane (see Fig. 4). The integral is restricted to states with energies ε between the Fermi energy ε_F and ε_F+eV (V is the voltage across the emitter point contact). Moreover, only states with positive $\partial\varepsilon/\partial k_z$ should be taken into account: states with negative $\partial\varepsilon/\partial k_z$ correspond to electrons coming from the high-voltage side of the point contact and these states are not occupied. For $eV \ll \varepsilon_F$, $\int dk_x \int dk_y = A$ is the area in momentum space of the projection of the Fermi surface on the plane $k_z=0$. From Eq. (5), an expression for the Sharvin resistance can be deduced:

$$R_S = 4\pi^3(\hbar/e^2)(A\,\Delta S_e)^{-1} \tag{6}$$

For free electrons ($A=\pi k_F^2$), this expression is identical to the expression in Eq. (2).

For the current density that is induced by I_e at the position of the collector point contact, an expression similar to Eq. (5) can be written down:

$$J_{ce} = 2e(2\pi)^{-3}\int dk_x \int dk_y \int dk_z \,\frac{1}{\hbar}\frac{\partial\varepsilon}{\partial k_z} \tag{7}$$

The energy restrictions are the same as for the integral in Eq. (5), but the integral is also restricted to those momentum states that correspond to electrons that started on their orbit somewhere inside the emitter point-contact area. These states are namely the only states above the Fermi level that are occupied. If ΔS_e is small, they are grouped in small spots on the Fermi surface. The area of each spot is given by the transformation of the position variables in the emitter point-contact area into the momentum variables at the position of the collector point contact (see Fig. 4):

$$\int dk_x \int dk_y = \int dx \int dy (dA/dS) = (dA/dS)\Delta S_e \tag{8}$$

Combining Eqs (5), (7), and (8), the ratio of collector current density and emitter current is given by

$$J_{ce}/I_e = (1/A)(dA/dS) \tag{9}$$

Thus to calculate the focusing signal, one should first find the orbits that the electrons can follow from the emitter to the collector point contact Each orbit then gives a contribution to the focusing signal proportional to dA/dS Orbits containing specular reflection at the crystal surface are not considered because their contribution to the focusing signal can be derived from the contribution of the direct orbits by proper scaling

In the semi-classical approximation, the orbits of electrons in a homogeneous magnetic field B directed along the y-axis, are determined by

$$\hbar \frac{d}{dt} k_x = eB \frac{dz}{dt} \quad , \quad \hbar \frac{d}{dt} k_z = -eB \frac{dx}{dt} \tag{10}$$

while ε and k_y are constants of the motion In momentum space, the electron orbit is the intersection of the Fermi surface and a plane k_y=constant In real space, the projection of the orbit on the xz-plane has the shape of the orbit in momentum space (this follows from Eq (10)) Although k_y is constant, the velocity component parallel to the magnetic field is generally not ($v_y = \hbar^{-1}(\partial\varepsilon/\partial k_y)$)

The orbits leading from the point $(x,y,0)$ inside the emitter to the collector, which is located in the origin, have to be found, in particular the points in k-space at the collector that correspond to these orbits and the dependence of these points on x and y Integration of Eq (10) yields that the starting points and the end points of the orbits in k-space have to obey

$$\Delta k_x = 0 \quad , \quad \Delta k_z = (eB/\hbar)x \tag{11}$$

while Δk_y=0 because k_y is a constant of the motion These conditions define a continuous curve of starting points (with $v_z>0$) on the Fermi surface and a curve of end points (with $v_z<0$) For a spherical Fermi surface, these curves are the intersections of the Fermi sphere with the planes $k_z = \pm(1/2)(eB/\hbar)x$ (see Fig 5), it is clear that for $B>2\hbar k_F/(ex)$, there are no solutions The electron orbits themselves lie in planes k_y=constant The actual planes of the orbits follow from the condition

$$-y = \int dt' v_y = \int dx' (v_y/v_x) = -\frac{\hbar}{eB} \int dk_z' \left.\frac{\partial k_x}{\partial k_y}\right|_{k_z,\varepsilon} \tag{12}$$

The integrations have to be performed along the electron orbits, the partial derivative should be calculated for constant k_z and ε The condition of Eq (12) can also be written as

$$\zeta(\Delta k_z, k_y) = (eB/\hbar)y \tag{13}$$

with

$$\zeta(\Delta k_z, k_y) = \int \mathrm{d}k'_z \left.\frac{\partial k_x}{\partial k_y}\right|_{k_z,\varepsilon} \tag{14}$$

Equation (13) is an implicit equation for k_y as a function of $\Delta k_z = (eB/\hbar)x$ and y. For a spherical Fermi surface there usually are two solutions. A short orbit FG and a long orbit MNPQ (Fig. 5). For $B = 2\hbar k_F/(ex)$ (and $y=0$), the two solutions coincide and for larger B there are no solutions.

Now that the orbits that lead from emitter to collector are known, it is possible to determine the magnitude of the collector current by calculating how many k-states contribute for given emitter area ΔS_e. This is precisely the meaning of the term $\mathrm{d}A/\mathrm{d}S$ in Eq. (9). We calculate this quantity at the end point of the orbit (i.e. at the collector point contact).

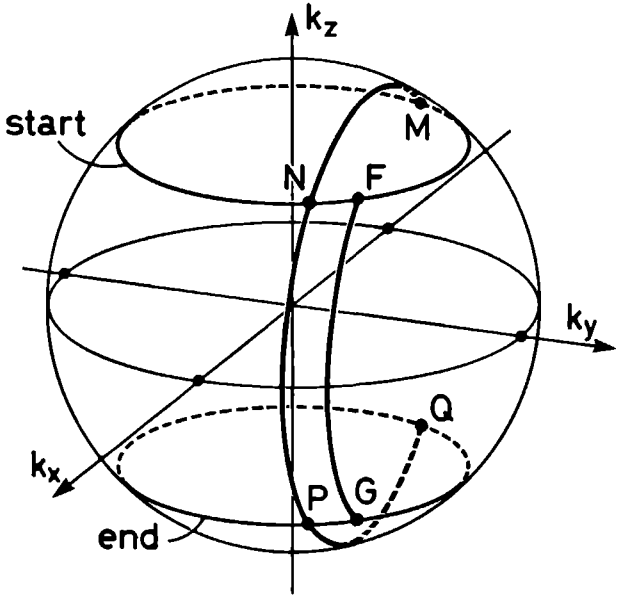

Fig. 5. The two orbits FG and MNPQ on a spherical Fermi surface that, in real space, connect the emitter and collector point contacts for given magnetic field.

$$dA = dk_x dk_y = \left.\frac{\partial(k_x)_c}{\partial(\Delta k_z)}\right|_{k_y} d(\Delta k_z) dk_y = (eB/\hbar)\left\{\left.\frac{\partial(\Delta k_z)}{\partial(k_x)_c}\right|_{k_y}\right\}^{-1} dx\, dk_y \qquad (15)$$

In this equation, the fact is used that, for constant k_y, there is a relation between the k_x-value of starting and end point and $\Delta k_z = (eB/\hbar)x$. Next, for constant x (or Δk_z), we may write

$$dk_y = \left\{\left.\frac{\partial y}{\partial k_y}\right|_{\Delta k_z}\right\}^{-1} dy = (eB/\hbar)\left\{\left.\frac{\partial\zeta(\Delta k_z, k_y)}{\partial k_y}\right|_{\Delta k_z}\right\}^{-1} dy \qquad (16)$$

using Eq. (13). The combination of the Eqs. (9), (15), and (16) yields

$$J_{ce}/I_e = A^{-1} dA/dS = (eB/\hbar)^2 A^{-1} W^{-1} \qquad (17)$$

with

$$W = \left.\frac{\partial(\Delta k_z)}{\partial(k_x)_c}\right|_{k_y} \left.\frac{\partial\zeta(\Delta k_z, k_y)}{\partial k_y}\right|_{\Delta k_z} \qquad (18)$$

The total focusing signal is found by adding the quantities W^{-1} of each orbit that leads from the emitter to the collector point contact.

Finally, the general result of Eqs. (17) and (18) will be applied to a spherical Fermi surface. Then the relation between Δk_z and $(k_x)_c$ is simply $(k_x)_c^2 + k_y^2 + (\Delta k_z/2)^2 = k_F^2$, so

$$\left.\frac{\partial(\Delta k_z)}{\partial(k_x)_c}\right|_{k_y} = \frac{-2\sqrt{k_F^2 - k_y^2 - (\Delta k_z/2)^2}}{(\Delta k_z/2)} \qquad (19)$$

We express everything in the quantities k_y and Δk_z, because they are related to the coordinates of the emitter point contact (Eqs. (11) and (13)). To calculate the function $\zeta(\Delta k_z, k_y)$ in Eq. (14), the integrations have to be performed along the orbits FG and MNPQ on the Fermi surface (see Fig. 5). As for constant ε ($=\varepsilon_F$), the components of the k-vector are related through $k_x^2 + k_y^2 + k_z^2 = k_F^2$, the integrand in Eq. (14) is

$$\left.\frac{\partial k_x}{\partial k_y}\right|_{k_z,\varepsilon} = -(k_y/k_x) = \frac{-k_y}{\sqrt{k_F^2 - k_y^2 - (k_z')^2}} \qquad (20)$$

Along the orbit, k_y is constant and k_z' is the integration variable that runs from $-(\Delta k_z/2)$ to $+(\Delta k_z/2)$ (note that, in the geometry of Fig. 4, x and therefore Δk_z are negative). Thus,

$$\zeta_{FG}(\Delta k_z, k_y) = \int_{-\Delta k_z/2}^{\Delta k_z/2} dk_z' \frac{-k_y}{\sqrt{k_F^2 - k_y^2 - (k_z')^2}} = -2k_y \arcsin\left[\frac{\Delta k_z/2}{\sqrt{k_F^2 - k_y^2}}\right] \qquad (21)$$

For the long orbit MNPQ, we have to add the contributions of MN and PQ:

$$\zeta_{MQ}(\Delta k_z,k_y) = \zeta_{FG}(\Delta k_z,k_y) + 4\int_{\Delta k_z/2}^{-\sqrt{k_F^2-k_y^2}} dk_z' \frac{-k_y}{\sqrt{k_F^2-k_y^2-(k_z')^2}}$$

$$= 2\pi k_y + 2k_y \arcsin\left[\frac{\Delta k_z/2}{\sqrt{k_F^2-k_y^2}}\right] \tag{22}$$

With these explicit expressions for the functions $\zeta(\Delta k_z,k_y)$ and with Eq. (19), the value of W for the two orbits can be calculated. The short orbit FG yields

$$W_{FG} = \frac{4k_y^2}{k_F^2-k_y^2} + \frac{4\sqrt{k_F^2-k_y^2-(\Delta k_z/2)^2}}{(\Delta k_z/2)} \arcsin\left[\frac{\Delta k_z/2}{\sqrt{k_F^2-k_y^2}}\right] \tag{23}$$

with $\Delta k_z=(eB/\hbar)x$, while k_y is implicitly given by $\zeta_{FG}(\Delta k_z,k_y)=(eB/\hbar)y$. The long orbit MNPQ yields

$$W_{MQ} = \frac{-4k_y^2}{(k_F^2-k_y^2)} - \frac{4\sqrt{k_F^2-k_y^2-(\Delta k_z/2)^2}}{(\Delta k_z/2)}\left\{\pi + \arcsin\left[\frac{\Delta k_z/2}{\sqrt{k_F^2-k_y^2}}\right]\right\} \tag{24}$$

Here, the other solution for k_y should be taken, which can be obtained from $\zeta_{MQ}(\Delta k_z,k_y)=(eB/\hbar)y$.

The implicitness of the relation between k_y and the position coordinates of the emitter, makes it impossible to obtain a general expression for the focusing signal as a function of magnetic field for fixed point-contact separation. An exception is the case where the magnetic field is perpendicular to the line EC, a geometry that is often used in experiments. Then $y=0$ and the two orbits FG and MNPQ both lie in the plane $k_y=0$ for all values of B. The focusing signal shows a peak for $(\Delta k_z/2)^2=(eB/\hbar)^2(x/2)^2=k_F^2$ because then $W_{FG}=W_{MQ}=0$. The peak occurs at a magnetic field value B_0 given by

$$B_0 = 2\hbar k_F/(eL) \tag{25}$$

in which $L=|x|$ is the separation of the point contacts. With the replacement $(\Delta k_z/2)=-(B/B_0)k_F$ (the minus sign takes into account the fact that x and therefore Δk_z are negative), the focusing signal (Eq. (17)) is given by

$$J_{ce}/I_e = (eB/\hbar)^2(\pi k_F^2)^{-1}(W_{FG}^{-1} + W_{MQ}^{-1})$$

$$= 4L^{-2}(B/B_0)^3[\pi^2 - 4\arccos^2(B/B_0)]^{-1}[1-(B/B_0)^2]^{-1/2} \tag{26}$$

The focusing signal decreases quadratically with increasing point-contact separation The divergence at $B = B_0$ is described by the last factor, for small B, the other terms give rise to a B^2 dependence of the signal This result can be compared with the result of the direct calculation by Benistant [20] Agreement is found if in the calculation of Ref 20 the limits for large mean free path and small collector area are taken and if a factor 2 is added to correct for a normalization error

Chapter 2.3

SAMPLE PREPARATION AND EXPERIMENTAL SET-UP

The Ag single-crystals on which the TEF experiments were performed, were grown in Leiden[21] from a melt of 6N purity The single-crystal rod was spark-cut[21] in order to obtain samples with (100) and (110) surfaces respectively The samples were polished with the use of diamond paste and etched in 20 ml of a NH_3 solution (>25%) with 5 to 10 drops added of a H_2O_2 solution (40%) In order to further purify the samples and to release mechanically induced strains, the samples were annealed[22] for 8 hours at 850 °C in 10^{-2} Pa air In this way, a residual resistivity ratio (RRR) of 15 000 is obtained This corresponds to an electron mean free path at low temperatures of about 0 7 mm, which is quite sufficient for TEF experiments The point contacts were made with 50-μm-diam Ag wires of 5N purity The wires were sharpened by electrochemically etching in a solution of 5% NaCN and 5% $K_4[Fe(CN)_6]$ $3H_2O$ in water [23] This yields sharp points with radii of the order of 1 μm The diameter of the actual point contact, however, is much smaller A typical resistance value of a Sharvin point contact of 1 Ω corresponds to a diameter of 38 nm

The measurements were done in a He bath at 4 2 K, or at 1 2 K if it was important to reduce thermal broadening The insert (see Fig 6) is of similar construction as that of Tsoi and Tsoi [24] The sample is mounted on a turntable and can be rotated from outside the dewar The point-contact wires are attached to levers and can be individually lowered onto the sample surface or lifted from outside The tail of the glass cryostat is left unsilvered in order to be able to observe the orientation of the sample with respect to the point contacts It also allows the measurement of the point-contact separation, which is typically between 40 μm and 200 μm The magnetic field is produced by a water-cooled iron-core electromagnet, which can be rotated in the horizontal plane A Hall probe mounted on one of the pole faces provides a voltage signal that is proportional to the magnetic field

The TEF signal is measured with the use of a phase-sensitive detection technique Through the emitter point contact an ac current (120 Hz) is sent, the collector voltage, which is of the order of 1 nV, is amplified with a transformer, a pre-amplifier, and a selective amplifier and is finally measured with a lock-in amplifier To study the dependence of the TEF signal on the electron energy, also a dc current is sent through the emitter point contact This current establishes a dc emitter voltage V and, if the ac modulation is much smaller than V, the ac part of the collector voltage is only due to electrons that are injected with an energy eV above the Fermi level This is only true if the equilibrium energy distribution of the electrons shows a sharp cut off at the Fermi level (i e if the temperature is low) To study the emitter current dependence of the TEF signal, in principle the same set-up is used However, to provide the large injection currents that are used in these experi-

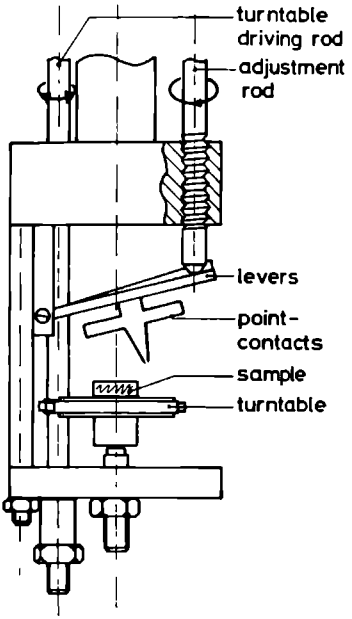

Fig. 6. Detail of the insert that is used in the TEF experiments The sample can be rotated from outside the dewar and the point-contact wires can be lowered and lifted.

ments, an extra power amplifier is added.

References

[1] Yu. V. Sharvin, Zh. Eksp. Teor. Fiz. **48**, 984 (1965) [Sov. Phys.-JETP **21**, 655 (1965)].

[2] Yu. V. Sharvin and L. M. Fisher, Pis'ma Zh. Eksp. Teor. Fiz. **1**, 54 (1965) [JETP Lett. **1**, 152 (1965)].

[3] Yu. V. Sharvin and N. I. Bogatina, Zh. Eksp. Teor. Fiz. **56**, 772 (1969) [Sov. Phys.-JETP **29**, 419 (1969)].

[4] V. S. Tsoi, Pis'ma Zh. Eksp. Teor. Fiz. **19**, 114 (1974) [JETP Lett. **19**, 70 (1974)].

[5] V S Tsoi, Zh Eksp Teor Fiz **68**, 1849 (1975) [Sov Phys -JETP **41**, 927 (1975)]
[6] V S Tsoi and I I Razgonov, Pis'ma Zh Eksp Teor Fiz **23**, 107 (1976) [JETP Lett **23**, 92 (1976)]
[7] V S Tsoi and I I Razgonov, Pis'ma Zh Eksp Teor Fiz **25**, 30 (1977) [JETP Lett **25**, 26 (1977)]
[8] V S Tsoi and I I Razgonov, Zh Eksp Teor Fiz **74**, 1137 (1978) [Sov Phys -JETP **47**, 597 (1978)]
[9] P J M W L Birker, H van Kempen, and P Wyder, J Phys (Paris) **C6**, 1128 (1978)
[10] V S Tsoi, J Bass, P A M Benistant, H van Kempen, E L M Payens, and P Wyder, J Phys F **9**, L221 (1979)
[11] P A M Benistant, G F A van de Walle, H van Kempen, and P Wyder, Phys Rev **B33**, 690 (1986)
[12] H Sato and F Kimura, J Phys F **14**, 1905 (1984)
[13] P A M Benistant, H van Kempen, and P Wyder, J Phys F **15**, 2445 (1985)
[14] H Sato and K Yonemitsu, J Phys F **16**, 2053 (1986)
[15] A P van Gelder, lecture notes, University of Nijmegen (1986)
[16] J C Maxwell, A Treatise on Electricity and Magnetism, Oxford (1904)
[17] A G M Jansen, A P van Gelder, and P Wyder, J Phys C **13**, 6073 (1980)
[18] S A Korzh, Zh Eksp Teor Fiz **68**, 144 (1975) [Sov Phys -JETP **41**, 70 (1975)]
[19] E L M Payens, doctoral thesis, University of Nijmegen (1979)
[20] P A M Benistant, thesis, University of Nijmegen (1984)
[21] We are grateful to Ing T J Gortenmulder and the late Dr B Knook of the Kamerlingh Onnes Laboratory, Leiden for growing the silver single-crystals from the melt, and Ir L W M Schreurs for orienting and spark-cutting the samples
[22] A C Ehrlich, J Mat Science **9**, 1064 (1974)
[23] J W Dozier and J D Rodgers, IEEE Trans **MTT-12**, 360 (1964)
[24] V S Tsoi and N P Tsoi, Zh Eksp Teor Fiz **73**, 289 (1977) [Sov Phys -JETP **46**, 150 (1977)]

New Method to Study the Electron-Phonon Interaction in Metals

P C van Son, H van Kempen, and P Wyder[(a)]
Research Institute for Materials University of Nijmegen NL 6525 ED Nijmegen The Netherlands
(Received 12 November 1986)

A new kind of point-contact spectroscopy is described The magnitude of the transverse electron-focusing signal in a Ag single crystal is measured as a function of the energy of the injected electrons For low energies, this is a direct measurement of the energy dependence of the electron-phonon interaction strength of electrons in a specific orbit on the Fermi surface Also for higher energies effects of the anisotropy of the electron-phonon interaction are observed

PACS numbers 72 15 Lh 72 10 Di 72 15 Gd

The electron-phonon interaction in metals and its anisotropy are studied in many different ways Most of the methods use the fact that, in a magnetic field, electrons move in cyclotron orbits [e g , the radio-frequency size effect (RFSE)] The energy-dependent part of the mean free path of electrons in a certain orbit is studied by measurement of the decrease of the signal for increasing temperature For a review on the use of RFSE and other methods for this purpose, see Gantmakher [1] Point-contact spectroscopy[2,3] is a method that allows direct measurement of the energy dependence Electrons are injected with a certain amount of energy at a Sharvin point contact[4] between two metals, if the electrons scatter back through the contact, the resistance will increase With that method it is not possible to select a specific cyclotron orbit, although via a weight factor over the Fermi surface information about the anisotropy can be obtained [5,6]

We used a new method to study the electron-phonon interaction in Ag The method is based on transverse electron focusing (TEF)[7-9] and combines the advantages of the methods described above In a TEF experiment, two point contacts are placed on the surface of a metal single crystal at a distance apart smaller than the mean free path (see the inset of Fig 1) Electrons are injected at the emitter point contact (E) and are bent back to the surface by a magnetic field For a certain value of the field, the electrons are focused on the collector point contact (C) and a voltage peak is found We measured the decrease of this voltage peak with increasing energy of the electrons This is a direct measurement of the energy dependence of the scattering rate of electrons in a specific cyclotron orbit Sharvin and Bogatina[10] used a slightly different setup (longitudinal electron focusing) to study the electron-phonon interaction in Sn The temperature dependence of the peak height could be related to scattering processes with phonons, but the energy dependence they found was dominated by the defocusing action of the magnetic field of the injection current

If in a TEF experiment on a metal with a spherical Fermi surface the magnetic field B is directed perpendicular to the line EC, only electrons with no velocity component along B will arrive at the collector The electrons that give rise to the focusing peak travel half a cyclotron orbit through the crystal If the magnetic field is rotated over an angle θ in the plane of the crystal surface, focusing still occurs It may be shown that the electrons responsible for the focusing peak now travel along a nonextremal cyclotron orbit over an angle $\pi+2\alpha$ (α being a function of θ) Electrons that are scattered will no longer contribute to the focusing peak If the scattering rate τ^{-1} is a function of the energy ϵ of the electron (relative to the Fermi energy), the TEF peak height P will be a function of the voltage V across the emitter point contact

$$P(eV) = P(0)\exp[-t/\tau(eV)] \qquad (1)$$

Here $t = (\pi+2\alpha)m/eB_0$ is the time during which the electron travels through the crystal, B_0 is the value of the magnetic field for which focusing occurs, and for m we

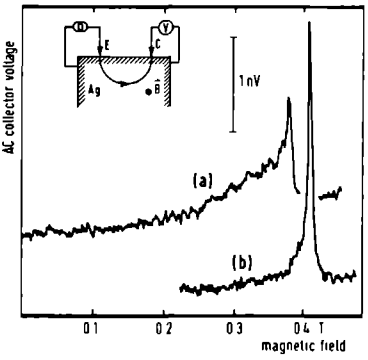

FIG 1 (a) Collector voltage vs magnetic field for Ag(100) The magnetic field is directed along [001] and the line connecting the point contacts is perpendicular to it (b) Same as (a), but with the magnetic field rotated over $\approx 35°$ Inset The TEF geometry with emitter (E) and collector (C) point contacts

take the free-electron mass

The scattering rate of electrons with phonons depends on the energy of the electrons and on the temperature It may be characterized by the function α^2F, the product of the average electron-phonon interaction matrix element squared and the phonon density of states

$$\frac{1}{\tau(\epsilon\, T)} = 2\pi \int d\omega\, \alpha^2F(\omega)[f(\epsilon+\hbar\omega) - f(\epsilon-\hbar\omega) + 2N(\omega) + 1] \tag{2}$$

Here f and N are the Fermi-Dirac and Bose-Einstein distribution functions, respectively, and $\hbar\omega$ is the phonon energy For $T=0$, the equation reduces to

$$\frac{1}{\tau(\epsilon,0)} = 2\pi \int_0^{\epsilon/\hbar} d\omega\, \alpha^2F(\omega) = \frac{2\pi b}{3\hbar}\epsilon^3 \tag{3}$$

The last step is valid for low energies where $\alpha^2F(\omega) = b(\hbar\omega)^2$ From the decrease of the TEF peak height with increasing electron energy, the coefficient b may be determined As the electron-phonon interaction is anisotropic, this value is an average value for the orbit that is selected by the focusing condition Effects of finite temperature can be neglected as long as $k_BT \ll \epsilon$

If the electron-phonon interaction is studied in an RFSE experiment, the temperature dependence of the scattering rate is measured In principle, one measures some average rate for electrons with energies within a range of the order of k_BT around the Fermi energy [11] Wagner and Albers,[12] however, showed that, in samples that are thick with respect to the electron mean free path, only the electrons at the Fermi level contribute The scattering rate of these electrons follows from Eq (2) and, with the assumption of a quadratic energy dependence of α^2F, is given by

$$1/\tau(0,T) = 8\,4(2\pi b/\hbar)(k_BT)^3 \tag{4}$$

Equations (3) and (4) may be used to compare measurements of the energy dependence and of the temperature dependence by expressing the coefficients in the single parameter b

The preparation of the Ag single-crystal samples that were used in the TEF experiments has been described elsewhere [8,9] All measurements were done in a pumped He bath (1 2 K) Point contacts were made by means of two 50-μm-diam Ag wires with sharp points etched to them, the contact resistances ranged from 0 1 to 1 Ω Both the sample and the magnetic field could be rotated in the horizontal plane with respect to the point contacts For the point-contact separation used ($\approx 50\,\mu$m), the relative directions of EC, magnetic field, and crystal axes could be determined only up to $\pm 5°$

A home-built current source provided a direct current and a small ac modulation (120 Hz) to the emitter point contact The ac voltage across the emitter was chosen not larger than 0 5 mV_{rms} to prevent smearing out of the energy dependence The ac voltage across the collector point contact was measured by use of phase-sensitive detection The collector voltage was first measured as a function of the magnetic field for zero dc emitter voltage (the usual TEF experiment) The energy dependence was then measured by sweeping of the dc voltage for several values of the magnetic field

Measurements were done for four different electron orbits in two Ag samples, with the normals along [100] and [110], respectively Figure 1(a) shows the TEF signal for a Ag(100) sample with the magnetic field along [001] and perpendicular to the line connecting the point contacts (orbit 1 in Fig 2) When the magnetic field is rotated over $\approx 35°$, a maximum is observed in the TEF peak height while the width of the peak has become smaller [see Fig 1(b)] In this configuration the electrons that give rise to the focusing peak follow a nonextremal belly orbit that does not come very close to the necks of the Fermi surface (orbit 2 in Fig 2) The differences in heights and widths of the TEF signal in different configurations can be explained qualitatively by the deviations of the Fermi surface of Ag from a sphere [9] Figures 3(a) and 3(b) show the corresponding measurements of collector voltage versus dc emitter voltage

On the Ag(110) sample, TEF measurements were done with $\angle(EC,[1\bar{1}0]) = 25°$ and $B \perp EC$ The electrons then follow an orbit which is already close to the necks (orbit 3 in Fig 2) By rotation of the magnetic field over 12°, the orbit is brought as close to the necks as possible (orbit 4 in Fig 2) In the latter configuration, also the roles of emitter and collector were interchanged (with the magnetic field reversed), and measurements were done for $B = 2B_0$ as well, when electrons are focused after being specularly reflected at the surface In all these measurements the same voltage dependence was found

The voltage dependence of the TEF peak height in different configurations shows the same features For low voltages, the signal decreases because the scattering rate of electrons with phonons increases with increasing

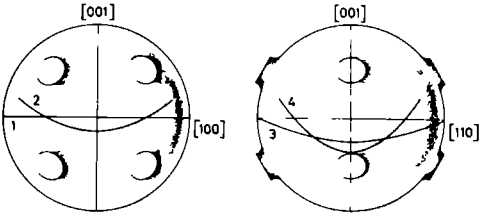

FIG 2 The Fermi surface of Ag with orbits 1–4 Orbits 1 and 3 are extremal orbits

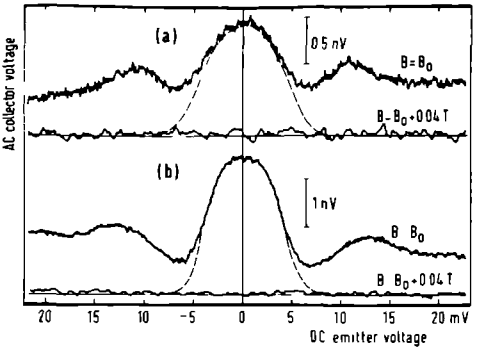

FIG 3 (a) Collector voltage vs dc emitter voltage for Ag(100) The magnetic field is directed along [001] and the line connecting the point contacts is perpendicular to it Traces are for the focusing peak of Fig 1(a) ($B=B_0$) and for $B=B_0+0.04T$ The dashed line is a fit with $b=60\ \mathrm{eV}^{-2}$ (b) Same as (a), but with the magnetic field rotated over $\approx 35°$ Traces are for the focusing peak of Fig 1(b) ($B=B_0$) and for $B=B_0+0.04T$ The dashed line is a fit with $b=75\ \mathrm{eV}^{-2}$

electron energy For higher voltages, a background signal is observed, which is due to electrons that have lost their energy close to the emitter These electrons again have a large mean free path The smaller the source of these electrons is, the narrower and higher their focusing peak will be The background signal has maximum that depends on the configuration [compare Figs 3(a) and 3(b)] It also shows a slight asymmetry for positive and negative emitter voltages, which is due to the magnetic field generated by the emitter current [13]

The parameter b was determined by fitting of the expected voltage dependence of the TEF signal [Eq (1)] to the measurements [see the dashed lines in Figs 3(a) and 3(b)] We assumed that the background signal is zero for $V_{dc}=0$ and that it increases monotonically for increasing absolute value of the emitter voltage In Table I, we compare our TEF results for the parameter b with measurements of the temperature dependence of RFSE lines by Gasparov[14] and by Johnson and Goodrich [15] These values of b are calculated from the coefficients of the temperature dependence with the use of Eq (4) The data for orbit 1 may be compared directly For the other orbits we tabulated how the b value is related to the value for the nearest orbit that was measured in Refs 14 and 15 Gasparov, Lebech, and Saermark[16] measured the temperature dependence of time-of-flight effect signals in Ag and found up to 30% higher values for the coefficient than the RFSE results of Ref 14 The temperature dependence of the magneto-acoustic effect in Ag[17] yields the same values as the RFSF results of Ref 15

Our values for b are lower, but they are not unreasonable in view of the discrepancy in the published values On the other hand, Gasparov[14] and Johnson and Goodrich[15] do qualitatively agree on the anisotropy of b, while the TFF measurements show rather the opposite trend, except for the orbit very close to the necks An explanation for this discrepancy may be found in the fact that the TEF experiment measures the electron-phonon interaction in the energy range 1–5 meV, while the measurements on temperature dependence probe the range 0 1–1 meV Although the results of both experiments are consistent with $\alpha^2F=b(\hbar\omega)^2$, the measurements only extend over a limited energy range and the ω dependence of α^2F and its anisotropy may well be more complicated

TABLE I Values of the parameter b in eV^{-2} for electrons in four different orbits on the Fermi surface of Ag The orbits are shown in Fig 2 For the RFSE measurements of the same (1) or nearby (2,3,4) orbits the values of b are calculated from the temperature dependence with the use of Eq (4)

Orbit	This work (TEF)	Ref 14 (RFSE)	Ref 15 (RFSF)
1	60 ± 15	115	76
2	75 ± 15	<115	<76
3	45 ± 10	$\gtrsim125$	$\gtrsim90$
4	100 ± 15	$\gg125$	$\gg90$

A comparison in terms of the coefficient b between TEF and point-contact spectroscopy is difficult because the latter measures some average value over the whole Fermi surface In addition, point-contact spectroscopy is not very sensitive for low energies when the electrons are scattered far from the emitter For high-electron energies however, the two methods are very similar The main difference is that in TEF the electrons that are scattered close to the emitter are detected at a collector point contact instead of at the emitter This means that scattering processes are selected in which the electrons are scattered into a specific direction, namely the starting direction of the focusing orbit Both the TEF signal and the point-contact spectrum[3] of Ag show a maximum for $\epsilon\approx12$ meV that corresponds to the main peak of α^2F The TEF signal also shows a dependence of the position of this maximum on the configuration (i e , on the focusing orbit), and so also for high energies TEF yields information about the anisotropy of the electron-phonon interaction

In conclusion, TEF is of great use to study the electron-phonon interaction in metals For low energies, it directly measures the energy dependence of the scattering rate of electrons in a specific orbit on the Fermi surface Other methods like RFSE study the energy dependence through the temperature dependence of the electron mean free path The results of the present TEF measurements on Ag do not in all aspects agree with the earlier RFSE results This may be because the methods

probe slightly different energy ranges For high electron energies, TEF is in principle very similar to point-contact spectroscopy The different experimental setup of TEF, however, yields very specific information about the anisotropy of the electron-phonon interaction

We are grateful to Ing T J Gortenmulder and the late Dr B Knook of the Kamerlingh Onnes Laboratory, Leiden, for growing the silver single crystals from the melt, and Ir L W M Schreurs for orienting and spark cutting the samples We thank Dr J A A J Perenboom for critical reading of the manuscript Part of this work is supported by the Stichting voor Fundamenteel Onderzoek der Materie (FOM), which is financially supported by the Nederlandse Organisatie voor Zuiver Wetenschappelijk Onderzoek (ZWO)

---

[a]Also at Max-Planck-Institut fur Festkorperforschung, Hochfeld-Magnetlabor, 166X, F-38042 Grenoble-Cedex, France

[1]V F Gantmakher, Rep Prog Phys **37**, 317 (1974)

[2]I K Yanson, Zh Eksp Teor Fiz **66**, 1035 (1974) [Sov Phys JETP **39** 506 (1974)]

[3]A G M Jansen, A P van Gelder, and P Wyder, J Phys C **13**, 6073 (1980)

[4]A Sharvin point contact is characterized by ballistic electron flow (the contact radius is small with respect to the electron mean free path)

[5]I K Yanson and A G Batrak, Pis ma Zh Eksp Teor Fiz **27**, 212 (1978) [JETP Lett **27**, 197 (1978)]

[6]H U Baranger, A H MacDonald, and C R Leavens, Phys Rev B **31**, 6197 (1985)

[7]V S Tsoi, Pis'ma Zh Eksp Teor Fiz **19**, 114 (1974) [JETP Lett **19**, 70 (1974)], V S Tsoi, Zh Eksp Teor Fiz **68**, 1849 (1975) [Sov Phys JETP **41**, 927 (1975)]

[8]V S Tsoi, J Bass, P A M Benistant, H van Kempen, E L M Payens, and P Wyder, J Phys F **9**, L221 (1979)

[9]P A M Benistant, thesis, University of Nijmegen, 1984 (unpublished)

[10]Yu V Sharvin and N I Bogatina, Zh Eksp Teor Fiz **56**, 772 (1969) [Sov Phys JETP **29**, 419 (1969)]

[11]P B Allen, Phys Rev B **11**, 2693 (1975)

[12]D K Wagner and R C Albers, J Low Temp Phys **20**, 593 (1975)

[13]P C van Son, H van Kempen, and P Wyder to be published

[14]V A Gasparov, Zh Eksp Teor Fiz **68** 2259 (1975) [Sov Phys JETP **41**, 1129 (1975)]

[15]P B Johnson and R G Goodrich, Phys Rev B **14**, 3286 (1976)

[16]V A Gasparov, J Lebech, and K Saermark, J Low Temp Phys **50**, 379 (1983)

[17]P B Johnson and J A Rayne, J Low Temp Phys **40**, 617 (1980)

J. Phys. F: Met Phys. 17 (1987) 1471–1475. Printed in the UK

COMMENT

Emitter current dependence of transverse electron focusing

P C van Son, H van Kempen and P Wyder†

Research Institute for Materials, University of Nijmegen, Toernooiveld, NL 6525 ED Nijmegen, The Netherlands

Received 18 November 1986

Abstract. In transverse electron focusing experiments in Ag an asymmetry is observed in the effect of a positive or negative emitter current on the position and height of the focusing peak. A simplified calculation shows that both effects may be explained qualitatively by the influence of the magnetic field of the emitter current on the orbits of the injected electrons.

In a transverse electron focusing (TEF) experiment (Tsoi 1974, 1975, Tsoi *et al* 1979) electrons are injected into a single crystal at a point contact (the emitter, E). The electrons are bent back to the surface by an applied magnetic field B_a (see the inset of figure 1). For a specific field value, a voltage peak is observed across a second point contact (the collector, C). Non-linearities in the relation between collector voltage and emitter current for TEF in Ag were shown to yield information about the electron–phonon interaction (van Son *et al* 1987). For high emitter currents, an asymmetry for positive and negative current is also observed both in peak height and in peak position.

In a slightly different geometry (longitudinal electron focusing in a Sn single crystal) Sharvin and Bogatina (1969) observed an asymmetric shift of the peak position, which they attributed to the influence of the magnetic field of the injection current on the electron orbits. In a theoretical paper on TEF, Kolesnichenko (1980) showed that such an asymmetry may also be due to the energy dependence of the cyclotron radius, and that an asymmetry in the peak height may be due to thermoelectric effects at the emitter. But these effects are only relevant for semimetals, which have a small Fermi energy. We observed an asymmetry in peak height and in peak position for TEF in Ag. We will describe a simplified calculation that takes the magnetic field of the emitter current into account, and that explains qualitatively both the asymmetry in peak height and shift.

The preparation of the Ag single-crystal sample that was used has been described elsewhere (Tsoi *et al* 1979). Point contacts were made by means of two 50 μm diameter Ag wires with sharp points etched to them. A home-built current source and a power amplifier provided a DC current and an AC current modulation to the emitter point contact. While sweeping the applied magnetic field the AC collector voltage was measured using phase-sensitive detection.

† Also at: Max-Planck-Institut fur Festkorperforschung, Hochfeld Magnetlabor, 166X, F 38042, Grenoble Cedex, France.

Figure 1 shows a TEF measurement in which a large asymmetry was found. The point contacts stood on the (100) surface of a Ag single crystal and were 185 μm apart. The magnetic field was directed perpendicular to the line connecting the point contacts and it made an angle of 10° with the [001] axis. This means that the focusing signal is due to electrons that travel along an almost circular extremal belly orbit on the Fermi surface of Ag. The three traces correspond to DC emitter currents $I_{DC}=0$, $+1.55$ and -1.55 A respectively; the AC modulation was 40 mA_{RMS}. The resistance of the emitter point contact was 19, 17 and 15 mΩ respectively. For these high currents the point-contact resistance is not always constant. This is probably due to heating of the contact or to Lorentz forces on the point-contact wire. The measurement with $I_{DC}<0$ (that is with electron injection into the Ag crystal) shows an increase in peak height with a factor 2.0 and a 5% higher focusing field. For positive I_{DC} (injection of 'holes'), focusing occurs at a 2% lower value of the applied magnetic field and the peak height is a factor 0.53 lower than the peak height for $I_{DC}=0$.

The DC emitter current affects the TEF signal through its magnetic field, but also by establishing a voltage V_{DC} across the emitter point contact. If the electron transport through the contact is ballistic (Sharvin point contact), the electrons are injected with an excess energy eV_{DC} above the Fermi level and may be scattered by emitting a phonon (van Son *et al* 1987). For the low-ohmic point contacts used, many non-equilibrium phonons will be present near the contact. The electrons will lose their excess energy close to the contact and the influence of V_{DC} will only be small.

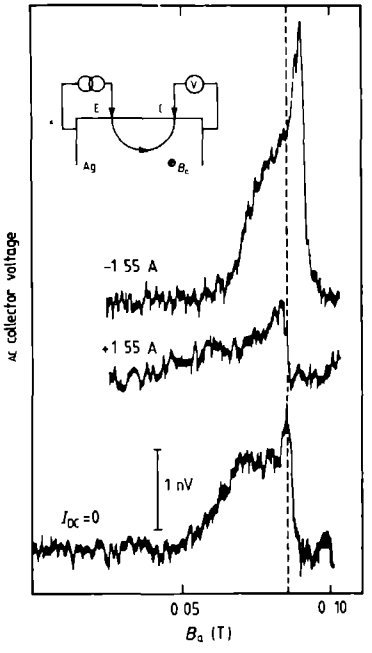

Figure 1. Measured TEF signal for three values of the DC emitter current and constant AC current modulation. The inset shows the geometry of a TEF experiment.

The asymmetry for positive and negative I_{DC} that is measured can only be due to the magnetic field of the current. This was confirmed in a TEF measurement with two point contacts of 0.8 and 0.01 Ω respectively. For fixed DC emitter voltage, the influence of the magnetic field of the emitter current will of course be larger as the point-contact resistance is smaller. If the high-ohmic point contact is used as the emitter, the peak heights for $V_{DC} = \pm 19$ mV are equal and are 20% smaller than the peak height for $V_{DC} = 0$, while the peak position does not shift. After interchanging the roles of the point contacts (and reversing the magnetic field), we find for $V_{DC} = -19$ mV a 40% higher TEF peak at a 5% larger magnetic field value compared with the peak for $V_{DC} = 0$.

In the calculation of the influence of I_{DC} on the TEF peak, we assume a spherical Fermi surface and we neglect effects of finite emitter voltage. If the applied magnetic field is directed perpendicular to the line connecting the point contacts, only electrons with no velocity component along B_a contribute to the focusing signal (see the inset of figure 2). The electrons that are injected at the origin return to the surface at a distance x_s, which is a function of B_a and of the injection angle φ_0:

$$x_s = 2R_c \cos(\varphi_0 - \pi). \tag{1}$$

$R_c = |mv_F/eB_a|$ is the cyclotron radius, v_F is the Fermi velocity and m and e are the mass and charge respectively of the charge carriers (for electrons $m > 0$ and $e < 0$; for 'holes' in a free-electron metal one has $m < 0$ and $e > 0$). The function $x_s(\varphi_0)$ has a maximum for $\varphi_0 = \pi$ with $x_s = 2R_c$ (curve $I_{DC} = 0$ in figure 2). At that point the density of electrons arriving at the surface shows a maximum and if, for a specific B_a, the point coincides with the collector position, a voltage peak is measured. The maximum value of the function $x_s(\varphi_0)$ thus determines the focusing value of the applied magnetic field while the curvature at the maximum determines the height of the focusing peak.

The influence of the magnetic field of the emitter current is determined by calculating how this field B_I makes the function $x_s(\varphi_0)$ change. To obtain an analytical expression for B_I, two major simplifications with regard to the current density have to be made: the emitter is assumed to be a mathematical point and the curvature of the electron orbits due

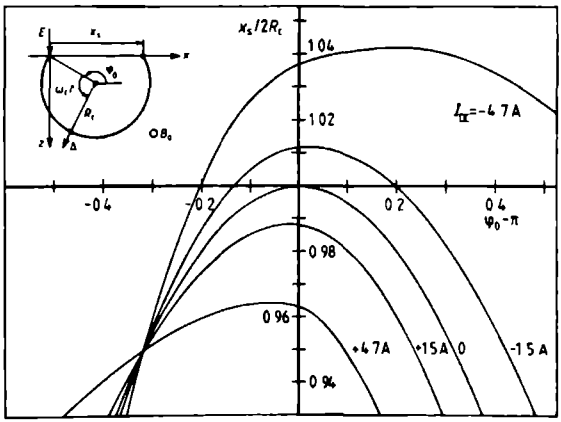

Figure 2. Calculated results of the function $x_s(\varphi_0)$ for Ag (equation (2)) for five values of the DC emitter current. Various symbols are defined in the inset.

to B_a is neglected. Then the current density $J(r)$ and the resulting field $B_I(r)$ are given by

$$J(r)=\frac{I_{DC}}{2\pi r^2}\frac{r}{r}$$

$$B_I(r)=\frac{\mu_0 I_{DC}}{2\pi}\frac{1-\cos\theta}{r\sin\theta}\frac{\varphi}{\varphi}$$

in which r, θ and φ are standard spherical coordinates.

Due to the field $B_I(r)$, the electron orbits are no longer circular but the orbits that are relevant for focusing are still confined to the xz plane because for these orbits B_I is directed perpendicular to this plane. We assume that the deviations from the original electron orbit are small, so that the field $B_I(r)$ felt by the electrons in a specific orbit becomes a known function of the time. In that case the deviation $\Delta(\omega_c t, \varphi_0)$ from the circular orbit is given by

$$\frac{d^2\Delta}{dt^2}=\frac{ev_F|B_I(\omega_c t,\varphi_0)|}{m}\frac{x}{|x|}\frac{I_{DC}}{|I_{DC}|}-\omega_c^2\Delta.$$

The first term is the acceleration due to the Lorentz force (note that the factor e/m is negative for both electrons and holes). The second term is due to the rotation of the coordinate system with the cyclotron frequency $\omega_c=eB_a/m$. The differential equation is integrated numerically from $\omega_c t=\omega_c t_0$ to $\omega_c t=3\pi-2\varphi_0$ with initial conditions $\Delta=d\Delta/dt=0$, thus yielding $\Delta_s(\varphi_0)$. The integration cannot be started at $\omega_c t=0$ because B_I diverges at the origin. Except for $\varphi_0=\pi$, the value of Δ_s depends somewhat on the value of $\omega_c t_0$. In the calculations we took $\omega_c t_0=10^{-3}$, which corresponds to a distance from the origin of the order of the experimental point-contact diameter. The function $x_s(\varphi_0)$ is then given by

$$x_s(\varphi_0)=2R_c\cos(\varphi_0-\pi)+\frac{\Delta_s(\varphi_0)}{\cos(\varphi_0-\pi)}. \tag{2}$$

All material parameters can be absorbed in a single scaling current $2\pi m v_F/\mu_0 e$, which is 39 A for Ag. In figure 2 the function $x_s(\varphi_0)$ is given for $I_{DC}=0$, ± 1.5 and ± 4.7 A. For $\varphi_0>\pi$, Δ_s is negative for positive I_{DC} and vice versa. This can easily be understood because for $\varphi_0>\pi$, B_I has the same (opposite) direction as B_a along the whole orbit for positive (negative) I_{DC}. For $\varphi_0<\pi$, B_I and B_a are parallel on part of the orbit while on the other part they are antiparallel. For a specific value of φ_0 this results in $\Delta_s=0$. From the maximum value of the function $x_s(\varphi_0)$ it follows that focusing occurs at a value of B_a up to 4% larger (smaller). The relative peak height is calculated by determining the width of the function $x_s(\varphi_0)$ for $x_s/(x_s)_{max}=0.999$. The results are 1.00 ($I_{DC}=0$):0.98 (+1.5 A):1.22 (+4.7 A):1.11 (−1.5 A):1.89 (−4.7 A). For negative I_{DC}, the peak height increases strongly, while for positive I_{DC} the peak height first decreases and later increases.

According to the calculation, the peak shifts and the relative peak heights should only depend on the value of I_{DC}. In the experiment this is not the case; in most other measurements the effects are smaller than in figure 1. These differences may be due to the deviations of the Fermi surface of Ag from a sphere, or to effects of finite emitter voltage. The calculated peak shifts (−1.2% and +1.2%) and relative peak heights (0.98 and 1.11) for $I_{DC}=\pm 1.5$ A are smaller than the measured values of figure 1 (−2%, +5%, 0.53 and 2.0 respectively) but the trend is correct. A quantitative agreement is not to be expected because of the simplifications that were made in the calculation. There is, however,

sufficient agreement to confirm the idea that the magnetic field of the emitter current is responsible for the observed asymmetry in both peak height and shift.

Acknowledgments

We are grateful to Ing T J Gortenmulder and the late Dr B Knook of the Kamerlingh Onnes Laboratory, Leiden for growing the silver single crystal from the melt, and to Ir L W M Schreurs for orienting and spark cutting the sample. Part of this work is supported by the Stichting voor Fundamenteel Onderzoek der Materie (FOM) which is financially supported by the Nederlandse Organisatie voor Zuiver Wetenschappelijk Onderzoek (ZWO).

References

Kolesnichenko Yu A 1980 *Fiz Nizk Temp* **6** 603 (transl *Sov J Low Temp Phys* **6** 289)
Sharvin Yu V and Bogatina N I 1969 *Zh Eksp Teor Fiz* **56** 772 (transl *Sov Phys–JETP* **29** 419)
van Son P C, van Kempen H and Wyder P 1987 *Phys Rev Lett* **58** 1567
Tsoi V S 1974 *Zh Eksp Teor Fiz , Pis Red* **19** 114 (transl *JETP Lett* **19** 70)
—— 1975 *Zh Eksp Teor Fiz* **68** 1849 (transl *Sov Phys–JETP* **41** 927)
Tsoi V S, Bass J, Benistant P A M, van Kempen H, Payens E L M and Wyder P 1979 *J Phys F Met Phys* **9** L221

Chapter 3

ANDREEV REFLECTION

Chapter 3.1

INTRODUCTION

Andreev reflection[1] is a very special kind of reflection process of electrons that may take place at an interface of a normal metal and a superconductor (N-S interface) In the ground state of a superconductor, the electrons are bound in Cooper pairs and there is an energy gap in the excitation spectrum If the incoming electron in the normal metal has a lower energy than this gap energy, it can not enter the superconductor as an excitation Instead, it enters the superconductor as a Cooper pair together with a second electron from the normal metal The hole (or "missing electron") that is created in the normal metal moves back in the direction from which the incident electron came This Andreev-reflection process gives rise to a so-called excess current because the returning hole gives an additional contribution to the current Andreev reflection is of practical importance because it is one of the origins of the non-linearities in the current-voltage (I-V) curves of superconducting weak links that are used in several devices Blonder, Tinkham, and Klapwijk[2] elaborated an Andreev-reflection model that describes well the measured excess current in the I-V curves of N-S point contacts In this chapter, the work on N-S point contacts is extended by studying the I-V curves of normal-metal point contacts on the N side of N-S bilayers If the electron mean free path in N is large enough, the point-contact resistance is influenced by the Andreev-reflection process at the N-S interface An advantage of this set-up is that the detector (i e the point contact) and the object of study (i e the N-S interface) are independent of each other in contrast to the N-S point contact

A superconductor is characterized by a finite value of the superconducting order parameter, in a normal metal it is zero However, near an N-S interface, this need not be true The presence of S induces a finite value of the order parameter in N, while the presence of N gives rise to a depression of the order parameter near the interface in S (proximity effect) In N-S point contacts, the pair potential varies on the scale of the point-contact diameter As this is much smaller than the coherence length of the superconductor, Blonder et al [2] used a step-function for the position dependence of the order parameter In Chapter 3 2, their model is extended in order to be able to deal with a gradual variation of the order parameter The influence of this effect on the probability of Andreev reflection is calculated, this will be relevant for the excess current of a point contact on an N-S bilayer Also the influence of a gradual variation of the order parameter on geometrical resonance effects is calculated These effects show up as oscillations in the transmission of a tunnel junction on an N-S bilayer and are a consequence of the Andreev-reflection process at the N-S interface Both the probability of Andreev reflection and the geometrical resonance effects begin to change if the region in which the pair potential varies with position, becomes of the order of the coherence length of the superconductor

In Chapter 3 3, measurements of the excess current of normal-metal point contacts on thin-film N S bilayers are discussed The results deviate from the excess current of an N-S point contact and, for thin N layers, they agree qualitatively with the theoretical results of Chapter 3 2 For large thicknesses of the N film, the finite mean free path of the electrons also influences the I-V curves From the shape of the I-V curve, in principle the position dependence of the order parameter at the N-S interface can be reconstructed However, to be able to do that, the mean free path should be incorporated in the model of Chapter 3 2

Finally, in Chapter 3 4 an experiment is described that combines Andreev reflection and electron focusing [3] The N film is now a thin single-crystal that is much thicker than the deposited thin-films but in which the electrons have a very large mean free path The Andreev-reflection process itself focuses the reflected holes back onto the point contact where the electrons were injected (retroreflection) A small magnetic field influences the orbits of electrons and holes and makes the excess current decrease The results deviate from a model that describes that effect This is partly due to the presence of for instance dislocations that scatter the electrons and holes over small angles The deviations for very small values of the magnetic field are not completely understood, the corresponding length scale implies that the wave character of the electrons has to be taken into account

Although Andreev reflection is directly related to the existence of Cooper pairs in a superconductor, there is an optical analogue of it, optical phase conjugation (for a review, see Ref 4) A phase-conjugate mirror has the same properties with respect to the reflection of light as the N-S interface has with respect to the reflection of electron and hole waves First, it also gives rise to retroreflection the incoming light beam is reflected over 180° independent of the angle of incidence Secondly, the phase of the light wave is conjugated (or time reversed) upon reflection The same happens to the electron and hole wave functions upon Andreev reflection For a phase-conjugate mirror based on the process of degenerate four-wave mixing, the analogy even holds in another aspect Such a mirror consists of a non-linear medium that is excited by two laser beams propagating in opposite directions The phase-conjugated reflected beam results from the interaction of the incident beam with the two pump beams in the non-linear medium The analogy with the Cooper pairs in a superconductor (that consist of electrons with opposite momenta) is clear The analogy of Andreev reflection and optical phase conjugation may be helpful in solving problems in one field with the use of results obtained in the other field

References

[1] A F Andreev, Zh Eksp Teor Fiz **46**, 1823 (1964) [Sov Phys JETP **19**, 1228 (1964)]

[2] G E Blonder, M Tinkham, and T M Klapwijk, Phys Rev **B25**, 4515 (1982)

[3] P A M Benistant, A P van Gelder, H van Kempen, and P Wyder, Phys Rev **B32**, 3351 (1985)

[4] M Ducloy, Festkorperprobleme **22**, 35 (1982)

Chapter 3.2

ANDREEV REFLECTION AND GEOMETRICAL RESONANCE EFFECTS FOR A GRADUAL VARIATION OF THE PAIR POTENTIAL NEAR THE NORMAL-METAL-SUPERCONDUCTOR INTERFACE

P. C. van Son,[a] H. van Kempen,[a] and P. Wyder[a,b]

[a] Research Institute for Materials, University of Nijmegen, Toernooiveld, NL-6525 ED Nijmegen, The Netherlands

[b] Max-Planck-Institut für Festkörperforschung, Hochfeld-Magnetlabor, 166X, F-38042 Grenoble Cedex, France

The probability of Andreev reflection is calculated as a function of the energy for quasiparticles that are incident on a normal-metal-superconductor (N-S) interface with a gradual variation of the pair potential. These calculations are an extension of the work of Blonder, Tinkham, and Klapwijk (Phys. Rev. **B25**, 4515 (1982)), who assumed a step-function for the position dependence of the pair potential. We integrate the Bogoliubov equations numerically in the region in which the pair potential varies with position and apply boundary conditions to find the quantities of interest. This approach is also used to calculate the geometrical resonances in the transmission of a tunnel junction on an N-S bilayer. For a step-like variation of the pair potential, the same expression for the transmission is found as with the usual density-of-states approach. Also results are given for a gradual variation of the pair potential at the interface. Both the probability of Andreev reflection and the geometrical resonance effects begin to change if the region in which the pair potential varies with position, becomes of the order of the coherence length of the superconductor.

PACS number: 74.50+r

I Introduction

In the BCS ground state of a superconductor, electrons with opposite momentum and spin are condensed in Cooper pairs This is due to an attractive phonon-mediated electron-electron interaction that is larger than the repulsive Coulomb interaction Below a specific threshold energy, no excited states exist The quasiparticle states above that threshold are mixtures of electron and hole wave functions The coupling of these wave functions is described in the Bogoliubov equations via a pair potential Δ In a normal metal, the pair potential is zero and there is no energy gap in the excitation spectrum If an electron in a normal metal is incident on an interface with a superconductor (N-S interface), the change in the pair potential causes total or partial Andreev reflection [1] The electron is then reflected as a hole while a Cooper pair is injected into the superconductor If the N-S interface is not perfect, the electron may also be ordinarily reflected and, if its energy is larger than the energy gap of the superconductor, it may be transmitted as an excitation as well Blonder, Tinkham, and Klapwijk[2] (BTK) showed that the Bogoliubov equations are very suitable to describe the reflection and transmission of quasiparticles at an N-S interface They assumed that, at the N-S interface, Δ increases instantaneously from zero in N to a constant value in S Then the solutions of the Bogoliubov equations in N and in S are simple, the probabilities of reflection and transmission are found by matching the two solutions at the N-S interface Ordinary scattering of quasiparticles at the interface is taken into account via appropriate boundary conditions The assumption of a step-function for $\Delta(x)$ is valid for the small-area N-S junctions in which BTK were primarily interested In other geometries, e g a point contact on an N-S bilayer, the Andreev-reflection process induces a correlation between electron and hole states near the interface in N Unless the effective electron-electron interaction in N is zero, this means that there is a finite pair potential in N (proximity effect[3]) On the other hand, the N metal causes a depression of the pair potential in S that decays away from the interface

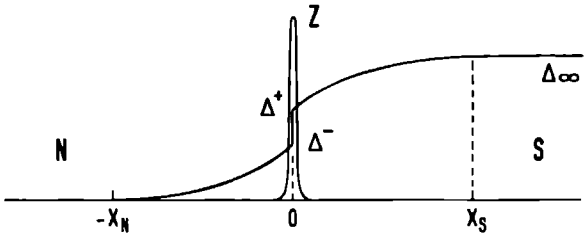

Fig 1 Position dependence of the pair potential Δ that is assumed in the calculation of the probabilities of reflection and transmission The parameter Z indicates the scattering potential at the N-S interface

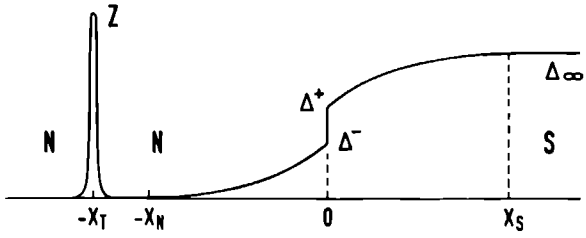

Fig 2 Position dependence of the pair potential Δ that is assumed in the calculation of the geometrical resonance effects The parameter Z indicates the tunnel junction

In this paper, we extend the calculations of BTK to study the effect of a gradual variation of the pair potential near the N-S interface on the reflection and transmission coefficients of quasiparticles Although in principle the position dependence of Δ should be calculated self-consistently,[3] we limit ourselves to an assumed $\Delta(x)$ (see Fig 1) In the region in which $\Delta(x)$ is not constant, the Bogoliubov equations are solved numerically At the N-S interface, a $\delta-$function potential is assumed to represent the scattering of quasiparticles and we allow a discontinuity of $\Delta(x)$ Like in the calculation of BTK, the $\delta-$function potential is dealt with by means of boundary conditions At the starting point and at the end point of the integration, the solution is matched to the solutions for zero Δ and for constant Δ in N and S respectively From the coefficients of the latter solutions, the probabilities of reflection and transmission are deduced The method is described in Section II, while in Section III results for different choices of $\Delta(x)$ are discussed and compared to the BTK results

Andreev reflection plays a crucial role in the origin of the geometrical resonance effects that are observed in the differential conductance of tunnel junctions on N-S bilayers (for a review, see Ref 4) The geometry is shown in Fig 2, the tunnel junction is represented by the $\delta-$function potential at $x=-x_T$ An electron at the tunnel junction in N that moves toward the N-S interface returns to the tunnel junction as a hole After ordinary reflection at the tunnel barrier and a second Andreev-reflection process, it again returns to the tunnel junction but now as an electron This electron wave-function interferes with the original electron wave-function Depending on the energy of the quasiparticle, the interference will be constructive or destructive, which leads to maxima and minima in the differential conductance versus voltage of the tunnel junction Usually, the differential conductance is interpreted as reflecting the density of states of excitations in N Then, the density of states in an N slab with on one side an N-S interface and on the other side a perfectly reflecting boundary is calculated by solving the Bogoliubov equations using Green's functions techniques [4,5] However, BTK have shown that their approach of matching solutions of the Bogoliubov equations can be applied to calculate the differential conductance of an N-S tunnel junction The transmission of a tunnel junction on an N-S bilayer can be analyzed the same

way If a step-function is chosen for $\Delta(x)$, we show that the results of the density-of-states approach and the BTK approach are identical However, the influence on the geometrical resonance effects due to a gradual variation of the pair potential is much easier studied using our extension of the BTK approach In Section IV, results for several choices of $\Delta(x)$ are given and compared to the result for a step-function

At an N-S interface, the Cooper pairs of the superconductor leak into the normal metal, so the pair amplitude changes gradually The pair potential is given by the product of the pair amplitude and the BCS potential that describes the effective electron-electron interaction [3] If the interaction is repulsive in N, the sign of the pair potential in N is opposite to that in S As an interesting sidestep, we discuss in Section V the influence of $\Delta(x)<0$ in N on the probability of Andreev reflection and on the geometrical resonance effects In Section VI, the conclusions are given

II Bogoliubov equations

Because in the ground state electrons with opposite momentum and spin are coupled, the elementary excitations of a superconductor are not just single-electron wave-functions An excitation with wave vector k is built up from the creation of an electron with wave vector k and the annihilation of an electron with wave vector $-k$ [6] The latter process can also be interpreted as the creation of a hole excitation with wave vector k In the Bogoliubov-equation formalism, the excitations are represented by a two-element column vector ψ (we will follow the notation of BTK as much as possible)

$$\psi(x,t) = \begin{bmatrix} f(x,t) \\ g(x,t) \end{bmatrix} \tag{1}$$

The functions $f(x,t)$ and $g(x,t)$ obey the Bogoliubov equations

$$i\hbar\frac{\partial f}{\partial t} = \left[-\frac{\hbar^2}{2m}\frac{\partial^2}{\partial x^2} - \mu(x) + V(x)\right] f(x,t) + \Delta(x) g(x,t) \tag{2a}$$

$$i\hbar\frac{\partial g}{\partial t} = -\left[-\frac{\hbar^2}{2m}\frac{\partial^2}{\partial x^2} - \mu(x) + V(x)\right] g(x,t) + \Delta(x) f(x,t) \tag{2b}$$

in which $\mu(x)$, $\Delta(x)$, and $V(x)$ are the electrochemical potential, the pair potential, and the ordinary potential respectively In the normal metal far from the N-S interface ($\Delta(x)=0$), Eq (2a) reduces to the Schrodinger equation for electrons Then Eq (2b) is the time-reversed Schrodinger equation, which may be interpreted as describing a hole excitation We have assumed that the potentials vary only in the x-direction, the direction normal to the N-S interface Then the y- and z-dependent parts of the wave function are plane waves

and can be disregarded; with k, the x-component of the wave vector is meant.

The Bogoliubov equations can be simplified by noting the different length scales in it. Except for a step at the N-S interface, $\mu(x)$ is assumed to be constant. For $V(x)$, a δ−function is taken to represent the scattering of quasiparticles at the N-S interface. The effects of the discontinuity of $\mu(x)$ and of the δ−function potential can be combined in a δ−function potential with an effective height.[7] It is accounted for in the boundary conditions of the solutions in N and in S and can therefore be omitted from the differential equation. The wave function oscillates on a scale k_F^{-1}, the inverse Fermi wave vector. As $\Delta(x)$ is much smaller than $\mu(x)=\hbar^2k_F^2/(2m)$, the effects of superconductivity on the wave function are limited to small deviations of the wave vector from k_F. For an excitation with energy E, it is therefore convenient to take trial solutions $f=\bar{u}(x)\exp[\mathrm{i}\,k_Fx-\mathrm{i}\,Et/\hbar]$ and $g=\bar{v}(x)\exp[\mathrm{i}\,k_Fx-\mathrm{i}\,Et/\hbar]$, in which the functions $\bar{u}(x)$ and $\bar{v}(x)$ are assumed to vary only on a scale that is much larger than k_F^{-1}. Neglecting higher order terms, the Bogoliubov equations can be written as:

$$\frac{\partial\bar{u}}{\partial x} = \mathrm{i}\,(\pi\xi_0\Delta_\infty)^{-1}\,[E\bar{u} - \Delta(x)\bar{v}] \tag{3a}$$

$$\frac{\partial\bar{v}}{\partial x} = -\mathrm{i}\,(\pi\xi_0\Delta_\infty)^{-1}\,[E\bar{v} - \Delta(x)\bar{u}] \tag{3b}$$

The functions $\bar{u}(x)$ and $\bar{v}(x)$ vary on the scale of the BCS coherence length $\xi_0=\hbar v_F/(\pi\Delta_\infty)=\hbar^2k_F/(\pi m\Delta_\infty)$, which is indeed much larger than k_F^{-1} (Δ_∞ is the value of the pair potential in S far from the interface). If for an excitation with negative wave vector the trial functions $f=\bar{v}(x)\exp[-\mathrm{i}\,k_Fx-\mathrm{i}\,Et/\hbar]$ and $g=\bar{u}(x)\exp[-\mathrm{i}\,k_Fx-\mathrm{i}\,Et/\hbar]$ are chosen, the same equations for $\bar{u}(x)$ and $\bar{v}(x)$ are obtained. Thus the general form of the wave function in the region in which $\Delta(x)$ varies with position is:

$$\psi = \begin{bmatrix}\bar{u}_a(x)\\ \bar{v}_a(x)\end{bmatrix}e^{\mathrm{i}k_Fx} + \begin{bmatrix}\bar{v}_b(x)\\ \bar{u}_b(x)\end{bmatrix}e^{-\mathrm{i}k_Fx} \tag{4}$$

in which the two sets of functions $(\bar{u}_{a,b}(x),\bar{v}_{a,b}(x))$ are solutions of Eq. (3). If $\Delta(x)=\Delta_\infty$ is constant, the solution of Eq. (3) is:

$$\begin{bmatrix}\bar{u}(x)\\ \bar{v}(x)\end{bmatrix} = \begin{bmatrix}\sqrt{E\pm(E^2-\Delta_\infty^2)^{1/2}}\\ \sqrt{E\mp(E^2-\Delta_\infty^2)^{1/2}}\end{bmatrix}e^{\pm\mathrm{i}\varkappa_Sx} \tag{5}$$

with $\varkappa_S=(E^2-\Delta_\infty^2)^{1/2}(\pi\xi_0\Delta_\infty)^{-1}$. For later use, we define $\varkappa_N=E(\pi\xi_0\Delta_\infty)^{-1}$. The solution is valid for all energies $E>0$ and is not limited to $E>\Delta_\infty$. If the usual BCS coherence factors

$$u_0^2 = 1-v_0^2 = \frac{1}{2}\left[1 + \frac{\sqrt{E^2-\Delta_\infty^2}}{E}\right] \tag{6}$$

are defined also for all $E>0$, the general solution of the Bogoliubov equations for constant $\Delta(x)=\Delta_\infty$ is:

$$\psi = \alpha\begin{bmatrix}u_0\\v_0\end{bmatrix}e^{i(k_F+\varkappa_S)x} + \beta\begin{bmatrix}v_0\\u_0\end{bmatrix}e^{-i(k_F-\varkappa_S)x} + \gamma\begin{bmatrix}u_0\\v_0\end{bmatrix}e^{-i(k_F+\varkappa_S)x} + \delta\begin{bmatrix}v_0\\u_0\end{bmatrix}e^{i(k_F-\varkappa_S)x} \tag{7}$$

This is up to first order in $(k_F\xi_0)^{-1}$ the wave function used by BTK. Far from the interface in N ($\Delta(x)=0$), the general solution is:

$$\psi = \alpha\begin{bmatrix}1\\0\end{bmatrix}e^{i(k_F+\varkappa_N)x} + \beta\begin{bmatrix}0\\1\end{bmatrix}e^{-i(k_F-\varkappa_N)x} + \gamma\begin{bmatrix}1\\0\end{bmatrix}e^{-i(k_F+\varkappa_N)x} + \delta\begin{bmatrix}0\\1\end{bmatrix}e^{i(k_F-\varkappa_N)x} \tag{8}$$

The four terms in Eq. (8) correspond to electrons ($|k|>k_F$) and holes ($|k|<k_F$) moving in positive (α,β) and negative (γ,δ) x-direction respectively.

Although Eq. (3) is a very convenient mathematical formulation of the Bogoliubov equations, it is a physically interesting sidestep to consider a different formulation. We take as a trial solution the wave function given in Eq. (7) but we temporarily define u_0, v_0, and $\varkappa_S$ in terms of the local value of $\Delta(x)$. If this trial solution with the proper time dependence is inserted in the Bogoliubov equations (Eq. (2)), equations for the position dependence of the coefficients α, β, γ, and δ are obtained. Neglecting terms of second order in $(k_F\xi_0)^{-1}$ and expressing u_0 and v_0 in terms of $\Delta(x)$, we find:

$$\frac{\partial\alpha}{\partial x} = \frac{\partial\Delta}{\partial x}\left[\frac{\alpha\Delta - \delta E e^{-2i\varkappa' x}}{2(E^2-\Delta^2)} + \frac{i\alpha x}{\pi\xi_0\Delta_\infty}\frac{\Delta}{\sqrt{E^2-\Delta^2}}\right] \tag{9a}$$

$$\frac{\partial\delta}{\partial x} = \frac{\partial\Delta}{\partial x}\left[\frac{\delta\Delta - \alpha E e^{2i\varkappa' x}}{2(E^2-\Delta^2)} - \frac{i\delta x}{\pi\xi_0\Delta_\infty}\frac{\Delta}{\sqrt{E^2-\Delta^2}}\right] \tag{9b}$$

with $\varkappa'=[E^2-\Delta^2(x)]^{1/2}(\pi\xi_0\Delta_\infty)^{-1}$. The equations for β and γ are found by replacing α with β and δ with γ. Equation (9) clearly shows the Andreev-reflection process: If Δ varies with position, the coefficients α and δ influence each other. These are the coefficients of an electron-like quasiparticle moving in the positive x-direction (α) and a hole-like quasiparticle moving in the negative x-direction (δ). The two coefficients β and γ also influence each other but there is no coupling between the two sets of coefficients. Only the potential $V(x)$ gives rise to a coupling between the two sets that correspond to excitations with positive and negative wave vector respectively. For numerical calculations, Eq. (9) is not very convenient because it contains a singularity at $\Delta(x)=E$. The singularity is limited to the coeffi-

cients and is due to the choice of the trial function The wave function itself shows no singularity This is confirmed by the fact that the formulation of the Bogoliubov equations in Eq (3) shows no singularity

We will analyze the probabilities of reflection and transmission of a quasiparticle incident on an N-S interface that has a geometry as given in Fig 1 At the interface ($x=0$), the scattering potential $V(x)=Z(\pi\xi_0\Delta_\infty)\delta(x)$ is located and there is a discontinuity in the pair potential $\Delta^+-\Delta^-$ The parameter Z describes the strength of ordinary scattering at the interface It contains a contribution of a $\delta-$function potential and a contribution due to the discontinuity of $\mu(x)$ (i e of the difference of k_{FN} and k_{FS}) For $x>x_S$ ($\Delta(x)=\Delta_\infty$) and for $x<-x_N$ ($\Delta(x)=0$), the solution of the Bogoliubov equations is given by Eq (7) and Eq (8) respectively Like BTK, we are interested in the situation with a single incoming electron wave in N and we would like to calculate the coefficients of the outgoing reflected electron and hole waves in N and the coefficients of the outgoing transmitted electron-like and hole-like waves in S These coefficients are defined for $x<-x_N$ and $x>x_S$ respectively and the corresponding wave functions have to be matched via a numerical solution of Eq (3) in the region $-x_N<x<x_S$ This means for instance that there is no incoming hole wave at $x=-x_N$ in N and that there are no incoming waves at $x=x_S$ in S These boundary conditions are not very suitable for a numerical solution because they apply at two different positions Therefore we choose the initial values of the coefficients of the outgoing waves at $x=x_S$ and integrate back to $x=-x_N$ If this is done for two independent sets of initial values, the relevant coefficients can be deduced (details are given in the Appendix) The result is the probability currents $A(E)$, $B(E)$, $C(E)$, and $D(E)$ ($A+B+C+D=1$) that correspond to a quasiparticle with energy E that is incident on the N-S interface $A(E)$ and $B(E)$ are related to Andreev-reflection and ordinary reflection processes respectively while $C(E)$ and $D(E)$ denote transmission without and with change in character (electron-like or hole-like) of the quasiparticle

Geometrical resonances are calculated for the geometry of Fig 2 The tunnel junction is represented by a (very high) $\delta-$function potential at $x=-x_T$ For simplicity, the $\delta-$function potential at the N-S interface is omitted The quantity of interest is the transmission of electrical current T, which is given by[2] $T(E)=1-B(E)+A(E)$ This function can be calculated in a similar way as the probability currents for the N-S interface of Fig 1 Only the boundary conditions have to be adapted because the geometry is different (details are given in the Appendix)

Negative values of $\Delta(x)$ in N can be directly inserted in Eq (3) In fact, if $(\tilde{u}(x),\tilde{v}(x))$ is a solution of Eq (3) with $\Delta(x)$, then $(\tilde{u}(x),-\tilde{v}(x))$ is the solution with $-\Delta(x)$ Often the phase of the wave function is not relevant but in the application of boundary conditions it will make a difference It will therefore be interesting to calculate the probability of Andreev reflection and the geometrical resonance effects also for $\Delta(x)<0$ in N

III Probability of Andreev reflection

Independent of the exact form of $\Delta(x)$, some observations can be made about the values of the probabilities of reflection $A(E)$ and $B(E)$, and of transmission $C(E)$ and $D(E)$ (proofs are given in the Appendix). The probabilities $C(E)$ and $D(E)$ are zero for $E<\Delta_\infty$, while, if $Z=0$, the probabilities B and D are zero for all E. If $\Delta(x)$ changes on a scale that is small compared to ξ_0, the BTK results are reproduced. We calculate the values of the probabilities for the geometry given in Fig. 1. The shape of $\Delta(x)$ is assumed to be parabolic with zero slope at $x=-x_N$ and $x=x_S$. For another shape of $\Delta(x)$, practically the same results are obtained as long as the effective length over which $\Delta(x)$ varies with position and the values of Δ^+ and Δ^- are the same. We take a small δ–function potential at the N-S interface ($Z=0.3$) and we set $2x_N/(\pi\xi_0)=2x_S/(\pi\xi_0)=3$. The probability of Andreev reflection is given in Fig. 3 as a function of energy for three sets of values (Δ^+,Δ^-). The curves for the other probabilities are omitted for clarity. For $E<\Delta_\infty$, $C=D=0$ and $B=1-A$. For $E>\Delta_\infty$, D tends to zero on the same scale as A, while B and C tend to their high-energy values $1-B=C=(1+Z^2)^{-1}$. The results for $A(E)$ are compared to the BTK result (the dashed lines in Fig. 3). The fact that $A\neq 0$ for $E>\Delta_\infty$ is a standard result of the quantum mechanics of a sharp potential step. If the potential rises more gradually, A becomes smaller. For $E<\Delta_\infty$, the effects of $\Delta^-\neq 0$ and $\Delta^+\neq\Delta_\infty$ are largest for low and higher energies respectively. In the curve for $\Delta^-=0.4\Delta_\infty$ and $\Delta^+=\Delta_\infty$, the influence of the δ–function potential at $x=0$ is smaller for low quasiparticle energy. This can be understood by realizing that, for $E<\Delta(x)$, the functions $\bar{u}$ and $\bar{v}$ are exponentially damped, so that the value of the wave function at $x=0$ is small. The maximum of A in the curve for $\Delta^-=0$ and $\Delta^+=0.6\Delta_\infty$ is due to a geometrical resonance effect. For $E>\Delta^+$, it is possible that for a specific energy, the incoming electron wave and the Andreev-reflected hole wave are both zero at $x=0$. Then the δ–function potential has no influence at all and A equals unity. In the curve for $\Delta^-=\Delta^+=0.5\Delta_\infty$, both effects are present.

IV Geometrical resonance effects

Geometrical resonances occur for instance in the geometry of Fig. 2. They are due to interference effects of the wave functions of quasiparticles that feel a pair-potential step on one side of the N slab and an ordinary potential on the other side. The resonances manifest themselves as sharp peaks or as oscillations in the differential conductance (or transmission) of the tunnel junction at $x=-x_T$. The geometrical resonance effects can be calculated in two different ways that correspond to two different interpretations. The usual interpretation is that the differential conductance of the tunnel junction measures the density of states of the excitations in the normal-metal slab backed by a superconductor. The density of states is obtained from the Bogoliubov equations (with a step-function for $\Delta(x)$) using Green's

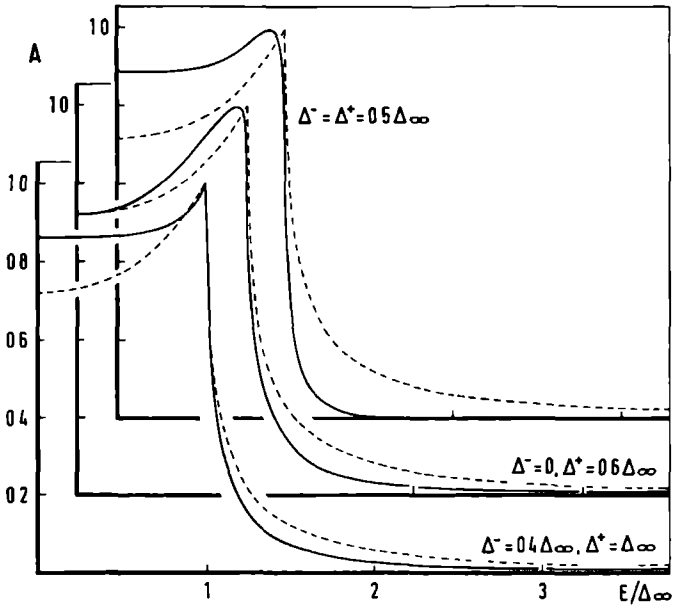

Fig 3 Energy dependence of the probability of Andreev reflection of a quasiparticle incident on the N-S interface of Fig 1 for three sets of (Δ^+,Δ^-) values The parameter $Z=0\,3$, while $2x_S/(\pi\xi_0)=2x_N/(\pi\xi_0)=3$ The dashed line is the BTK result for $Z=0\,3$

functions techniques [4 5] For $E<\Delta_\infty$, the probability of Andreev reflection is unity and "bound states" of the quasiparticles are found at specific energy values For $E>\Delta_\infty$, the density of states shows maxima that are due to "quasi-bound states" A completely different approach is to calculate the transmission T of electrical current of the complete structure of Fig 2 Such a calculation has already been done analytically, for arbitrary Z and for a step-like variation of $\Delta(x)$, by Hahn[8] as an extension of the calculations of BTK In the Appendix, T/T_0 is given in the limit of large Z ($T_0=(1+Z^2)^{-1}$ is the transmission coefficient of the tunnel junction if no superconductor is present) This result is identical to the result of the density-of-states approach The sharp peaks in the transmission for specific energies $E<\Delta_\infty$ are due to the fact that, for those energies, $A=1$ and $B=0$, so $T=2$ independent of the value of Z This can be understood by realizing that, for specific energies, it is possible to have a solution of the Bogoliubov equations with an incident electron wave function and an Andreev-reflected hole wave function that both are zero at $x=-x_T$ Such a

solution is not influenced by a δ-function potential at that point

Although the two interpretations are completely different, in the limit of a step-function for $\Delta(x)$, the results are identical However, effects of a gradual variation of $\Delta(x)$ near the N-S interface are calculated more easily using the transmission approach We calculate the transmission of the structure of Fig 2 in the limit of large Z for $2x_N/(\pi\xi_0)=2x_S/(\pi\xi_0)=3$ and $2x_T/(\pi\xi_0)=4$ We omit the δ-function potential at $x=0$ because the combination of two such potentials leads to oscillations on a very small energy scale due to interference effects of the $\exp[ik_F x]$-parts of the wave functions This effect makes the numerical calculation much more complicated Moreover, in a real sample, the thickness is not constant on the scale of k_F^{-1}, so results for several thicknesses have to be averaged, which makes the small-scale oscillations disappear again To avoid these complications, we limit ourselves to a single δ-function potential at $x=-x_T$ In experiments, the most left N layer in Fig 2 is often replaced with an S layer because the peak in the density of quasiparticle states in a superconductor reduces the effect of thermal smearing Because of the tunnel barrier at $x=-x_T$, the geometrical resonance effects are hardly influenced by the nature of the top layer We take a top N layer because then the calculation is simpler.

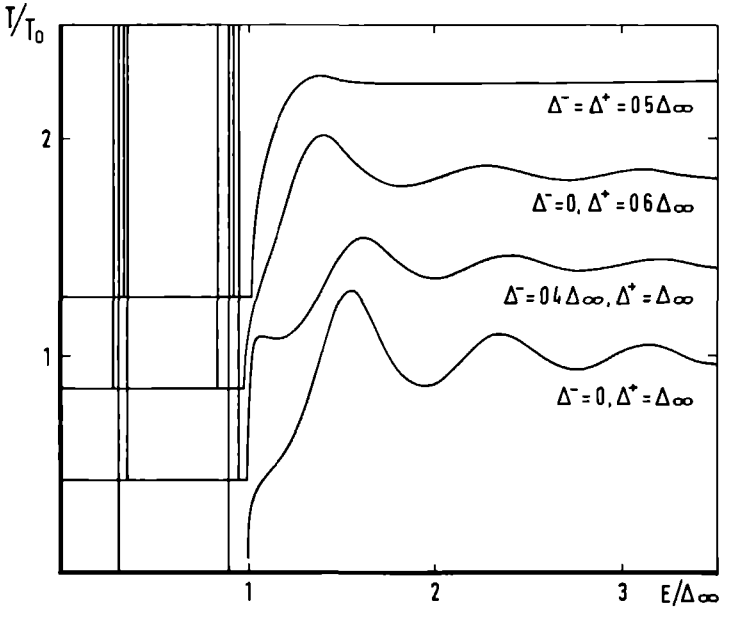

Fig 4 Energy dependence of the normalized transmission coefficient of the tunnel junction of Fig 2 for four sets of (Δ^+,Δ^-) values The vertical lines for $E<\Delta_\infty$ correspond to the singularities of T/T_0 Z is assumed to be infinite, while $2x_S/(\pi\xi_0)=2x_N/(\pi\xi_0)=3$ and $2x_T/(\pi\xi_0)=4$

The results of the calculation for four sets of (Δ^+,Δ^-)-values (including a step-like $\Delta(x)$) are given in Fig 4 For $E \gg \Delta_\infty$, the amplitude of the oscillations scales with the discontinuity $(\Delta^+ - \Delta^-)$ at the interface For energies only slightly larger than Δ_∞, the amplitude is also influenced by the shift of the maxima For $E < \Delta_\infty$, the positions of the peaks have shifted too These energy shifts can be related to phase shifts of the wave function The shifts to higher energies of the maxima in the curve for $\Delta^- = 0\,4\Delta_\infty$ and $\Delta^+ = \Delta_\infty$, are due to the fact that the effective thickness of the N slab is smaller in this case than for a step-like variation of $\Delta(x)$

V Negative pair potential

In the BCS theory of superconductivity, the effective electron-electron interaction between electrons with opposite momentum and spin is represented by a single potential $-V_{BCS}$ For $V_{BCS} > 0$ (attractive interaction), a superconducting ground state of the electrons is found, while, for $V_{BCS} < 0$, $\Delta = 0$ is the only solution As the effective electron-electron interaction is the sum of an attractive phonon-mediated interaction and the repulsive Coulomb interaction, it may be negative in metals that do not show superconductivity even at very low temperatures At an N-S interface, the superconductor in general induces a pair amplitude of the electrons in N If in N $V_{BCS} < 0$, then the pair potential, which is the product of the pair amplitude and V_{BCS}, will be negative However, N also influences S and the position dependence of $\Delta(x)$ should in principle be calculated self-consistently Possibly, the large negative value of Δ^- that we assume in our calculation does not occur in such a self-consistent calculation

In Fig 5, results are given for the probability of Andreev reflection and for the geometrical resonance effects for a negative tail of $\Delta(x)$ in N ($\Delta^- = -0\,4\Delta_\infty$, $\Delta^+ = 0\,6\Delta_\infty$) Figure 5(b) is very similar to the previous results for positive $\Delta(x)$ in N The positions of the maxima are shifted somewhat in energy and the amplitude of the oscillations for $E > \Delta_\infty$ scales with the discontinuity in Δ at the interface (and apparently not with the discontinuity of $|\Delta|$ as also might have been expected) The probability of Andreev reflection shown in Fig 5(a) confirms the observation that the discontinuity of Δ rather than of $|\Delta|$ is important because, for $E > \Delta_\infty$, the curve is almost equal to the BTK result For $E < \Delta_\infty$, the probability of Andreev reflection differs strongly from the results for positive $\Delta(x)$ in N The influence of the δ-function potential is enhanced rather than diminished while, for large enough values of Z, A even becomes zero (B then equals 1) This can not be due to a geometrical resonance effect because in the region beyond the point where $|\Delta(x)| = E$ in N, the functions $\bar{u}(x)$ and $\bar{v}(x)$ are not oscillating Possibly, the contributions to the Andreev-reflected wave due to the decrease of Δ in N and due to the increase of Δ at the interface and in S partly or completely compensate each other

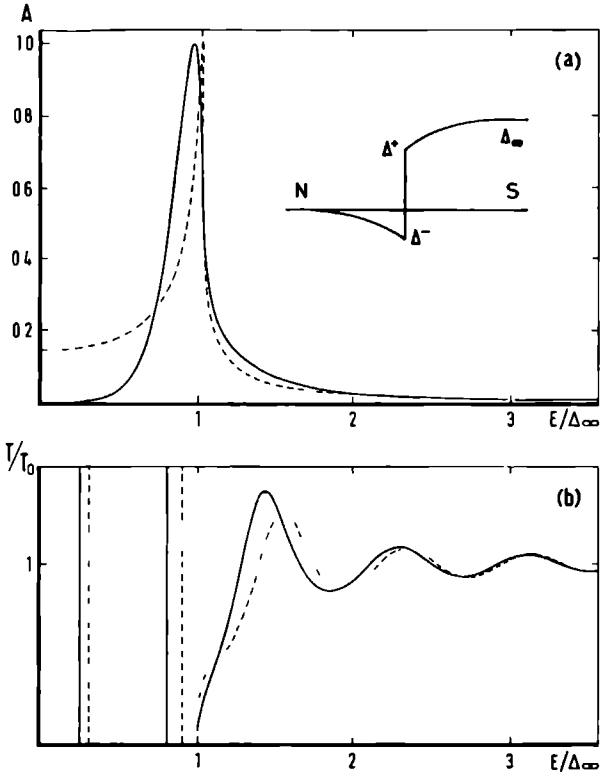

Fig 5 (a) Energy dependence of the probability of Andreev reflection of a quasiparticle incident on the N-S interface of Fig 1 for $\Delta^- = -0\,4\Delta_\infty$ and $\Delta^+ = 0\,6\Delta_\infty$ The parameter $Z = 0\,9$, while $2x_S/(\pi\xi_0) = 2x_N/(\pi\xi_0) = 3$ The dashed line is the BTK result for $Z = 0\,9$ The inset shows the position dependence of Δ near the interface (b) Energy dependence of the normalized transmission coefficient of the tunnel junction of Fig 2 for $\Delta^- = -0\,4\Delta_\infty$ and $\Delta^+ = 0\,6\Delta_\infty$ The parameter Z of the tunnel junction is assumed to be infinite, while $2x_S/(\pi\xi_0) = 2x_N/(\pi\xi_0) = 3$ and $2x_T/(\pi\xi_0) = 4$

VI Conclusion

We showed that the probabilities of reflection and transmission of a quasiparticle incident on an N-S interface with a gradually changing pair potential can be calculated by numerically solving the Bogoliubov equations near the interface and by applying appropriate boundary conditions This method can also be applied to find the geometrical resonance effects in the transmission of a tunnel junction on an N-S bilayer For a step-like variation of the pair potential at the N-S interface, the results of the usual density-of-states calculations

are reproduced. However, the influence of a gradual variation of the pair potential is calculated more easily with the method described in this paper. Both the probability of Andreev reflection and the geometrical resonance effects begin to change if the region in which the pair potential varies with position becomes of the order of the coherence length of the superconductor. As the pair potential usually varies on this scale, the influence of that variation should be taken into account in a careful comparison of theory and experiment.

Acknowledgment

We would like to thank Dr. G. Schön for valuable comments. Part of this work is supported by the Stichting voor Fundamenteel Onderzoek der Materie (FOM), which is financially supported by the Nederlandse Organisatie voor Zuiver Wetenschappelijk Onderzoek (ZWO).

Appendix

In order to obtain the probabilities of reflection and transmission of an incoming quasiparticle from the numerical solution of the Bogoliubov equations (Eq. (3)), appropriate boundary conditions have to be applied. The integration is performed from $x=x_S$ to $x=-x_N$ (see Fig. 1) for two independent sets of initial values at $x=x_S$ that only contain outgoing quasiparticles. From the two solutions (denoted with the indices 1 and 2), the probabilities of reflection and transmission of a quasiparticle incident in N can be reconstructed. For $x \geq x_S$, the general solution is given in Eq. (7); we choose the two independent solutions:

$$\psi_1 = \begin{bmatrix} u_0 \\ v_0 \end{bmatrix} e^{\imath(k_F+\varkappa_S)x} \quad , \quad \psi_2 = \begin{bmatrix} v_0 \\ u_0 \end{bmatrix} e^{-\imath(k_F-\varkappa_S)x} \tag{A1}$$

For $-x_N \leq x \leq x_S$, the wave function is of the form:

$$\psi_j = \begin{bmatrix} \tilde{u}_{a_j}(x) \\ \tilde{v}_{a_j}(x) \end{bmatrix} e^{\imath k_F x} + \begin{bmatrix} \tilde{v}_{b_j}(x) \\ \tilde{u}_{b_j}(x) \end{bmatrix} e^{-\imath k_F x} \tag{A2}$$

in which the four sets of functions $(\tilde{u}_{a_j}(x),\tilde{v}_{a_j}(x))$ and $(\tilde{u}_{b_j}(x),\tilde{v}_{b_j}(x))$ $(j=1,2)$ are solutions of Eq. (3). The boundary conditions at $x=x_S$ demand that ψ and $\partial\psi/\partial x$ are continuous. In the latter condition, terms that are proportional to $\partial\tilde{u}/\partial x$, $\partial\tilde{v}/\partial x$, and $\varkappa_S$ may be neglected with respect to terms proportional to k_F (except in the exponent). Then the initial conditions of the numerical integration are:

$$\bar{u}_{a1}(x_S)=\bar{u}_{b2}(x_S)=u_0 e^{i\kappa_S x_S} \quad , \quad \bar{v}_{a1}(x_S)=\bar{v}_{b2}(x_S)=v_0 e^{i\kappa_S x_S} \tag{A3a}$$

$$\bar{u}_{b1}(x_S)=\bar{u}_{a2}(x_S)=0 \quad , \quad \bar{v}_{b1}(x_S)=\bar{v}_{a2}(x_S)=0 \tag{A3b}$$

Only a single integration of Eq. (3) has to be performed from $x=x_S$ to $x=0$ because two sets of functions are equal to zero (the differential equation is homogeneous) and the other two sets are identical.

The potential $V(x)=Z(\pi\xi_0\Delta_\infty)\delta(x)$ is taken into account via the boundary conditions at $x=0$ (indices + and − indicate the values of the functions for $x \downarrow 0$ and $x \uparrow 0$ respectively):

$$\psi^+ = \psi^- \tag{A4a}$$

$$(\partial\psi^+/\partial x) - (\partial\psi^-/\partial x) = 2k_F Z\psi^+ \tag{A4b}$$

The wave function ψ is given in Eq. (A2). The boundary conditions are simplified by realizing that $\bar{u}_{b2}^+=\bar{u}_{a1}^+$, $\bar{v}_{b2}^+=\bar{v}_{a1}^+$, and that the other functions are zero. If we again neglect terms proportional to $\partial\bar{u}/\partial x$ and $\partial\bar{v}/\partial x$ in Eq. (A4b), we find as initial conditions for the integration for $x \leqslant 0$:

$$\bar{u}_{a1}^- = (1+iZ)\bar{u}_{a1}^+ \quad , \quad \bar{v}_{a1}^- = (1+iZ)\bar{v}_{a1}^+ \quad , \quad \bar{u}_{b1}^- = -iZ\bar{v}_{a1}^+ \quad , \quad \bar{v}_{b1}^- = -iZ\bar{u}_{a1}^+ \tag{A5a}$$

$$\bar{u}_{a2}^- = iZ\bar{v}_{a1}^+ \quad , \quad \bar{v}_{a2}^- = iZ\bar{u}_{a1}^+ \quad , \quad \bar{u}_{b2}^- = (1-iZ)\bar{u}_{a1}^+ \quad , \quad \bar{v}_{b2}^- = (1-iZ)\bar{v}_{a1}^+ \tag{A5b}$$

Because the differential equation, Eq. (3), is homogeneous, common prefactors of $\bar{u}$ and $\bar{v}$ may be split off. This means that for $-x_N \leqslant x \leqslant 0$, the two solutions for the wave function can be written:

$$\psi_1 = (1+iZ)\begin{bmatrix}\bar{u}_{a0}(x)\\ \bar{v}_{a0}(x)\end{bmatrix}e^{ik_F x} - iZ\begin{bmatrix}\bar{v}_{b0}(x)\\ \bar{u}_{b0}(x)\end{bmatrix}e^{-ik_F x} \tag{A6a}$$

$$\psi_2 = iZ\begin{bmatrix}\bar{u}_{b0}(x)\\ \bar{v}_{b0}(x)\end{bmatrix}e^{ik_F x} + (1-iZ)\begin{bmatrix}\bar{v}_{a0}(x)\\ \bar{u}_{a0}(x)\end{bmatrix}e^{-ik_F x} \tag{A6b}$$

The sets of functions $(\bar{u}_{a0}(x),\bar{v}_{a0}(x))$ and $(\bar{u}_{b0}(x),\bar{v}_{b0}(x))$ are two solutions of Eq. (3) with initial conditions $\bar{u}_{a0}^-=\bar{u}_{a1}^+$, $\bar{v}_{a0}^-=\bar{v}_{a1}^+$, and $\bar{u}_{b0}^-=\bar{v}_{a1}^+$, $\bar{v}_{b0}^-=\bar{u}_{a1}^+$ respectively. In Eq. (6), it is clear that only if $Z\neq 0$, wave functions with positive and negative wave vector get mixed.

For $x \leqslant -x_N$, the general solution for the wave function is in principle given by Eq (8). The solutions ψ_1 and ψ_2 we started with in Eq. (A1), correspond to a single outgoing

electron-like quasiparticle and to a single outgoing hole-like quasiparticle respectively. Such solutions have to correspond in N to mixtures of incoming electron and hole wave functions with their respective reflected waves. Therefore, for $x \leqslant -x_N$, the wave function is written as:

$$\psi_j = \nu_j \left\{ \begin{bmatrix} 1 \\ 0 \end{bmatrix} e^{i(k_F + \varkappa_N)x} + a_e \begin{bmatrix} 0 \\ 1 \end{bmatrix} e^{i(k_F - \varkappa_N)x} + b_e \begin{bmatrix} 1 \\ 0 \end{bmatrix} e^{-i(k_F + \varkappa_N)x} \right\}$$

$$+ \eta_j \left\{ \begin{bmatrix} 0 \\ 1 \end{bmatrix} e^{-i(k_F - \varkappa_N)x} + a_h \begin{bmatrix} 1 \\ 0 \end{bmatrix} e^{-i(k_F + \varkappa_N)x} + b_h \begin{bmatrix} 0 \\ 1 \end{bmatrix} e^{i(k_F - \varkappa_N)x} \right\} \tag{A7}$$

The coefficients a_e and b_e are the amplitudes of the Andreev-reflected wave and the ordinarily reflected wave respectively for an incident electron wave with amplitude 1. The coefficients a_h and b_h are in magnitude equal to a_e and b_e respectively but may differ in the phase factor. By applying the boundary conditions at $x = -x_N$ (namely continuity of ψ and of $\partial\psi/\partial x$), the coefficients $a_{e,h}$ and $b_{e,h}$ can be expressed in the solutions of the numerical integration $\bar{u}_{a0}(-x_N) = \bar{u}_a$, $\bar{v}_{a0}(-x_N) = \bar{v}_a$, $\bar{u}_{b0}(-x_N) = \bar{u}_b$, and $\bar{v}_{b0}(-x_N) = \bar{v}_b$. The result is:

$$a_e = \frac{(1+Z^2)\bar{u}_a\bar{v}_a - Z^2\bar{u}_b\bar{v}_b}{(1+Z^2)\bar{u}_a^2 - Z^2\bar{u}_b^2} e^{-2i\varkappa_N x_N} \tag{A8a}$$

$$b_e = \frac{iZ(1-iZ)(\bar{u}_b\bar{v}_a - \bar{u}_a\bar{v}_b)}{(1+Z^2)\bar{u}_a^2 - Z^2\bar{u}_b^2} e^{-2i\varkappa_N x_N} \tag{A8b}$$

while $a_h = a_e$ and $b_h = -b_e(1+iZ)/(1-iZ)$. The amplitudes of the transmitted waves corresponding to a single incident electron wave (c_e and d_e) or corresponding to a single incident hole wave (c_h and d_h) can be deduced by writing for $x \geqslant x_S$:

$$\psi_j = \nu_j \left\{ c_e \begin{bmatrix} u_0 \\ v_0 \end{bmatrix} e^{i(k_F + \varkappa_S)x} + d_e \begin{bmatrix} v_0 \\ u_0 \end{bmatrix} e^{-i(k_F - \varkappa_S)x} \right\}$$

$$+ \eta_j \left\{ c_h \begin{bmatrix} v_0 \\ u_0 \end{bmatrix} e^{-i(k_F - \varkappa_S)x} + d_h \begin{bmatrix} u_0 \\ v_0 \end{bmatrix} e^{i(k_F + \varkappa_S)x} \right\} \tag{A9}$$

These ψ_j should be equal to the wave functions we started with in Eq. (A1). The coefficients ν_j and η_j are known from the foregoing calculation, so the amplitudes $c_{e,h}$ and $d_{e,h}$ can be determined:

$$c_e = \frac{(1-iZ)\bar{u}_a}{(1+Z^2)\bar{u}_a^2 - Z^2\bar{u}_b^2} e^{-i\varkappa_N x_N} \tag{A10a}$$

$$d_e = \frac{iZ\bar{u}_b}{(1+Z^2)\bar{u}_a^2 - Z^2\bar{u}_b^2} e^{-i\varkappa_N x_N} \tag{A10b}$$

while $c_h = c_e(1+iZ)/(1-iZ)$ and $d_h = -d_e$. Following BTK, we define probability currents A, B, C, and D for the various wave-function components. These are given by $A = |a_{e,h}|^2$, $B = |b_{e,h}|^2$, $C = |c_{e,h}|^2(|u_0|^2 - |v_0|^2)$, and $D = |d_{e,h}|^2(|u_0|^2 - |v_0|^2)$. If the region near the N-S interface in which $\Delta(x)$ is not constant is much smaller than ξ_0, the integration of Eq. (3) over this region hardly changes $\bar{u}$ and $\bar{v}$. It can easily be shown that then $\bar{u}_a = \bar{v}_b = u_0 \exp[i\varkappa_S x_S]$ and $\bar{v}_a = \bar{u}_b = v_0 \exp[i\varkappa_S x_S]$. As $\varkappa_S x_S$ and $\varkappa_N x_N$ are very small in this limit, Eqs. (A8) and (A10) reduce to the BTK results. So deviations from the BTK results are only to be expected if $\Delta(x)$ varies on the scale of ξ_0. Two observations of BTK can be shown to hold also for this more general situation. First, if $Z=0$, there is no ordinary reflection and no transmission with change of character of the quasiparticle ($B=D=0$). Secondly, if $E<\Delta_\infty$, u_0 and v_0 are complex conjugates, so $C=D=0$. If also $Z=0$, $B=0$ and A necessarily equals 1. This also follows from the calculation because the initial values of $\bar{u}$ and $\bar{v}$ are complex conjugates (note that for $E<\Delta_\infty$, $\varkappa_S$ in Eq. (A3a) is imaginary). Then during integration of Eq. (3), the functions remain complex conjugate and, for $Z=0$, $A = |(\bar{v}_a/\bar{u}_a)\exp[-2i\varkappa_N x_N]|^2 = 1$.

To calculate the geometrical resonance effects, the foregoing discussion has to be adapted only slightly. The geometry is given in Fig. 2. The tunnel junction is represented by a δ-function potential with very large Z at $x=-x_T$, while at the N-S interface no barrier is assumed to be present to avoid interference effects due to the $\exp[ik_F x]$-parts of the wave functions. The quantity to be calculated is the transmission coefficient T of the whole geometry. That will be very low but it should be scaled with $T_0=(1+Z^2)^{-1}$, the transmission coefficient if no superconductor is present. If the charge current is evaluated at $x<-x_T$ in N, T is given by $T=1-B+A$. Because there is no δ-function potential at the N-S interface, the two solutions given by Eq. (A2) can be evaluated all the way to $x=-x_N$. The result is two numbers $\bar{u}_{a1}(-x_N)=\bar{u}_{b2}(-x_N)=\bar{u}_a$ and $\bar{v}_{a1}(-x_N)=\bar{v}_{b2}(-x_N)=\bar{v}_a$; the other four functions are identically zero. For $-x_T \leqslant x \leqslant -x_N$, the solutions are given by Eq. (8), with the coefficients being determined by the boundary conditions at $x=-x_N$:

$$\psi_1 = \bar{u}_a e^{i\varkappa_N x_N} \begin{bmatrix} 1 \\ 0 \end{bmatrix} e^{i(k_F+\varkappa_N)x} + \bar{v}_a e^{-i\varkappa_N x_N} \begin{bmatrix} 0 \\ 1 \end{bmatrix} e^{i(k_F-\varkappa_N)x} \tag{A11a}$$

$$\psi_2 = \bar{u}_a e^{i\varkappa_N x_N}\begin{bmatrix}0\\1\end{bmatrix}e^{-i(k_F-\varkappa_N)x} + \bar{v}_a e^{-i\varkappa_N x_N}\begin{bmatrix}1\\0\end{bmatrix}e^{-i(k_F+\varkappa_N)x} \tag{A11b}$$

Now, for $x \leqslant -x_T$, the wave functions of Eq. (A7) are chosen and, at $x=x_T$, they are matched to the above solutions using the boundary conditions of Eq. (A4). The results for the coefficients $a_{e,h}$ and $b_{e,h}$ are:

$$a_e = \frac{\bar{u}_a \bar{v}_a e^{-2i\varkappa_N x_N}}{\bar{u}_a^2 + Z^2[\bar{u}_a^2 - \bar{v}_a^2 e^{4i\varkappa_N(x_T-x_N)}]} \tag{A12a}$$

$$b_e = \frac{-iZ(1-iZ)[\bar{u}_a^2 - \bar{v}_a^2 e^{4i\varkappa_N(x_T-x_N)}]}{\bar{u}_a^2 + Z^2[\bar{u}_a^2 - \bar{v}_a^2 e^{4i\varkappa_N(x_T-x_N)}]} e^{-2i(k_F+\varkappa_N)x_T} \tag{A12b}$$

while $a_h = a_e$ and $b_h = -b_e \exp[4ik_F x_T](1+iZ)/(1-iZ)$. In the limit of very large Z, the normalized transmission coefficient T/T_0 of the tunnel junction is given by:

$$\frac{T}{T_0} = 1 + 2\mathrm{Re}\left[\frac{\bar{v}_a^2 e^{4i\varkappa_N(x_T-x_N)}}{\bar{u}_a^2 - \bar{v}_a^2 e^{4i\varkappa_N(x_T-x_N)}}\right]$$

$$= \mathrm{Re}\left[\frac{\bar{u}_a^2 e^{-2i\varkappa_N(x_T-x_N)} + \bar{v}_a^2 e^{2i\varkappa_N(x_T-x_N)}}{\bar{u}_a^2 e^{-2i\varkappa_N(x_T-x_N)} - \bar{v}_a^2 e^{2i\varkappa_N(x_T-x_N)}}\right] \tag{A13}$$

The latter expression for T/T_0 is most suitable to discuss the energy range $E<\Delta_\infty$. As has been discussed before, for those energies, $\bar{u}_a$ and $\bar{v}_a$ are complex conjugates. Then the numerator is real while the denominator is purely imaginary. This means that T/T_0 equals zero except if the denominator is zero, which is the case if the phase factors obey:

$$\tan[2\varkappa_N(x_T-x_N)] = \mathrm{Im}(\bar{u}_a^2)/\mathrm{Re}(\bar{u}_a^2) \tag{A14}$$

For specific values of the energy of the quasiparticles, this condition may be fulfilled and T/T_0 diverges. From Eq. (A12) it follows that, for these energies, $B=0$ and $A=1$, so $T=2$ independent of the height of the tunnel barrier. This can be understood by realizing that, for specific values of the phase of the coefficient a_e, it will be possible to have an incident electron wave function and an Andreev-reflected hole wave function that both are zero at $x=-x_T$. Such a wave function is not influenced by the presence of a δ-function potential at that point (note that there is no δ-function potential at the N-S interface).

If at the N-S interface, the pair potential $\Delta(x)$ varies only on a scale that is much smaller than ξ_0, no numeric integration has to be performed. The solution is then given by $\bar{u}_a = u_0$ and $\bar{v}_a = v_0$, while $\varkappa_N x_N = \varkappa_S x_S = 0$. Most other calculations of geometrical resonance

effects assume such a step-like variation of $\Delta(x)$. The condition for the peaks of T/T_0 for $E<\Delta_\infty$, Eq. (A14), then is:

$$\tan(2\varkappa_N x_T) = \frac{\sqrt{\Delta_\infty^2 - E^2}}{E} \tag{A15}$$

This is exactly the condition that has already been found by de Gennes and Saint-James.[9] The expression for T/T_0, Eq. (A13), reduces to:

$$\frac{T}{T_0} = 1 + 2\mathrm{Re}\left[\frac{v_0^2 e^{4i\varkappa_N x_T}}{u_0^2 - v_0^2 e^{4i\varkappa_N x_T}}\right] \tag{A16}$$

This expression has also been obtained by calculating the density of states of the normal-metal slab using Green's functions to solve the Bogoliubov equations.[4,5] So in the limit of a step-like variation of $\Delta(x)$, the two methods yield identical results.

References

[1] A. F. Andreev, Zh. Eksp. Teor. Fiz. **46**, 1823 (1964) [Sov. Phys.-JETP **19**, 1228 (1964)].

[2] G. E. Blonder, M. Tinkham, and T. M. Klapwijk, Phys. Rev. **B25**, 4515 (1982).

[3] P. G. de Gennes, Superconductivity of Metals and Alloys (Benjamin, New York, 1966).

[4] P. Nédellec, Ann. Phys. (Paris) **2**, 253 (1977).

[5] Gerald B. Arnold, Phys. Rev. **B18**, 1076 (1978).

[6] M. Tinkham, Introduction to Superconductivity (McGraw-Hill, New York, 1975).

[7] G. E. Blonder and M. Tinkham, Phys. Rev. **B27**, 112 (1983).

[8] Artur Hahn, Phys. Rev. **B31**, 2816 (1985).

[9] P. G. de Gennes and D. Saint-James, Phys. Lett. **4**, 151 (1963).

Chapter 3.3

NEW METHOD TO STUDY THE PROXIMITY EFFECT AT THE NORMAL-METAL-SUPERCONDUCTOR INTERFACE

P. C. van Son,[a] H. van Kempen,[a] and P. Wyder[a,b]

[a] Research Institute for Materials, University of Nijmegen, Toernooiveld, NL-6525 ED Nijmegen, The Netherlands

[b] Max-Planck-Institut fur Festkörperforschung, Hochfeld-Magnetlabor, 166X, F-38042 Grenoble Cedex, France

The excess current of a point contact on a Ag-Pb bilayer has been measured for several thicknesses of the Ag film. The excess current is due to Andreev reflection and contains information about the position dependence of the superconducting order parameter near the interface. If the Ag film is very thin, the excess current is that of a normal-metal-superconductor point contact, though slightly changed due to the depression of the order parameter at the surface of the bilayer. For larger thicknesses, the combination of the proximity effect and the limited mean free path of the electrons yields very different current-voltage characteristics.

PACS number: 74.50+r

If a normal metal N is in good electrical contact with a superconductor S, the Cooper pairs of S leak into N and the pair amplitude varies gradually with position near the N-S interface The length scale of this proximity effect[1] is determined by the coherence length, which is typically of the order of 0 1 μm The pair potential Δ is the product of the pair amplitude and the BCS coupling constant, which is smaller in N than in S The position dependence of Δ near the N-S interface is shown schematically in Fig 1 Experimentally, the proximity effect can be studied for instance by measuring the screening properties of an N-S bilayer in a magnetic field [1,2] Another approach employs a tunnel junction on the N side of an N-S bilayer [1,3] If the N layer is thin compared to the coherence length, the pair potential at the tunnel-junction interface in N is finite and this is reflected in the differential resistance of the junction

We employed a point contact on the N side of an N-S bilayer to study the probability of Andreev reflection[4] of quasiparticles incident on an N-S interface like that in Fig 1 An electron at an N-S interface in N can condense into a Cooper pair together with a second electron from N with opposite momentum and spin The hole (or missing electron) that is created in N moves back in the direction from which the incident electron came (retroreflection) If it returns through the point contact, the hole gives rise to an excess current that can be measured The Andreev-reflection process has been studied both theoretically[5] and experimentally[6] for N-S point contacts Then however, the order parameter varies on the scale of the point-contact diameter, which is much smaller than the coherence length Therefore, in Ref 5 a step-function was used for the position dependence of Δ The theory has been extended to include a gradual variation of Δ near the N-S interface and then yields slightly different results for the probability of Andreev reflection [7] Measurements have been done of the excess current of a point contact on a Ag single-crystal backed by a Pb film [8] In these samples, the thickness of the N layer (200 μm and 20 μm respectively) was much larger than the coherence length and the influence of the proximity effect in these experiments was small compared to that of other effects Here, we present measurements on thin-film Ag-Pb bilayers, which show features that can be related to the influence

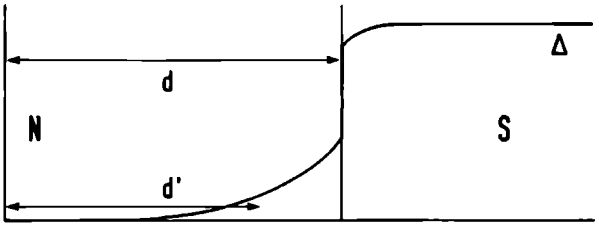

Fig 1 Position dependence of Δ near an N-S interface The thickness of the N layer is d while d' is an effective thickness of the non-superconducting layer

of the proximity effect on the probability of Andreev reflection Two regimes can be distinguished that are characterized by the ratio of the mean free path of the electrons and the thickness of the Ag layer

The theory[5-7] yields the probability of Andreev reflection A of an electron incident on an N-S interface as a function of its energy E (relative to the Fermi energy) If E is smaller than the pair potential Δ in the superconductor, A equals unity For $E>\Delta$, the electron can be transmitted into the superconductor as an excitation but there is still a small probability of Andreev reflection The value of A is smaller as the variation of Δ at the interface is smoother The incident electron can also be ordinarily reflected at the N-S interface due to impurities or due to the discontinuity of the Fermi wave vector In the theory, these effects are modeled with a $\delta-$function potential barrier at the N-S interface with a height that is proportional to a parameter Z, for $Z\neq 0$, A is no longer unity for $E<\Delta$ However, if Δ extends sufficiently far in N, the influence of the potential barrier is small, especially for electrons with low energies [7]

The diameter of the point contact on the N-S bilayer is much smaller than the electron mean free path (Sharvin junction[9]) The electrons do not scatter close to the contact and they are injected in all directions with energies between 0 and eV (V is the voltage across the point contact) At the N-S interface, the electrons are transmitted, ordinarily reflected or Andreev reflected respectively If the thickness of the N layer is large compared to the point-contact diameter, only the Andreev-reflected holes return through the point contact Only the Andreev-reflection process namely gives rise to retroreflection The excess current due to the holes is measured as a decrease of the point-contact resistance The voltage dependence of the differential resistance $R(V)$ reflects the energy dependence of the probability of Andreev reflection

$$\frac{R(V)}{R_S} = \frac{1}{1 + A(eV)\Lambda(eV)} \tag{1}$$

R_S is the point-contact resistance if no superconductor would be present (Sharvin resistance) The parameter $\Lambda(eV)$ describes the effect of the finite mean free path l of the electrons and holes, it is given by an integral over all angles of injection

$$\Lambda(eV) = \pi^{-1} \int_0^{2\pi} \mathrm{d}\phi \int_0^{\pi/2} \mathrm{d}\theta \, \sin\theta \cos\theta \exp[-2d'(eV)/(l\cos\theta)] \tag{2}$$

The first factor $\cos\theta$ weighs the contribution to the current of the electrons injected with polar angle θ $d'(eV)$ is the effective thickness that the electrons have to traverse before they are Andreev reflected (see Fig 1) Unless $l>>d'$, the dependence of d' on the energy of the electrons yields an additional contribution to the voltage dependence of the differential resistance

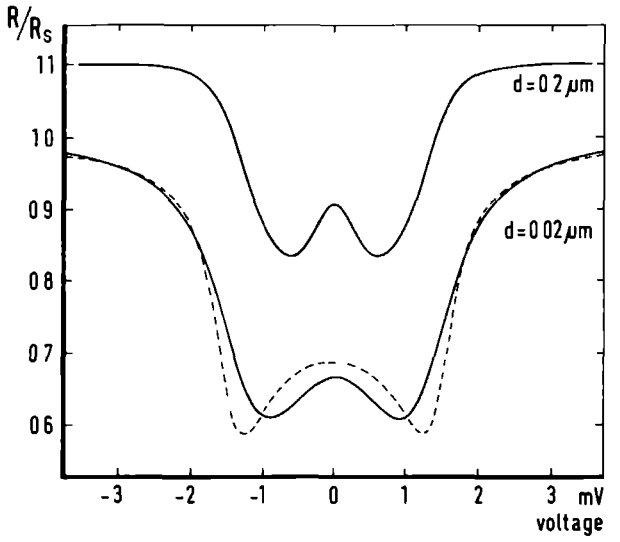

Fig 2 Measured differential resistance versus voltage of a point contact on a Ag-Pb bilayer for two samples with different Ag-film thicknesses The point-contact resistances were $R_S=46\ \Omega$ ($d=0\ 02\ \mu m$) and $R_S=17\ \Omega$ ($d=0\ 2\ \mu m$) The curve with $d=0\ 2\ \mu m$ has been shifted upward for clarity The dashed line is a theoretical curve

We studied thin-film Ag-Pb bilayers that were evaporated on glass slides in a single run The Pb film was evaporated at a rate of 4 nm/s to a thickness of 0 4 μm The thickness of the Ag film was varied between 0 02 μm and 0 9 μm for different samples The evaporation rate of Ag was 0 5 nm/s while the pressure during evaporation was typically $2\ 10^{-4}$ Pa The point contact was made with a 50-μm-diam Ag or Cu wire with a sharp point etched to it electrochemically All measurements were done in a pumped He bath (1 2 K) The differential resistance of the point contact was measured as a function of the voltage by standard phase-sensitive-detection techniques

On each sample many point contacts were made with resistances varying from less than 1 Ω to more than 100 Ω For the combination of a thin Ag film and a low point-contact resistance, effects of heating[6] are observed Most $R(V)$ curves show a common shape that is characteristic of the thickness of the Ag film Quantitatively, there is a variation in the scale of the resistance change of sometimes more than a factor two for the thicker films This may be due to inhomogeneities of the films or due to imperfections of the point contacts The $R(V)$ curves that we show here are the ones that were observed most frequently

In Fig 2, the $R(V)$ curves are shown of point contacts on two samples with Ag-film thicknesses $d=0\ 02$ μm and $d=0\ 2$ μm respectively The dashed line corresponds to Eq (1) with $\Lambda=1$ and with the energy dependence of A according to the theory of Blonder et al [5] We incorporated thermal broadening ($T=1\ 2$ K) and we used the literature value $\Delta_{Pb}=1\ 40$ meV, the best agreement was found for $Z=0\ 5$ By using Eq (1), it is assumed that the ordinarily reflected electrons do not return through the point contact This is justified because, for $R_S=46\ \Omega$, the point-contact diameter is 3 nm, and this is much smaller than the distance to the N-S interface where the ordinary reflection is assumed to take place In the measured $R(V)$ curve, the maximum value of A is reached for smaller E than in the calculated curve This feature agrees qualitatively with the numerical results of Ref 7 It is shown there to be due to the depression of Δ near the interface in S The value of Δ in the Ag layer is not relevant because the layer thickness is much smaller than the coherence length As far as Andreev reflection is concerned, variations of Δ on a length scale that is much smaller than the coherence length are equivalent to a step-like position dependence [7] Compared to the measurement on the thin sample, the excess current of a point contact on the sample with $d=0\ 2$ μm is smaller Here, the mean free path of the electrons starts to play a role and the $R(V)$ curve is also influenced by the energy dependence of Λ

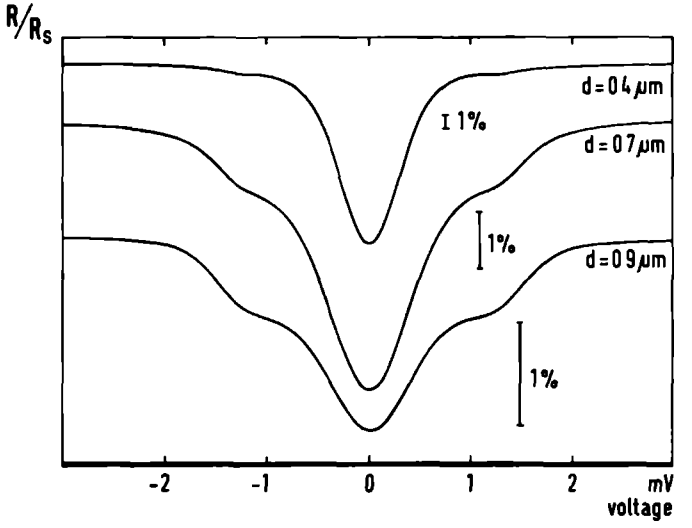

Fig 3 Measured differential resistance versus voltage of a point contact on a Ag-Pb bilayer for three samples with different Ag-film thicknesses The point-contact resistances were $R_S=1\ 6\ \Omega$ ($d=0\ 4$ μm), $R_S=1\ 2\ \Omega$ ($d=0\ 7$ μm), and $R_S=4\ 3\ \Omega$ ($d=0\ 9$ μm) Note the different vertical scales

Table I Mean free path l and effective thickness $d-d'(0)$ of the superconducting layer in N that are deduced from the measurements shown in Fig 3

d (μm)	$1-R/R_S$ for $V=0$	$1-R/R_S$ for $eV\lesssim\Delta_{Pb}$	l (μm)	$d-d'(0)$ (μm)
0 4	14%	0 7%	0 3	0 3
0 7	4 6%	1 2%	0 5	0 3
0 9	1 8%	0 75%	0 6	0 2

The $R(V)$ curves of point contacts on bilayers with larger Ag-film thicknesses are very different In Fig 3, the results are shown of three samples with Ag-film thicknesses $d=0\,4$ μm, $d=0\,7$ μm, and $d=0\,9$ μm respectively The excess current decreases with increasing thickness because the mean free path of the electrons and holes is smaller than their path length The $R(V)$ curves are dominated by the energy dependence of Λ (i e of d') It is too simple to say that the Andreev-reflection process takes place at the point where $\Delta(x)=E$ because the exponentially decaying wave function in the region where $E<\Delta(x)$ also plays a role Nevertheless, electrons with high energy will effectively be Andreev reflected further away from the point contact than electrons with lower energy and they are therefore scattered more severely This effect explains the decrease of the excess current for small voltages in the $R(V)$ curves of Fig 3 The flattening of the $R(V)$ curve for $eV\lesssim\Delta_{Pb}$ corresponds to the jump of Δ at the N-S interface As the relative magnitude of $d'(eV)$ compared to d decreases for larger Ag-film thicknesses, the ratio of the excess currents for low and for high voltage also decreases In Table I, we estimate the values of l and of $d-d'(0)$ for the three samples from the resistance values for $eV=0$ and for $eV\lesssim\Delta_{Pb}$ using Eqs (1) and (2) From the measurement on the sample with $d=0\,02$ μm, we estimate $A\simeq 0\,5$ (for both values of V) We assume that the electrons with $E\lesssim\Delta_{Pb}$ are reflected at the N-S interface because the coherence length in Pb is smaller than that in Ag The resulting values of $d-d'(0)$ are of the same order of magnitude as the coherence length in Ag,[1] $\xi_N=[\hbar v_F l/(6\pi k_B T)]^{1/2}=0\,4$ μm This confirms the validity of the concept of an effective thickness of the N layer In principle, from the $R(V)$ curves, the position dependence of Δ near the N-S interface can be reconstructed For that however, the effect of the finite mean free path should be included in the theory of Ref 7

In conclusion, the excess current of point contacts on thin-film Ag-Pb bilayers shows features that are due to the proximity effect at the N-S interface For thin Ag films, the whole bilayer is superconducting Still, the voltage dependence of the excess current slightly deviates from that of an N-S point contact due to the depression of the pair potential near the interface in the superconductor For thick Ag films, the voltage dependence of the excess current is very different, it can be explained by combining the proximity effect and the limited mean free path of the electrons and holes In principle, the latter results can be

used to reconstruct the position dependence of the pair potential near the N-S interface

We would like to thank D Schouren for doing much of the experimental work Part of this work is supported by the Stichting voor Fundamenteel Onderzoek der Materie (FOM), which is financially supported by the Nederlandse Organisatie voor Zuiver Wetenschappelijk Onderzoek (ZWO)

References

[1] G Deutscher and P G de Gennes, in Superconductivity, ed R D Parks (Marcel Dekker, New York, 1969) Chapter 17

[2] J C Weber, A C Mota, and D Marek, in Proc of the 17th Int Conf on Low Temp Physics LT-17, eds U Eckern, A Schmid, W Weber, and H Wuhl (North Holland, Amsterdam, 1984) p 1023

[3] E L Wolf and D M Burnell, *ibid* , p 1031

[4] A F Andreev, Zh Eksp Teor Fiz **46**, 1823 (1964) [Sov Phys -JETP **19**, 1228 (1964)]

[5] G E Blonder, M Tinkham, and T M Klapwijk, Phys Rev **B25**, 4515 (1982)

[6] G E Blonder and M Tinkham, Phys Rev **B27**, 112 (1983)

[7] P C van Son, H van Kempen, and P Wyder, to be published (see Chapter 3 2)

[8] P A M Benistant, A P van Gelder, H van Kempen, and P Wyder, Phys Rev **B32**, 3351 (1985), P C van Son, H van Kempen, and P Wyder, to be published (see Chapter 3 4)

[9] Yu V Sharvin, Zh Eksp Teor Fiz **48**, 984 (1965) [Sov Phys -JETP **21**, 655 (1965)]

Chapter 3.4

EXCESS CURRENT OF A POINT CONTACT ON A NORMAL-METAL SINGLE-CRYSTAL BACKED BY A SUPERCONDUCTOR

P. C. van Son,[a] H. van Kempen,[a] and P. Wyder[a,b]

[a] Research Institute for Materials, University of Nijmegen, Toernooiveld, NL-6525 ED Nijmegen, The Netherlands

[b] Max-Planck-Institut für Festkorperforschung, Hochfeld-Magnetlabor, 166X, F-38042 Grenoble Cedex, France

Electrons that are injected into a Ag single-crystal slab at a point contact are focused back onto the contact as holes after Andreev reflection at a Ag-Pb interface. A small applied magnetic field shifts the position of the focusing spot on the scale of the point-contact diameter. The excess current due to the holes is measured both as a function of magnetic field and as a function of voltage. The results do not completely agree with a simple ballistic model. The deviation for large magnetic field can be understood qualitatively by assuming that the orbits of electrons and holes are deflected over small angles for instance by the long-range strain field of dislocations. There is not yet a complete and consistent explanation for the observed structure of the excess current for small magnetic field and voltage. The corresponding length scales imply that the wave character of the quasiparticles has to be taken into account.

PACS numbers: 74.50+r, 72.15.Lh, 72.15.Rn

At an interface between a normal metal and a superconductor (N-S interface), an incident electron in the normal metal can condense into a Cooper pair in the superconductor together with a second electron from the normal metal The hole (or missing electron) that is created in the normal metal moves back in the direction from which the incident electron came (Andreev reflection, Andreev 1964) This retroreflection process has been studied for instance in electron-focusing experiments (Bozhko *et al* 1982, Benistant *et al* 1983) Electrons are injected at a point contact into a normal-metal single-crystal in which they have a large mean free path They are reflected at an N-S interface and the holes are focused by a magnetic field onto a second point contact, where they are detected

We also did a focusing experiment and used a single point contact both as the emitter and as the detector (Benistant *et al* 1985, see the inset of Fig 1(a)) If the magnetic field is zero, the holes return through the point contact and, because they have the opposite charge as the injected electrons, the current increases (excess current) The point at which the quasiparticles return to the upper surface can be shifted by applying a small magnetic field The shift is detected through the decrease of the excess current In the present experiment, the normal metal was much thinner than in the experiment of Benistant *et al* (1985) This means that much larger magnetic fields had to be applied to obtain the same shift, although the field was still much smaller than the critical field of the superconductor For large magnetic fields, we obtained similar results as Benistant *et al* (1985), for small fields, we found new and unexpected structure that was not resolved in their measurements The deviations from the simple ballistic model for large magnetic fields can be ascribed to scattering of the quasiparticles over small angles for instance due to dislocations For the structure at small magnetic fields several possible explanations will be discussed

If the mean free path of the quasiparticles is of the order of the thickness of the normal metal, the quasiparticle flow should be treated ballistically both at the point contact (which then is a Sharvin junction, Sharvin 1965) and in the normal metal The quasiparticles that are injected at the point contact return to the surface with a small shift in their position The shift depends on the magnetic field B and on the polar and azimuthal angles θ and ϕ of the direction of injection The z-axis is perpendicular to the top surface of the normal metal crystal and the magnetic field is directed along the y-axis It can be derived by straightforward geometrical considerations that, for small fields, the magnetic shift δ, in units of the contact radius b, is given by

$$\delta = \frac{d^2}{bR_c\cos^3\theta}\sqrt{1+\sin^2\phi(\cos^4\theta-1)} \qquad (1)$$

with d the thickness of the normal metal The magnetic field dependence is contained in R_c, the cyclotron radius of the quasiparticle orbit For each direction of injection, the contribution of the returning quasiparticles to the excess current is given by the relative overlap η of the point-contact area and the same area shifted over a distance $b\delta(\theta,\phi)$ If the point-contact area is circular, $\eta(\theta,\phi)=(2/\pi)\arccos(\delta/2)-(\delta/\pi)(1-\delta^2/4)^{1/2}$ (for $\delta\geq 2$, $\eta=0$)

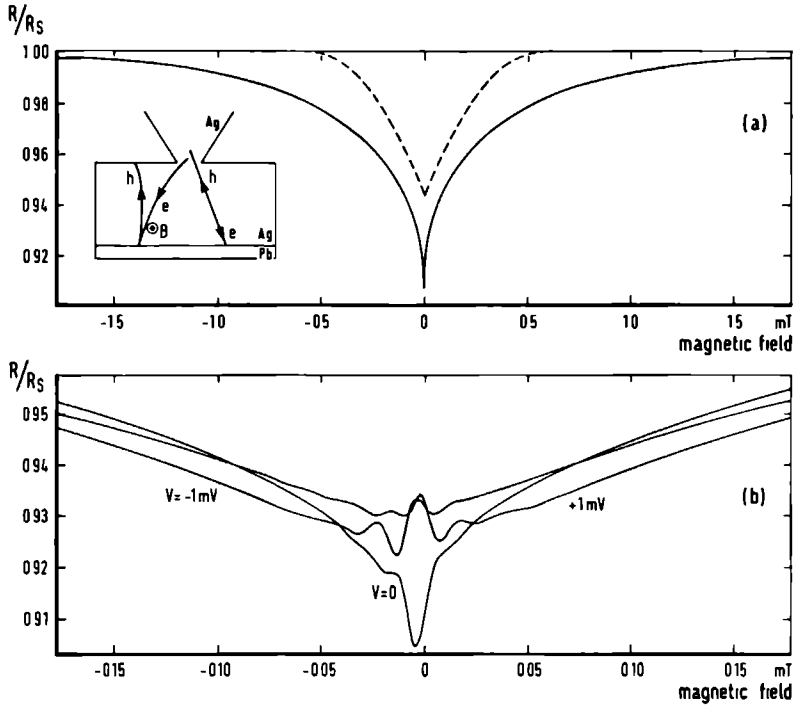

Fig. 1. (a) The magnetic field dependence of the resistance of a point contact with $R_S = 1.58\ \Omega$ ($b = 15$ nm). The dashed curve follows from the ballistic model (Eq. (2)) with $l = d = 20\ \mu$m and $A = 1$. The inset shows the electron and hole orbits with and without magnetic field. (b) The magnetic field dependence of the resistance of the same point contact on a magnified field scale for three values of the point-contact voltage V.

The total excess current I_e divided by the injected current I_i is found by integrating over all directions (the integral in Eq. (2) of Benistant *et al* (1985) is not completely correct):

$$I_e/I_i = (A/\pi)\int_0^{\pi/2} d\theta \sin\theta\cos\theta \int_0^{2\pi} d\phi\, \eta(\theta,\phi)\exp[-2d/(l\cos\theta)] \qquad (2)$$

In this equation also the mean free path l of the quasiparticles and the probability of Andreev reflection A are taken into account. The point-contact resistance R is given by $R/R_S = (1+I_e/I_i)^{-1}$, in which R_S is the point-contact resistance without excess current. For an ideal sample (infinite l and A equal to unity), the point-contact resistance drops to $0.5\,R_S$ in zero magnetic field, because then for each injected electron a hole returns through the contact ($\delta = 0$, $\eta = 1$).

The probability of Andreev reflection depends on the energy of the incident electron and on the amount of elastic scattering at the N-S interface. This dependence has been calculated using the Bogoliubov equations (see for instance Blonder *et al* 1982) and it is shown in the inset of Fig. 2. For energies higher than the energy gap Δ of the superconductor, A decreases because for these energies quasiparticle states are available in the superconductor. For energies below the gap, electrons are either Andreev reflected or they are reflected elastically. If a voltage V is applied to a Sharvin point contact, electrons are injected with energies E relative to the Fermi energy up to eV. In experiments on the voltage dependence of the excess current of N-S point contacts, good agreement with theory is found (Blonder and Tinkham 1983). In the model of Blonder *et al* (1982), Δ is assumed to rise at the interface instantaneously from zero to its value in the superconductor. This is a good approximation for an N-S point contact. In the present experiment, the proximity effect causes a more gradual rise of Δ and the energy dependence of A will be slightly different (van Son *et al* 1987a).

The sample consisted of a thin Ag single-crystal slab on which on one side a Pb film was evaporated. The preparation of the Ag slab was the same as that described by Benistant *et al* (1985). During annealing, the thickness decreased to between 20 and 40 μm; the measurements were done on the thin side of the sample. The thickness of the evaporated

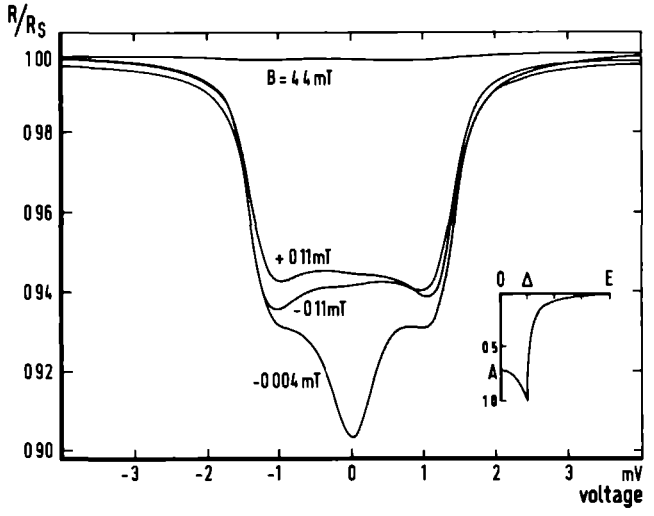

Fig. 2. The voltage dependence of the resistance of the point contact of Fig. 1 for four values of the magnetic field B. The inset shows the theoretical energy dependence (Blonder *et al* 1982) of the probability of Andreev reflection A for an N-S interface with only little elastic scattering.

Pb film was 0 8 μm All measurements were done in a pumped He bath (1 2 K) The point contact was made with a 50-μm-diam Ag or Cu wire with a sharp point etched to it The point-contact resistance was measured both as a function of magnetic field and as a function of voltage, using standard ac modulation and phase sensitive detection techniques The magnetic field in the plane of the sample was provided by a pair of Helmholtz coils Two other pairs compensated for the earth magnetic field in the two perpendicular directions Directly outside the dewar, the magnetic field was smaller than 10^{-5} T, if necessary, the compensating field was adjusted slightly to optimize the signal

Figures 1(a) and 1(b) show the magnetic field dependence of the resistance of a point contact with $R_S = 1\ 58\ \Omega$ ($b = 15$ nm) The dashed curve in Fig 1(a) follows from the ballistic model (Eq (2)) with $d = 20$ μm and $A = 1$ The mean free path is arbitrarily chosen equal to d to make the calculated excess current of the same order of magnitude as the measured excess current Compared to the prediction of the ballistic model, the measured excess current extends to much larger values of the applied magnetic field In addition, for small B, there is a sharp "extra" contribution to the excess current that also cannot be explained by the model The voltage dependence of the resistance of the same point contact is shown in Fig 2 Above the gap energy $\Delta_{Pb} = 1\ 4$ meV, the excess current disappears as expected But for low voltages, there is also an "extra" contribution to the excess current that cannot be explained by the energy dependence of A The contribution of the extra excess current for $B = V = 0$ to the total excess current depends on the point contact and varies between 10% and 80%

The extra excess current is not present in the magnetic field sweeps for constant nonzero voltage (Fig 1(b)) and in the voltage sweeps for constant nonzero magnetic field (Fig 2) It also disappears if the compensation of the earth magnetic field is not good enough The shoulders of the $V = 0$ curve in Fig 1(b) depend strongly on the compensation of the earth magnetic field and in some point contacts they can be eliminated by adjusting the compensating field The $V \neq 0$ curves in Fig 1(b) and the $B \neq 0$ curves in Fig 2 show a clear asymmetry but they are still more or less symmetric for reversal of both magnetic field and voltage The sign of the asymmetry (i e whether the wiggles in the magnetic field dependence shift to positive or to negative B values for positive voltage) is different for different point contacts

Figures 3(a) and 3(b) show the magnetic field dependence and the voltage dependence respectively of the resistance of a very high-ohmic point contact with $R_S = 96\ \Omega$ ($b = 1\ 9$ nm) The arrows in Fig 3(a) indicate the values of the magnetic field above which the excess current is zero in the ballistic model The curve is quite similar to Fig 1(a) if the magnetic field is scaled with the point-contact radius In the voltage dependence (Fig 3(b)), the excess current already decreases for voltages smaller than the gap voltage

For very low-ohmic point contacts ($R_S \simeq 0\ 1\ \Omega$), still new effects are found in the voltage dependence of the resistance (Fig 4) The excess current shows small wiggles and a sharp peak at $V = 0$ The decrease of the excess current for very small values of V has to be

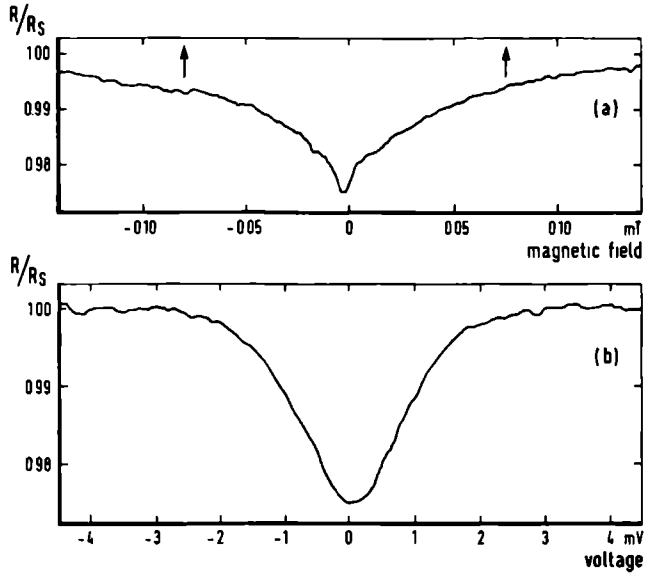

Fig. 3. (a) The magnetic field dependence of the resistance of a point contact with $R_S = 96\ \Omega$ ($b = 1.9$ nm). The two arrows indicate the magnetic field values above which the excess current is zero in the ballistic model. (b) The voltage dependence of the resistance of the same point contact.

due to an effect of the emitter current instead of the voltage because, contrary to the gap structure, the peak is hardly influenced by thermal smearing (compare the two curves in Fig. 4).

We will first discuss the deviations from the ballistic model for large magnetic fields. An excess current is still observed for fields in which the minimum magnetic shift is larger than the point-contact diameter. This means that the quasiparticles must obtain an extra shift of the order of the point-contact diameter that may compensate the magnetic shift. For small magnetic fields, this extra shift has to be much smaller because the excess current in Fig. 1 still shows a sharp cusp and is not smeared out. The magnetic field dependences of the resistance in Figs. 1(a) and 3(a) are quite similar if the magnetic field is scaled with the point-contact radius. This is consistent with the ballistic model because the magnetic shift δ is proportional to B/b (Eq. (1)). Apparently, the extra shift is also (approximately) proportional to the magnetic field.

The measurements of Benistant *et al* (1985) were done on a sample with a 200-μm-thick normal-metal slab (compared to 20 μm of our sample). This implies a much smaller magnetic field scale because δ is proportional to Bd^2 (Eq. (1)). They also found that the

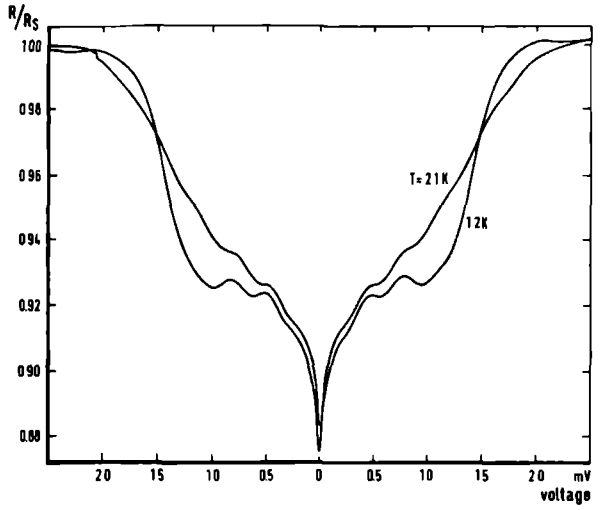

Fig 4 The voltage dependence of the resistance of a point contact with $R_S = 0.07\ \Omega$ for two temperatures T

excess current extended to larger B values than predicted by the ballistic model They did not find a sharp cusp at $B=0$, probably because the compensation of the earth magnetic field, which is more critical for thicker samples, was not good enough They tried to explain the large width of the excess current by ad hoc assuming that the quasiparticles are not exactly retroreflected at the N-S interface but return in a small cone centered around the direction of incidence According to our results, the extra shift is proportional to B, so also the solid angle of the cone should depend linearly on B However, the solid angle found by Benistant *et al* (1985) is of the same order of magnitude as the solid angle that can be derived from Fig 3(a), while the corresponding magnetic field values differ by an order of magnitude As we will show, the alternative explanation mentioned by Benistant *et al* (1985), small deflections of the quasiparticle orbits due to dislocations, agrees better with the experimental observations

Dislocations are accompanied by a long-range strain field that deflects the electrons that pass through it over small angles (Chang and Higgins 1975) After Andreev reflection, the holes return along almost the same orbit and they will be almost exactly deflected back * The net effect of these processes is that the quasiparticles obtain an extra shift that

* this is analogous to optical wavefront rectification with the aid of a phase-conjugate mirror (for a review of optical phase conjugation, see for instance Ducloy (1982)) The analogy of Andreev reflection of electron waves and optical phase conjugation (especially

in magnitude depends on the shift caused by other mechanisms. This can explain the observed dependences of the extra shift on B and d. For $B=0$, all shifts should be zero and the point-contact resistance should be 0.5 R_S. Apparently, the quasiparticle orbits are not exactly reversed, although the excess current is much larger than in the experiment of Benistant *et al* (1985) on a much thicker sample. Another possible mechanism like impurity scattering does not play a role because, according to the resistance ratio of the crystal rod from which the sample was cut, the electron mean free path for large-angle scattering is 700 μm. Nor can the probability of Andreev reflection be very small because, if the extra excess current is suppressed by a small magnetic field, the measured voltage dependence agrees well with the theoretical prediction for an almost perfect interface.

The origin of the structure of the excess current for small magnetic fields is much less clear. We will first discuss it and ignore the wave character of the quasiparticles. The extra contribution to the excess current for $B=0$ in Fig. 1(b) already decreases in magnetic fields in which the magnetic shift is much smaller than the point-contact diameter (for $B=0.01$ mT, the mean shift is approximately 0.6 nm). One explanation is that the extra shift due to the dislocations is already of the order of the point-contact diameter for these small magnetic fields. However, that would not be consistent with the observed magnetic field dependence of the extra shift for large B. An alternative explanation is the presence in the point-contact area itself of scattering centers like crystal defects or impurities. For $B=V=0$, the quasiparticles return exactly to the point where they were injected and their transmission probability is unity. If the quasiparticles are shifted, they may encounter a scattering center on their way back, the average transmission probability is smaller than unity, and the excess current decreases. If the distribution of scattering centers is not completely random, the transmission probability may even show wiggles as a function of B. This mechanism would also imply that the point-contact diameter is larger than the value that is calculated from the value of the resistance. However, this effect is too small to explain the large width of the excess current for large magnetic fields.

The disappearance of the extra excess current in the voltage dependence of the resistance for $B=0$ can also be explained by each of the two mechanisms because a finite voltage (or a finite current in low-ohmic point contacts) gives rise to small shifts too. If an electron with energy E relative to the Fermi energy E_F is incident on an N-S interface, it forms a Cooper pair with an electron with energy $-E$ and almost opposite momentum. The momentum of the Andreev-reflected hole has a slightly smaller z-component than the momentum of the incident electron because it lies within the Fermi sphere. The difference of the two momenta is taken up by the Cooper pair. As a consequence, the angle of reflection differs from the angle of incidence by a small amount $\delta\theta=(E/E_F)\tan\theta$. For a 20-μm-thick sample, this effect gives rise to a mean shift of approximately 0.7 nm for $V=0.5$ mV. The magnetic field of the injection current also influences the quasiparticle trajectories. The

---

degenerate four-wave mixing) holds in remarkably many aspects (van Son 1987).

shifts can be calculated if the region close to the point contact is neglected, so that a radial current distribution can be assumed The result is a mean shift of approximately 1 nm/mA for a sample thickness of 20 μm This effect becomes more important than the effect of the voltage for point-contact resistances below 1 Ω, which is consistent with the observation that for these point contacts the dip in the resistance for $V=0$ becomes narrower

For a very high-ohmic point contact (Fig 3), the small shifts that cause the disappearance of the extra excess current in Figs 1 and 2 are of the order of the point-contact diameter Therefore, there is no clear distinction between a "normal" and an "extra" excess current For the same reason, the voltage dependence of the excess current is dominated by the energy dependent shift of the quasiparticles instead of by the energy dependence of the probability of Andreev reflection

The asymmetry that is observed in the magnetic field sweeps for constant nonzero voltage and in the voltage sweeps for constant nonzero magnetic field, has to be due to an asymmetry of the sample region that is traversed by the quasiparticles The magnetic field direction namely is the only special direction in the plane of the sample and in an axial symmetric sample it should not matter This is consistent with the observation that the sign of the asymmetry is different in different point contacts The symmetry that is observed for reversal of both magnetic field and voltage restricts the number of possible explanations of the asymmetry

Although explanations can be given for the experimental observations, there is not yet a complete and consistent picture of the origin of the structure of the excess current for small magnetic field and voltage This may be due to the fact that, so far, we have ignored the wave character of the quasiparticles although the length scales in the discussion are of the order of the de Broglie wavelength of the electrons Interference effects are responsible for the oscillations of the differential resistance of a tunnel junction on an N-S bilayer (for a review of these and other geometrical resonance effects, see Nedellec 1977) An electron starting at the tunnel barrier returns to it as a hole after Andreev reflection at the N-S interface The phase of the wave function has changed only slightly because the phase velocity of the hole is opposite to its normal velocity Only the small difference in the wave vectors of electron and hole leads to a phase shift $\chi=(2Ed)/(\hbar v_F)$ for quasiparticles that move perpendicular to the film The hole is ordinarily reflected at the tunnel barrier and after a second Andreev-reflection process, an electron wave arrives at the tunnel barrier while the phase shift has doubled This electron wave interferes with the original electron wave, thereby creating bound states with energy levels spaced by $\Delta E=(\pi\hbar v_F)/(2d)$ The bound states give rise to peaks in the density of states of the normal-metal film Usually these peaks are measured with a tunnel junction but, if there is some elastic scattering in the contact, these interference effects also lead to oscillations in the excess current of a point contact (Hahn 1985) However, for a 20-μm-thick Ag film, the period of the oscillations is 0 07 meV, which is much smaller than the oscillation period in Fig 4 The maximum of the excess current for $V=0$ in Figs 2 and 4 can also not be explained by these interference ef-

fects. In the model there is namely no maximum for $E=0$ because the Andreev-reflection process itself introduces a phase shift too.

However, interference effects may still play an important role in a different mechanism, for instance if there are scattering centers in the point-contact area. An incident electron wave is scattered in the point contact and enters the crystal in the form of partial waves that move in different directions. These electron waves return to the point contact after Andreev reflection as hole waves, each with a phase that depends on the direction of injection. The hole partial waves now interfere with each other, which is an essentially different situation as with the geometrical resonances. For $B=V=0$, all hole waves have the same phase and the interference is constructive. For $V\neq 0$, phase shifts are introduced by the difference in the wave vector of electron and hole wave. For a partial wave with polar angle θ, the phase shift is given by $\chi=(2Ed)/(\hbar v_F \cos\theta)$. The phase difference between partial waves with for instance $\theta=0$ and $\theta=\pi/4$ is equal to 2π for $E=0.35$ meV, which is the right order of magnitude to describe the decrease of the extra excess current in Fig. 2. The shape of the excess current will of course depend on the distribution over θ of the partial waves that correspond to a single incoming wave and on the transmission probability of the hole wave through the point contact.

The magnetic field also introduces phase differences between partial waves that move in different directions. In general, the phase shift of the wave function due to a magnetic field is given by $\chi=(e/\hbar)\int \boldsymbol{A}\cdot \mathrm{d}\boldsymbol{s}$ (Aharonov and Bohm 1959), in which $\boldsymbol{A}$ is the vector potential. This effect yields flux quantization in superconductors but it has also been demonstrated in different experimental set-ups without using superconductors (Chambers 1960, Sharvin and Sharvin 1981). Usually, the phase shift along a closed loop is calculated via the enclosed flux, which is gauge invariant. In the present situation, the expression for χ in terms of $\boldsymbol{A}$ has to be used because the charge of the quasiparticle changes sign upon Andreev reflection. The phase shift of a quasiparticle wave on its way to the N-S interface and back is given by $\chi=\pi(Bd^2/\Phi_0)\tan\theta\cos\phi$ ($\Phi_0=h/(2e)=2.07\cdot 10^{-15}$ Wb is the flux quantum). The gauge is chosen such that $\boldsymbol{A}=0$ in the superconductor; a gauge transformation would introduce an extra phase shift upon Andreev reflection such that χ is constant (de Gennes 1966). If we again compare partial waves with $\theta=0$ and $\theta=\pi/4$, a phase difference of 2π is reached for $B=0.01$ mT, which is of the right order of magnitude to describe the decrease of the extra excess current in Fig. 1. With this interpretation, the extra excess current is a special manifestation of the Aharonov-Bohm effect.

Two paths may be followed to find out which mechanisms are relevant for the explanation of the shape of the extra excess current for small magnetic field and voltage. One approach is to make the N layer again much thinner. For vanishing thickness of the N layer, the voltage dependence of the excess current should become that of an N-S point contact. The magnetic shift in such a sample is negligible unless the magnetic field is of the order of the critical field of the superconductor. Measurements of the voltage dependence of the excess current of point contacts on thin-film Ag-Pb bilayers show an extra excess current if

the thickness of the Ag film is larger than 0 4 μm (van Son *et al* 1987b) In these films, the electron mean free path is of the same order of magnitude as the thickness, while due to the proximity effect at the N-S interface, the effective thickness that the quasiparticles experience depends on their energy This combination can explain the voltage dependence of the excess current in these samples However, it can not explain the decrease of the extra excess current for very small magnetic field in the measurements on the present sample nor the oscillations

The second approach is to use a tunnel junction instead of a point contact on a 20-μm-thick sample and to study the influence of a small magnetic field on the interference effects that give rise to the bound states Note that the phase shifts due to the magnetic field upon the two traversals of the N layer do not compensate because for the second traversal, the charge is different and ϕ has changed into $\phi+\pi$ In the much thinner samples that are usually used, the phase is hardly affected by a small magnetic field Tomasch and Wolfram (1966) studied geometrical resonance effects in very thick films (thicknesses up to 33 μm) but they looked at interference effects in a superconducing film and there a small magnetic field does not penetrate

In conclusion, the magnetic field dependence of the excess current of a point contact on a normal-metal single-crystal slab backed by a superconductor deviates both for small and for large magnetic fields from the prediction of a simple ballistic model Also the voltage dependence shows more structure than just the energy dependence of the probability of Andreev reflection at the N-S interface The deviation for large magnetic field can be understood qualitatively by assuming that the quasiparticle orbits are deflected over small angles for instance by the long-range strain field of dislocations For small magnetic field and voltage, an extra contribution to the excess current is observed Several features of the extra excess current can be qualitatively understood but there is not yet a complete and consistent description The length scales that are involved imply that the wave character of the quasiparticles has to be taken into account Possibly, the extra excess current is due to an interference effect of the quasiparticle waves

We acknowledge stimulating discussions with Prof Dr T M Klapwijk, Dr A P van Gelder, and Dr P A M Benistant We are grateful to Ing T J Gortenmulder and late Dr B Knook of the Kamerlingh Onnes Laboratory, Leiden for growing the silver single crystal from the melt, and Ir L W M Schreurs for orienting and spark-cutting the sample Part of this work is supported by the Stichting voor Fundamenteel Onderzoek der Materie (FOM), which is financially supported by the Nederlandse Organisatie voor Zuiver Wetenschappelijk Onderzoek (ZWO)

References

Aharonov Y and Bohm D 1959, Phys Rev **115**, 485

Andreev A F 1964, Zh Eksp Teor Fiz **46**, 1823
[Sov Phys JETP **19**, 1228]

Benistant P A M , van Kempen H , and Wyder P 1983,
Phys Rev Lett **51**, 817

Benistant P A M , van Gelder A P , van Kempen H ,
and Wyder P 1985, Phys Rev **B32**, 3351

Blonder G E , Tinkham M , and Klapwijk T M 1982,
Phys Rev **B25**, 4515

Blonder G E and Tinkham M 1983, Phys Rev **B27**, 112

Bozhko S I , Tsoi V S , and Yakovlev S E 1982, Pis'ma
Zh Eksp Teor Fiz **36**, 123 [JETP Lett **36**, 152]

Chambers R G 1960, Phys Rev Lett **5**, 3

Chang Y K and Higgins R J 1975, Phys Rev **B12**, 4261

Ducloy M 1982, Festkorperprobleme **22**, 35

de Gennes P G 1966, Superconductivity of Metals and
Alloys, Benjamin (New York)

Hahn Artur 1985, Phys Rev **B31**, 2816

Nédellec P 1977, Ann Phys (Paris) **2**, 253

Sharvin Yu V 1965, Zh Eksp Teor Fiz **48**, 984
[Sov Phys -JETP **21**, 655]

Sharvin D Yu and Sharvin Yu V 1981, Pis'ma Zh Eksp
Teor Fiz **34**, 285 [JETP Lett **34**, 272]

van Son P C 1987, thesis, University of Nijmegen (Chapter 3 1)

van Son P C , van Kempen H , and Wyder P 1987a,
to be published (see Chapter 3 2)

van Son P C , van Kempen H , and Wyder P 1987b,
to be published (see Chapter 3 3)

Tomasch W J and Wolfram T 1966, Phys Rev Lett **16**, 352

Chapter 4

ELECTRON SPIN POLARIZATION

Chapter 4.1

INTRODUCTION

The ground state of the electron system of a metal is described by the band structure, which gives the energies and the wave vectors of the electron states in the periodic lattice of the metal ions Up to the Fermi energy, each state is occupied by two electrons of opposite spin For some metals and metallic compounds, a lower ground-state energy is found if the symmetry of spin-up and spin-down electrons is dropped These materials are (anti-) ferromagnetic or ferrimagnetic, because the magnetism is due to the conduction electrons, it is called itinerant electron magnetism (for a review, see Ref 1) The spin dependence of the electron energy levels is due to the exchange interaction that results from the combination of the Pauli exclusion principle and the Coulomb interaction of the electrons The result is, that in a magnetically ordered material, the electrons with different spin have different band structures Recently, a new class of materials was discovered, half-metallic ferromagnets,[2] which show this in an extreme way In these materials, electrons of one spin are metallic (i e the Fermi level lies in one of the bands) while the electrons of the other spin are semiconducting (i e the (same) Fermi level lies in the gap between two bands) Examples are the Heusler compound NiMnSb and magnetite (Fe_3O_4), which is a half-metallic ferrimagnet [3] Various experimental methods exist that probe the band structure of a material and that are sensitive to the electron spin [4] For the transport properties of metals, only the electrons at the Fermi level are important In the half-metallic materials, these electrons are spin polarized for 100% In paramagnetic metals, the spin polarization is zero in zero magnetic field while in ordinary ferromagnetic metals it is in between these limits It should be possible to observe transport effects that are due to the spin polarization of the electrons at the Fermi level Such effects will be most prominent in half-metallic materials

In Chapter 4 2, an experiment is described in which the magnetic field dependence of the contact potential is measured The electron possesses a magnetic moment that is coupled to its spin so, in an applied magnetic field, the energy levels of spin-up and spin-down electrons shift in opposite directions If the electron spin polarization at the Fermi level is not zero, the result is a net shift of the Fermi level, which is related to the contact potential The effect has been observed in a polycrystalline Ni film, but the interpretation is complicated by the fact that the lattice constant of a ferromagnetic metal changes in a high magnetic field (volume magnetostriction) This effect influences the band structure and gives rise to an additional shift of the Fermi level

In Chapter 4 3, a theoretical description is given of the current transport at an interface of a (half-metallic) ferromagnet and a paramagnetic metal In a paramagnetic metal, the current is distributed equally over spin-up and spin-down electrons but in a ferromagnetic metal it is not Because the band structures are different, the conductivities of spin-up and

spin-down electrons are different and the current is distributed according to these conductivities At the interface, a redistribution of the current has to take place This process is accompanied by a difference of the electrochemical potentials of spin-up and spin-down electrons near the interface and it gives rise to an additional interface resistance Within this framework, recent experiments of Johnson and Silsbee[5] are discussed

References

[1] F Gautier, in Magnetism of Metals and Alloys, ed M Cyrot (North Holland, Amsterdam, 1982) Chapter 1

[2] R A de Groot, F M Mueller, P G van Engen, and K H J Buschow, Phys Rev Lett **50**, 2024 (1983)

[3] Akira Yanase and Kiiti Siratori, J Phys Soc Japan **53**, 312 (1984), R A de Groot and K H J Buschow, J Magn Magn Mat **54-57**, 1377 (1986)

[4] Carl Rau, J Magn Magn Mat **30**, 141 (1982)

[5] Mark Johnson and R H Silsbee, Phys Rev Lett **55**, 1790 (1985)

Chapter 4.2

NEW METHOD TO STUDY THE ELECTRON SPIN POLARIZATION AT THE FERMI LEVEL OF A FERROMAGNETIC METAL

P C van Son,[a] H van Kempen,[a] and P Wyder[a b]

[a] Research Institute for Materials, University of Nijmegen, Toernooiveld, NL-6525 ED Nijmegen, The Netherlands

[b] Max-Planck-Institut fur Festkorperforschung, Hochfeld-Magnetlabor, 166X, F-38042 Grenoble Cedex, France

An applied magnetic field shifts the energy levels of spin-up and spin-down electrons in opposite directions In a ferromagnetic metal, the resulting redistribution of the electrons over the spin bands gives rise to a shift of the Fermi level that is proportional to the degree of spin polarization of the electrons with the Fermi energy The shift can be measured as a magnetic field dependence of the contact potential Results have been obtained for polycrystalline Ni films The influences of interface effects and of effects due to magnetostriction are discussed

PACS numbers 75 80 +q, 71 25 Pi, 73 40 Cg

In a ferromagnetic metal, spin-up and spin-down electrons have different band structures, so for instance the two densities of states at the Fermi level are generally not equal If a magnetic field is applied to a ferromagnetic metal, the position of its Fermi level shifts This effect originates from the spin polarization of the electrons at the Fermi level and can be used to determine this quantity The measurement of the Fermi-level shift due to an applied magnetic field constitutes a new method to determine the electron spin polarization at the Fermi energy Because of its specific sensitivity for the spin polarization at the Fermi energy, the method is well suited to study half-metallic ferromagnets [1] According to band-structure calculations, the spin polarization at the Fermi level is $\pm 100\%$ in these materials For the electrons of one spin direction, the Fermi level lies within a band (metal-like) while, for the other spin direction, the (same) Fermi level lies in the gap between two bands (semiconductor-like)

Changes of the Fermi level due to an applied magnetic field can be measured as a field dependence of the contact potential They give rise to a voltage signal across a capacitor that consists of the metal under study and a reference metal the Fermi level of which does not change This method has already been used to measure Fermi-level oscillations in metal single-crystals[2] and in the two-dimensional electron gas in semiconductor structures [3] However, these oscillations are related to the de-Haas-van-Alphen effect and have a completely different origin than the Fermi-level shift discussed in this paper We have demonstrated the existence of the Fermi-level shift in measurements on polycrystalline Ni films We will discuss two effects that prevent a quantitative analysis of the results so far

An applied magnetic field shifts the energy levels of spin-up and spin-down electrons in opposite directions because of the magnetic moment of the electrons (Zeeman splitting) With the term spin-up electrons, we mean electrons with their magnetic moment parallel to the magnetic field Due to the Zeeman shifts, a redistribution of the electrons over the spin bands takes place until the Fermi levels in the spin-up and spin-down bands are equal again In Fig 1(a), this process is shown for a paramagnetic metal, in which it yields the Pauli spin paramagnetism Figure 1(a) also shows that the Fermi level does not shift This is due to the fact that the densities of states of spin-up and spin-down electrons with the Fermi energy are equal The Zeeman energy is much smaller than the Fermi energy, so that higher order effects due to the energy dependence of the density of states are negligible

For a ferromagnetic metal, the situation is completely different In Fig 1(b), a schematic band structure is drawn with symmetric free-electron bands and two narrow d-bands that are split due to the exchange interaction The energies of these d-bands have been chosen in such a way that a large (negative) electron spin polarization results at the Fermi level If now a magnetic field B is applied parallel to the direction of the magnetization, a shift ΔE_F of the Fermi level occurs (see Fig 1(b))

$$\Delta E_F = -\frac{1}{2} g \mu_B B \frac{N_\uparrow(E_F) - N_\downarrow(E_F)}{N_\uparrow(E_F) + N_\downarrow(E_F)} = -\frac{1}{2} g \mu_B B P \qquad (1)$$

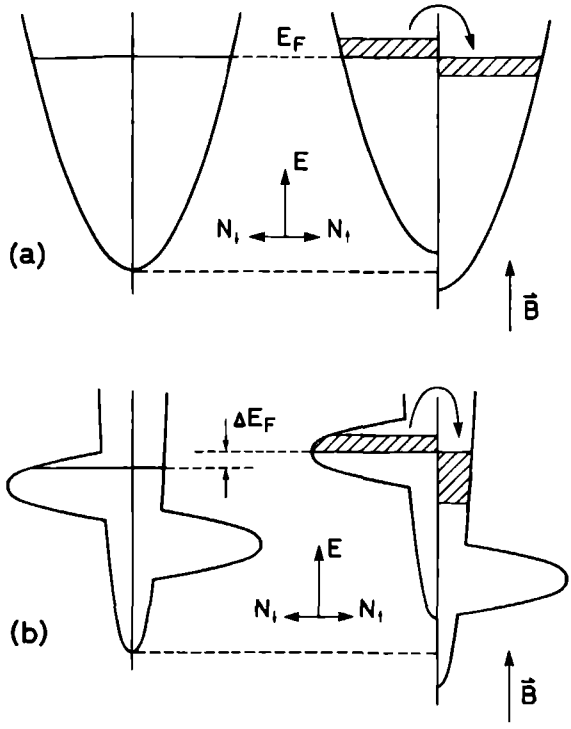

Fig 1 Schematic densities of states of spin up and spin-down electrons If a magnetic field is applied, a redistribution of the electrons over the spin bands takes place For a paramagnetic metal (a), the Fermi level does not shift while, for a ferromagnetic metal (b), it does

The Fermi-level shift is proportional to the electron spin polarization at the Fermi level P, $N_{\uparrow\downarrow}(E_F)$ are the densities of states at the Fermi energy of spin-up and spin-down electrons respectively, μ_B is the Bohr magneton, and g is the spectroscopic g-factor of the electrons The product $(1/2)g\mu_B B$ is the Zeeman energy, which, for $g=2$, is equal to 57 9 μeV in a magnetic field of 1 T For a half-metallic ferromagnet, $P=\pm 1$ and the Fermi level follows the full Zeeman shift of the metal-like electrons

Two types of samples were fabricated to measure the Fermi-level shift In one type, a 10-μm-thick mylar foil was used as the dielectric medium of the capacitor Onto one side an Al film was evaporated and onto the other side a Ni film was evaporated The Ni film was evaporated at a pressure of $3\ 10^{-4}$ Pa with a rate of 0 2 nm/s The foil had a large area ($\simeq$100 cm^2) and it was folded and rolled to fit into the sample holder The other type of

samples employed an Al_2O_3 film as the dielectric medium In a single run, the Al_2O_3 film was evaporated in between two metal films onto a glass substrate with an area of ≈ 1 cm^2 For these samples, the Ni films were evaporated at a pressure of $4\ 10^{-5}$ Pa with a rate of 0 4 nm/s The Al_2O_3 films, with thicknesses between 0 1 μm and 0 25 μm, were evaporated at a pressure of $8\ 10^{-4}$ Pa with a rate of 0 1 nm/s The top metal film was etched away along the edges of the substrate to remove short-circuits and to be able to make contact with the bottom film The capacitances C of all the samples on which measurements were done were in between 5 nF and 35 nF while the dissipation factor $D=(2\pi f R_p C)^{-1}$ was always smaller than 0 05 for a frequency of $f=100$ Hz This means that the parallel resistance of the samples R_p was high enough to be neglected

The experimental set-up is shown in Fig 2 The DC voltage source is not essential and its role will be discussed later on The sample capacitor sits in a large magnetic field that lines up all the magnetic domains of the ferromagnetic metal A small modulation of the field gives rise to a modulation of the Fermi level of the ferromagnetic metal (Fig 2(b)) If the modulation is fast compared to the time constant RC, the charge on the capacitor hardly changes and the Fermi-level modulation is measured as a voltage modulation across the resistor R The DC magnetic field is provided by a water-cooled iron-core electro-magnet The field modulation is due to a pair of Helmholtz coils in between the pole faces In most measurements, the frequency of the modulation was 83 Hz while the rms-amplitude was 3 0 mT If the direction of the current in one of the two Helmholtz coils is reversed, the modulation amplitude at the position of the sample is more than a factor 10 lower The voltmeter in Fig 2(a) stands for the combination of a differential pre-amplifier, a selective

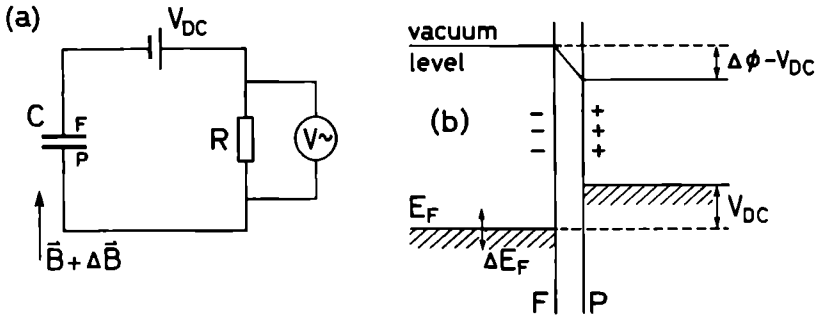

Fig 2 (a) Experimental set-up The sample is a capacitor of a ferromagnetic (F) and a paramagnetic (P) metal and it is located in a modulated magnetic field (b) Energy-level scheme of the capacitor The modulation of the magnetic field gives rise to a modulation of the Fermi level in F that is measured The charge on the capacitor is determined by the electrostatic potential difference $\Delta\phi - V_{DC}$

amplifier and a lock-in amplifier The resistor R of 10 MΩ is included to avoid charging of the capacitor due to for instance the input offset current of the pre-amplifier

The voltage signal to be measured is of the order of 0 1 μV while the inductive and capacitative pick-up are up to two orders of magnitude larger, despite good twisting and shielding The inductive pick-up can be further reduced by rotating the sample while the capacitative pick-up is smaller for larger sample capacitances A large sample capacitance has also the advantage that the parallel capacitance of the two twisted leads to the sample (≈0 1 nF) can be neglected Apart from looking at the phases of the signals, the Fermi-level modulation can be distinguished from the inductive and capacitative pick-up by reversing the direction of the DC magnetic field As the field modulation does not change, the inductive and capacitative pick-up stay the same, but the Fermi-level modulation changes sign One still has to be careful about interfering effects that do not stay exactly the same if the direction of the DC magnetic field is reversed, such as vibrations of the sample holder due to eddy currents

In Table I, the measured Fermi-level shifts for various samples are given * On sample 1 (Ni-mylar-Al) several checks were performed The Fermi-level modulation is the same for DC magnetic-field values of ±0 6 T and ±1 0 T and for frequencies of 27 Hz, 83 Hz, and 510 Hz If the Helmholtz coils are switched antiparallel, the signal decreases below 1 μeV/T The Fermi-level modulation in sample 2 (Ni-Al_2O_3-Cu) reproduces that of sample 1 The null result of sample 3 (Al-Al_2O_3-Au) shows that the effect is indeed due to the presence of a ferromagnetic metal while the null result of sample 4 (Ni-Cu-Al_2O_3-Cu) shows that it is a contact-potential effect Sample 5 (Ni-Al_2O_3 Ni) should also have shown a null result because, in the experiment, the relative Fermi-level shift of the films on either side of the dielectric medium is measured Apparently, in this sample the two Ni films are not equivalent This may be due to different amounts of gas contamination in the films or due to different structures of the interface of the Ni film and the dielectric film

On sample 1, also measurements were done with a DC voltage applied to the capacitor by means of a lithium battery (see Fig 2 and Table I, V_{DC} is the voltage of the ferromagnetic film with respect to that of the paramagnetic film) At first sight, no effect of the applied voltage is to be expected However, due to magnetostriction of the ferromagnetic film, the capacitance C is modulated and this leads to an additional voltage modulation Because the charge on the capacitor $Q=C(\Delta\phi-V_{DC})$ is constant on a time scale that is short with respect to RC, the relative changes of capacitance and of voltage are equal in magnitude

---

* We also fabricated samples that contained a Fe_3O_4 single-crystal, which is a half-metallic ferrimagnet Onto the crystal, an Al_2O_3 film and a Cu-film counterelectrode were evaporated No reproducible results have been obtained so far, probably due to vibrations of these samples The vibrations may have been caused by eddy currents (these samples are much thicker than the thin film samples) or by the torque that these magnetically anisotropic single-crystal samples experience in a magnetic field We thank Dr V A M Brabers of the Technical University of Eindhoven for kindly providing us with a Fe_3O_4 single-crystal

Table I Measured Fermi-level shifts due to an applied magnetic field for various samples

	sample	V_{DC} (V)	$\partial E_F/\partial B$ (μeV/T)
1a	Ni - mylar - Al	0	−20 (±1)
1b	Ni - mylar - Al	+3 7	−12 (±1)
1c	Ni - mylar - Al	−3 7	−28 (±1)
2	Ni Al_2O_3 - Cu	0	−19 (±2)
3	Al - Al_2O_3 - Au	0	0 (±2)
4	Ni - Cu - Al_2O_3 - Cu	0	0 (±2)
5	Ni - Al_2O_3 - Ni	0	−14 (±2)

and have opposite signs The effect is zero if the applied voltage V_{DC} equals the contact-potential difference $\Delta\phi$ of the two metals This is precisely how a contact-potential difference is measured with a Kelvin probe [4] As for sample 1 $\Delta\phi = +1$ V, the corrected value of the Fermi-level shift is -18 μeV/T For sample 2, the correction will even be smaller because Al_2O_3 is less tensile than mylar and because the contact-potential difference of Ni and Cu is only $\Delta\phi = +0\ 5$ V On the samples with Al_2O_3, no measurements with $V_{DC} \neq 0$ could be done either because the dielectric film broke down or because current spikes in the circuit made the measurement impossible

The statement that magnetostriction is responsible for the modulation of the capacitance is supported by a quantitative analysis From the results 1a-1c in Table I, the relative change of the capacitance due to a magnetic field change is found to be $(1/C)\partial C/\partial B = -(1/V)\partial V/\partial B = +2\ 2 \cdot 10^{-6}\ T^{-1}$ (note that changes of voltage and of Fermi level have opposite signs) For a saturated ferromagnetic metal, the magnetostriction effect only yields an isotropic volume change (volume magnetostriction) For Ni, the relative volume change $\partial\omega$ is[5] $\partial\omega/\partial B = -0\ 55\ 10^{-6}\ T^{-1}$ Although this is of the right order of magnitude, the sign is not the expected one An increase in volume of the ferromagnetic film should correspond to an increase of the capacitance because the area increases and because the thickness of the dielectric film decreases However, if no precautions are taken to measure the volume magnetostriction in Ni isothermally, the influence of magnetocaloric heating alters the negative volume change into a positive change of the same order of magnitude [5] As our measurements are not done isothermally, we should use the latter value that has the expected sign

From the (corrected) value of the Fermi-level shift, the spin polarization of the electrons at the Fermi surface in Ni can be evaluated using Eq (1) If we take[6] $g_{Ni} = 2\ 19$, we find $P = +28\%$ Several other experimental methods that measure the electron spin polarization exist like for instance spin-polarized photoemission spectroscopy and electron-capture spectroscopy (for a review, see Ref 7) Most of them are spin-sensitive spectroscopic

methods that are used to probe single-crystal surfaces in UHV For Ni, most of these methods yield negative P values that depend on the orientation of the crystal surface that is selected A method that more resembles our experiment is spin-selective tunneling from a ferromagnetic film to a superconducting film [8] Here, the spin polarization of the electrons that tunnel through the barrier is +25% for a Ni-Al_2O_3-Al tunnel junction Both this and our experiment measure the electron spin polarization in a very narrow energy range of order $k_B T$ around the Fermi energy The tunneling experiments are done at low temperatures $T<1$ K (0 1 meV) while we do our measurements of the Fermi-level shift at room temperature (25 meV) The spectroscopic methods can probe a wide energy range but have a lower energy resolution Band-structure calculations yield a large negative value of P [7] (the schematic band structure in Fig 1(b) is roughly that of Ni) However, for a comparison of the experimental results with each other and with the calculated band structure, a careful analysis has to be made of the weight in each experiment of the different electron states In addition, we will discuss two effects that obscure the direct proportionality (Eq (1)) of the Fermi-level shift and the electron spin polarization at the Fermi energy in the present experiment (1) the influence of the interface of Ni and the dielectric film and (2) the influence of the volume change of the Ni film that apparently occurs These effects may be responsible for the discrepancy between our result and the calculated band structure of Ni

Like the other methods, the contact-potential method measures the properties of the surface of the Ni film and these can be different from those of the bulk Moreover, the properties of the surface layer depend strongly on the adjacent material For instance, the spin polarization measured with electron capture spectroscopy has been shown to decrease due to H-chemisorption on a clean Ni surface [7] Also the polarization of the tunnel current depends on the barrier material and on its preparation [8] Our result of sample 5 indicates that the two Ni films are not equivalent, which may be due to an interface effect On the other hand, the equivalence of the results of sample 1 and sample 2 indicates that interface effects do not play a large role there Preparation of the samples under UHV conditions and good control of the interfaces will be needed to solve this point Another possibility is to do the measurements in UHV on clean surfaces The two capacitor plates should be held close together at a constant distance However, it will be hard to keep the capacitance sufficiently constant in a modulated magnetic field (note that the actual capacitance variation in the measurement on sample 1 is only $\partial C/C = 7\ 10^{-9}$) Another approach would be to measure the Fermi level shift due to an applied DC magnetic field directly as a DC change of the contact potential with a standard Kelvin probe in UHV However, it will be hard to measure the small shift that way

The volume magnetostriction not only influences the measurements by modulating the capacitance, it also has a more fundamental influence If the volume of a metal changes, its band structure changes and therefore its Fermi level shifts Preliminary calculations for Ni[9] yield $\partial E_F/(\partial\omega/\omega) = -11$ eV As the relative volume change is of the order of $\partial\omega/\omega \sim 10^{-6}\ T^{-1}$, this effect yields a Fermi-level shift of the order of 10^{-5} eV/T This means

that the measured shift contains a contribution due to the electron spin polarization at the Fermi level and a contribution due to the volume change of the metal However, note that the latter effect is a secondary effect The volume magnetostriction is the reaction of the lattice to the Zeeman shifts of the electron energy levels In principle, the band structure of Ni should be calculated with and without an applied magnetic field If in the calculation the lattice constant is allowed to change, both the volume magnetostriction and the net Fermi-level shift are obtained Unfortunately, the effect of magnetocaloric heating, which is not negligible for Ni, can not be incorporated in such a calculation

In conclusion, we have shown that the Fermi level of a ferromagnetic metal shifts if a magnetic field is applied The shift is due to the electron spin polarization at the Fermi level and can be used in principle to determine that quantity The Fermi-level shift has been measured as a change of the contact-potential difference of a ferromagnetic and a paramagnetic metal For a polycrystalline Ni film, the shift is -18 μeV/T, which would correspond to an electron spin polarization at the Fermi surface of Ni of +28% This number does not agree with band-structure calculations The discrepancy may be due to the fact that, in the determination of the electron spin polarization, the influence of interface effects and of effects due to magnetostriction have been neglected These effects need further experimental and theoretical attention respectively

We acknowledge helpful discussions with Dr R A de Groot and we thank E van Leuken for the calculation of the Fermi-level shift of Ni due to a volume change We thank Prof Dr J C Fuggle for critical reading of the manuscript Part of this work is supported by the Stichting voor Fundamenteel Onderzoek der Materie (FOM), which is financially supported by the Nederlandse Organisatie voor Zuiver Wetenschappelijk Onderzoek (ZWO)

References

[1] R A de Groot, F M Mueller, P G van Engen, and K H J Buschow, Phys Rev Lett **50**, 2024 (1983)

[2] D Shoenberg, Magnetic oscillations in metals (Cambridge University Press, 1984) pp 150 153

[3] R T Zeller, F F Fang, B B Goldberg, S L Wright, and P J Stiles, Phys Rev **B33**, 1529 (1986), D Weiss, V Mosser, V Gudmundsson, R R Gerhardts, and K v Klitzing, Solid State Commun **62**, 89 (1987)

[4] N A Surplice and R J D'Arcy, J Phys E **3**, 477 (1970)

[5] K Azumi and J E Goldman, Phys Rev **93**, 630 (1954) and references therein

[6] A J P Meyer and G Asch, J Appl Phys **32**, 330S (1961)

[7] Carl Rau, J Magn Magn Mat **30**, 141 (1982) and references therein

[8] R Meservey, P M Tedrow, and J S Moodera, J Magn Magn Mat **35**, 1 (1983)

[9] E van Leuken and R A de Groot, private communication

Chapter 4.3

CURRENT CONVERSION AT THE FERROMAGNETIC-NONFERROMAGNETIC METAL INTERFACE

P C van Son, H van Kempen, and P Wyder

The electrical transport properties of ferromagnetic metals can be described in terms of a two-current model (see the review article by Fert and Campbell[1]) The model is based on the suggestion by Mott[2] that, at temperatures that are low with respect to the Curie temperature, most scattering events will conserve the direction of the electron spin Therefore, spin-up and spin-down electrons will be almost independent and carry current in parallel As in ferromagnets the band structures of spin-up and spin-down electrons are different, the two conductivities will in general not be equal An extreme example of this is found in a new class of materials, half-metallic ferromagnets,[3] in which for instance the spin-down electrons are semiconducting while the spin-up electrons show metallic behavior and carry all of the current

When a current flows from a ferromagnetic metal (F) to a nonferromagnetic metal (N), its distribution over spin-up and spin-down current has to change An analogous situation occurs at an interface of a normal metal (N) and a superconductor (S) The conversion of a normal current into a supercurrent gives rise to an electrochemical potential difference between quasiparticles and Cooper pairs in the superconductor near the interface The effect has been measured as an excess resistance of the N-S interface and also in the form of a voltage across a detector junction that was located close to an injector junction (see the review articles of Pippard[4] and of Clarke[5] respectively) In a two-probe (injector-detector) experiment, Johnson and Silsbee[6] have demonstrated that similar nonequilibrium effects occur if a current is sent across an F-N interface The experiment is referred to as a spin-injection experiment and the effects have been described theoretically in terms of the injection of a nonequilibrium magnetization in N[7] and the detection of that magnetization as a voltage across a detector junction [8] Recently, this approach has been elaborated by Johnson and Silsbee [9] Although the two approaches are equivalent, a consistent description in terms of different electrochemical potentials of spin up and spin-down electrons is more straightforward and more general In fact, it can not only be used to describe the current conversion at an N-S interface and at an F-N interface but it can in principle be applied to any system for which a two-current model is valid (semiconductors)

We will describe the current-conversion process at the F-N interface and the accompanying excess interface resistance in terms of different electrochemical potentials of spin-up and spin-down electrons. If F is a half-metallic ferromagnet (HMF), the situation is directly analogous to the situation at the N-S interface: In both cases, the current conversion takes place on only one side of the interface. In the description of the general F-N interface, both sides of the interface have to be taken into account. As a further important generalization, the influence of a finite conductance of the interface itself is calculated. Next, we will describe the position dependence of the electrochemical potentials in the detector probe in a two-probe experiment and, finally, the relation will be discussed between our approach and the theory of Johnson and Silsbee.[9]

We will consider the one-dimensional case: The ferromagnetic metal occupies the halfspace $x<0$, the normal metal occupies the halfspace $x>0$, and a current with density j flows in the positive x-direction (see Fig. 1). Indices F and N refer to the ferromagnetic and the normal metal respectively. It is assumed that, for both F and N, the rate of scattering events without spin flip of spin-up ($\uparrow$) and spin-down ($\downarrow$) electrons is much larger than the spin-flip rate τ_{sf}^{-1}. This implies that at any point two electrochemical potentials $\mu_\uparrow$ and $\mu_\downarrow$ may be defined, which need not be equal. The conductivity σ and the current density are separated into two components: $\sigma_\uparrow=\alpha\sigma$, $\sigma_\downarrow=(1-\alpha)\sigma$, $j_\uparrow=\beta j$, and $j_\downarrow=(1-\beta)j$. The current determines the gradient of the electrochemical potential:

$$\partial\mu_{\uparrow,\downarrow}/\partial x = -(e/\sigma_{\uparrow,\downarrow})j_{\uparrow,\downarrow} \tag{1}$$

Far from the interface, spin-up and spin-down electrons will be in equilibrium ($\mu_\uparrow=\mu_\downarrow$), so $\beta(x\ll 0)=\alpha_F$ and $\beta(x\gg 0)=\alpha_N=1/2$. At the F-N interface, α changes abruptly but β has to be continuous (unless there is very strong spin-flip scattering at the interface). In a region near the interface, $\partial\beta/\partial x\neq 0$ and $(\mu_\uparrow-\mu_\downarrow)\neq 0$; the potential difference is the driving force of the current conversion. The potential difference obeys a diffusion equation, which in steady state is given by:

$$\frac{\mu_\uparrow-\mu_\downarrow}{\tau_{sf}} = D\frac{\partial^2(\mu_\uparrow-\mu_\downarrow)}{\partial x^2} \tag{2}$$

$D=(1/3)v_F l$ is the diffusion constant, v_F is the Fermi velocity, and l is the electron mean free path. For the normal metal $D_{N\uparrow}=D_{N\downarrow}=D_N$, but for the ferromagnet a weighted average should be chosen: $D_F=(1-\alpha_F)D_{F\uparrow}+\alpha_F D_{F\downarrow}$. From Eq. (2) it follows that the potential difference decays exponentially on the scale of the spin-flip diffusion length $\Lambda=(D\tau_{sf})^{1/2}$.

The boundary conditions at the F-N interface demand that $\beta(x=0)=\beta_I$ is continuous and that $\mu_\uparrow$ and $\mu_\downarrow$ are continuous. This determines the value of β_I (naturally $\alpha_N\leq\beta_I\leq\alpha_F$):

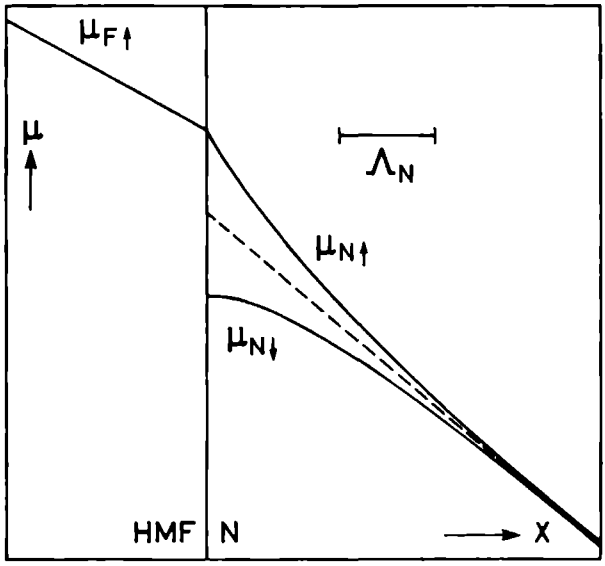

Fig. 1. The position dependence of the electrochemical potentials $\mu_\uparrow$ and $\mu_\downarrow$ near a HMF-N interface ($\mu_{F\downarrow}$ has been omitted because it is irrelevant). The dashed line in N represents μ_0; in the HMF, $\mu_0=\mu_{F\uparrow}$.

$$(2\beta_I-1) = \frac{(2\alpha_F-1)}{1+4\alpha_F(1-\alpha_F)(\sigma_N^{-1}\Lambda_N)/(\sigma_F^{-1}\Lambda_F)} \tag{3}$$

We took $\alpha_N=\frac{1}{2}$ but it is simple to extend the theory to an interface of two ferromagnetic metals. For a HMF ($\alpha_F=1$), we find $\beta_I=1$ because all spin flip has to take place in N.

For the discussion of $\mu_\uparrow$ and $\mu_\downarrow$, it is convenient to define μ_0 as the value that the electrochemical potential would have without a nonequilibrium current distribution:

$$\partial\mu_0/\partial x = -(e/\sigma)j \tag{4}$$

If far from the interface one takes $\mu_0=\mu_\uparrow=\mu_\downarrow$, it can be shown that $\mu_0=\alpha\mu_\uparrow+(1-\alpha)\mu_\downarrow$. We will first consider the HMF-N interface. The position dependence of the electrochemical potentials is drawn in Fig. 1. The dashed line in N represents μ_0. The $\mu_{F\downarrow}$-curve has been omitted because, in the HMF, μ_0 is determined completely by $\mu_{F\uparrow}$. Moreover, $\mu_{F\downarrow}$ will tend to $\mu_{F\uparrow}$ away from the interface but the length scale of that process, Λ_F, is not well defined for a HMF. Although $\mu_\uparrow$ and $\mu_\downarrow$ are continuous at the interface, μ_0 is not: The current-conversion process in N gives rise to an additional voltage drop. The interface resistance equals $(\sigma_N^{-1}\Lambda_N)$: Over a length Λ_N only half of the conductivity of N is used, so

the resistance of this slab is $2(\sigma_N^{-1}\Lambda_N)$ instead of $(\sigma_N^{-1}\Lambda_N)$

At a general F-N interface, the current-conversion process takes place both in F and in N The interface resistance R_I is given by

$$R_I = \frac{\mu_{F0}(x=0)-\mu_{N0}(x=0)}{ej} = \frac{(2\alpha_F-1)^2(\sigma_N^{-1}\Lambda_N)(\sigma_F^{-1}\Lambda_F)}{(\sigma_F^{-1}\Lambda_F)+4\alpha_F(1-\alpha_F)(\sigma_N^{-1}\Lambda_N)} \tag{5}$$

In Fig 2, the potential differences $(\mu_\uparrow-\mu_0)$ and $(\mu_\downarrow-\mu_0)$ are drawn as a function of the position near the interface The lengths Λ_F and Λ_N over which the potential differences extend in F and N respectively, do not depend on the parameters of the other metal The magnitude of the potential differences is determined by the ease with which the current-conversion process can take place and, for this process, F and N are two parallel channels If $(\sigma_F^{-1}\Lambda_F)\ll 4\alpha_F(1-\alpha_F)(\sigma_N^{-1}\Lambda_N)$, all spin flip takes place in F, $\beta_I=\frac{1}{2}$, and the potential differences do not depend on $(\sigma_N^{-1}\Lambda_N)$ However for a HMF ($\alpha_F=1$), all spin flip has to take place in N, however large $(\sigma_N^{-1}\Lambda_N)$ is

So far, we have assumed that the conductance of the interface itself is infinite, the interface resistance R_I of Eq (5) is purely due to the current-conversion process This is not generally true because an incoming electron at an interface of two different metals may be

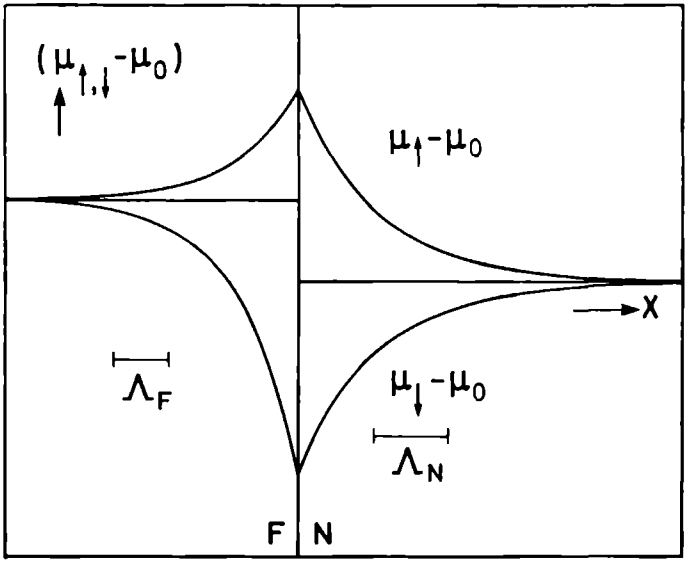

Fig 2 The position dependence of the potential differences $(\mu_\uparrow-\mu_0)$ and $(\mu_\downarrow-\mu_0)$ near an F-N interface

reflected as well as transmitted If the metals are separated by a tunnel junction, the conductance will even be very small The conductance per unit area of the interface G is built up from the contributions of spin-up and spin down electrons $G_\uparrow = \alpha_I G$, $G_\downarrow = (1-\alpha_I)G$ The finite value of G gives rise to discontinuities of the electrochemical potentials at the interface

$$\Delta\mu_{\uparrow\downarrow} = \mu_{F\uparrow\downarrow}(x=0) - \mu_{N\uparrow\downarrow}(x=0) = (e/G_{\uparrow\downarrow})j_{\uparrow\downarrow} \tag{6}$$

If we assume that there is no spin-flip scattering at the interface, the spin polarization of the current $(2\beta(x)-1)$ is still continuous Its value at the interface is given by

$$(2\beta_I - 1) = \frac{(2\alpha_F - 1)\dfrac{\sigma_F^{-1}\Lambda_F}{\alpha_F(1-\alpha_F)} + (2\alpha_I - 1)\dfrac{G^{-1}}{\alpha_I(1-\alpha_I)}}{\dfrac{\sigma_F^{-1}\Lambda_F}{\alpha_F(1-\alpha_F)} + \dfrac{G^{-1}}{\alpha_I(1-\alpha_I)} + 4\sigma_N^{-1}\Lambda_N} \tag{7}$$

For $G^{-1}=0$ (infinite interface conductance), the result of Eq (3) is reproduced On the other hand, if the interface conductance is small $(G^{-1}/[\alpha_I(1-\alpha_I)] \gg (\sigma_F^{-1}\Lambda_F)/[\alpha_F(1-\alpha_F)], 4\sigma_N^{-1}\Lambda_N)$, the spin polarization of the current at the interface is completely determined by the spin asymmetry of the interface conductance $(\beta_I = \alpha_I)$ Independent of the value of G, the spin polarization of the current at a HMF-N interface is equal to that in the HMF $(\beta_I = \alpha_F)$ because all spin flip has to take place in N

The current-conversion process near the interface and the finite conductance of the interface itself give rise to an interface resistance that is given by

$$R_I = \frac{1}{G} + \frac{(2\alpha_F-1)^2 G\alpha_I(1-\alpha_I) + (\sigma_F\Lambda_F^{-1})\alpha_F(1-\alpha_F)[1-4\alpha_I(1-\alpha_I)] + (\alpha_F-\alpha_I)^2(\sigma_N\Lambda_N^{-1})}{G\alpha_I(1-\alpha_I)(\sigma_N\Lambda_N^{-1}) + (\sigma_F\Lambda_F^{-1})\alpha_F(1-\alpha_F)[4G\alpha_I(1-\alpha_I) + \sigma_N\Lambda_N^{-1}]} \tag{8}$$

We will consider the same three limiting cases For $G^{-1}=0$, the result of Eq (5) is reproduced, while for small G, R_I is given by

$$R_I = \frac{1}{G} + \frac{(\sigma_F^{-1}\Lambda_F)}{\alpha_F(1-\alpha_F)}(\alpha_F-\alpha_I)^2 + (\sigma_N^{-1}\Lambda_N)[1-4\alpha_I(1-\alpha_I)] \tag{9}$$

Because in this limit $\beta_I = \alpha_I$, the full interface conductance is utilized, the last two terms are the contributions to the interface resistance due to the current conversion in F and in N respectively For a HMF-N interface, R_I is given by

$$R_I = G^{-1}/\alpha_I + \sigma_N^{-1}\Lambda_N \tag{10}$$

Because now $\beta_I = \alpha_F = 1$, there is no current conversion in HMF but only part of the interface conductance is utilized

The current-conversion process at an F N interface gives rise to an excess interface resistance However, the different electrochemical potentials of spin-up and spin-down electrons can also be measured directly with a voltmeter Two different voltage probes should then be attached to the nonequilibrium region close to the injector junction For the superconducting analogue, the situation is simple A normal-metal probe measures the electrochemical potential of the quasiparticles and a superconducting probe measures that of the Cooper pairs To measure directly $\mu_\uparrow$ and $\mu_\downarrow$ near an F-N interface, one would need two HMF probes that are magnetized in opposite directions However, an F and an N probe also measure a potential difference This can be seen in Fig 2, which may also be interpreted as giving the position dependence of the potentials in two voltage probes attached at $x=0$ to a sample with $\mu_\uparrow \neq \mu_\downarrow$ Because in a voltage probe no net current flows, μ_0 is constant in each probe The potential difference of the two probes is proportional to the difference $(\mu_\uparrow - \mu_\downarrow)$ in the sample However, note that the spin-up and the spin-down current are not zero and that the detector probes contribute to the current conversion in the sample they are attached to The effect can be made small for instance by making the cross-section of the probes small or by coupling the detector probes to the sample through tunnel junctions

In a recent paper,[9] Johnson and Silsbee have given a thermodynamic analysis of the transport across an interface of a ferromagnetic and a paramagnetic metal They extend the thermoelectric system by including a nonequilibrium magnetization of the electrons In the thermoelectric system, the flows of charge and heat are driven by an electric field and a temperature gradient The thermomagnetoelectric system also contains the flow of nonequilibrium magnetization and an extra driving force that is related to it That driving force is the gradient of the magnetization potential $-H^*$, which is formally argued to be a thermodynamic variable In the application of their theory to the transport of electric current across an interface of a ferromagnetic and a paramagnetic metal, they take into account both the current redistribution in the metals and the spin asymmetry of the conductance of the junction itself Their results are completely equivalent to the results of our model The magnetization potential $-H^*$ and the electric potential V in the theory of Ref 9 are directly related to the electrochemical potentials $\mu_\uparrow$ and $\mu_\downarrow$ of the spin-up and the spin-down electrons in our model

$$-H^* = \frac{\mu_\uparrow - \mu_\downarrow}{2\mu_B} \quad , \quad V - V_0 = \frac{\mu_\uparrow + \mu_\downarrow}{2e} \tag{11}$$

Here, μ_B is the Bohr magneton and V_0 is a constant that depends on the definition of the zeroes of the potentials

Concerning the description of the transport of electric current across an F-N interface, the two theories are mathematically identical and differ only in the physical interpretation Near the interface, the spin system is allowed to be out of equilibrium while the energy distribution of the electrons is assumed to be in equilibrium (with a specific voltage and tem-

perature). The physical justification for that is the fact that the spin-flip time is much longer than the other relevant relaxation times. On this basis, we divided the electron system in two only weakly coupled subsystems of spin-up and spin-down electrons respectively, that are each in equilibrium with the same electric potential and temperature but with different chemical potentials. This is a more general approach than to introduce formally a magnetization potential of the system as a whole. Moreover, as the nonequilibrium effects are detected by means of a voltmeter (which measures the electrochemical potential and not the electric potential nor the magnetization potential), the description in terms of different electrochemical potentials of spin-up and spin-down electrons is more straightforward.

In conclusion, the nonequilibrium effects that occur if a current is sent across an F-N interface have been described in terms of different electrochemical potentials of spin-up and spin-down electrons. The description is analogous to the description of the disequilibrium of quasiparticles and Cooper pairs near an N-S interface across which a current is sent. It will be applicable to any system for which a two-current model is valid. The approach is more general than the description of the effects in terms of a magnetization potential.

We thank Dr. R. A. de Groot for asking the basic question and for his continued interest in this work. We thank J. A. M. M. van Haaren for bringing Ref. 6 to our notice. Part of this work is supported by the Stichting voor Fundamenteel Onderzoek der Materie (FOM), which is financially supported by the Nederlandse Organisatie voor Zuiver Wetenschappelijk Onderzoek (ZWO).

References

[1] A. Fert and I. A. Campbell, J. de Physique, Colloque C1, **32**, C1-46 (1971).

[2] N. F. Mott, Proc. Roy. Soc. (London) **A153**, 699 (1936); **A156**, 368 (1936); Adv. Phys. **13**, 325 (1964).

[3] R. A. de Groot, F. M. Mueller, P. G. van Engen, and K. H. J. Buschow, Phys. Rev. Lett. **50**, 2024 (1983).

[4] A. B. Pippard, in Proceedings of the NATO Advanced Study Institute on Nonequilibrium Superconductivity, Phonons, and Kapitza Boundaries, edited by K. E. Gray (Plenum Press, New York, 1981), Chapter 12.

[5] John Clarke, *ibid.*, Chapter 13

[6] Mark Johnson and R. H. Silsbee, Phys. Rev. Lett. **55**, 1790 (1985)

[7] A. G. Aronov, Pis'ma Zh. Eksp. Teor. Fiz. **24**, 37 (1976) [JETP Lett. **24**, 32 (1976)]

[8] R. H. Silsbee, Bull. Magn. Reson. **2**, 284 (1980)

[9] Mark Johnson and R. H. Silsbee, Phys. Rev. **B35**, 4959 (1987)

Summary

Several kinds of experiments are described that were done to study the behavior of the conduction electrons in metals In most experiments, the trajectories of the electrons through the metal played an important role, for instance when scattering processes were studied or the reflection of electrons at a surface or at an interface Point contacts proved very useful in fixing the begin and end points of the electron trajectories and in varying the energy with which the electrons were injected into the metal An applied magnetic field was used to influence the trajectories of the electrons by means of the Lorentz force In some experiments, use was made of the interaction of the applied magnetic field and the magnetic moment of the electron

Transverse-electron-focusing experiments were done on high-purity Ag single-crystals Two point contacts were put on the surface of the crystal, separated by a distance much smaller than the electron mean free path Electrons were injected at one point contact and an applied magnetic field focused the electrons onto the second point contact, where they were detected If the energy of the injected electrons was increased, the focusing signal decreased when the mean free path of the electrons for phonon emission became smaller than the separation of the point contacts In this way, the energy dependence of the electron-phonon interaction in Ag was measured By studying different electron orbits between the two point contacts, the anisotropy of the electron-phonon interaction was determined For high injection energies, the focusing signal was not zero, this signal is due to electrons that loose their energy very close to the point contact where they are injected In this regime, the focusing signal also contains information about the electron-phonon interaction, although the interpretation is less simple than for low energies For high injection currents, an asymmetry was observed in the focusing signal for positive and negative values of the current A calculation shows that this effect is due to the influence of the magnetic field of the injection current on the orbits of the electrons

At an interface of a normal metal and a superconductor, an incident electron in the normal metal can be retroreflected as a hole while a Cooper pair is injected into the superconductor (Andreev reflection) If the hole returns through the point contact where the electron was injected, an excess current is observed Measurements were done of the excess current of a point contact on a thin Ag single-crystal backed by a Pb film The orbits of electrons and holes were influenced by an applied magnetic field For large fields, the excess current can be explained by assuming that, in the Ag single-crystal, the electrons and holes are scattered over small angles, for instance by dislocations The structure in the excess current for small fields is not yet completely understood, the corresponding length scale implies that the wave character of the electrons has to be taken into account Also measurements were done of the excess current of point contacts on thin-film Ag-Pb bilayers Here, the sample thickness was of the order of the coherence length of the superconductor The

excess current showed features that could be ascribed to the gradual variation of the pair potential near the interface (proximity effect). A quantitative comparison with numerical calculations of the probability of Andreev reflection for such an interface could not be made. In most of the experiments, the limited mean free path of electrons and holes played an important role while this effect had not been incorporated in the theory. On the other hand, the limited mean free path allows in principle the reconstruction of the position dependence of the pair potential near the interface from the measured excess current.

The third subject involves two effects that are related to the fact that, in a ferromagnetic metal, the degeneracy of spin-up and spin-down electron states is lifted. In an applied magnetic field, the energy levels of spin-up and spin-down electrons shift in opposite directions. If the densities of states of the two spin bands at the Fermi level are not equal, a net shift of the Fermi level results. This shift was measured as a magnetic field dependence of the contact potential of a polycrystalline Ni film. The interpretation of the result is complicated by the fact that the volume change of a ferromagnetic metal in an applied magnetic field yields an additional shift of the Fermi level. The second effect has to do with the transport properties of the conduction electrons. In a ferromagnetic metal, the current is not distributed equally over spin-up and spin-down electrons because their conductivities are different. At an interface of a ferromagnetic and a paramagnetic metal, a current redistribution has to take place. This process is accompanied by a difference of the electrochemical potentials of spin-up and spin-down electrons. With this theoretical model, the results of recent measurements done by others are readily understood.

Samenvatting

Verschillende soorten experimenten worden beschreven waarin het gedrag van de geleidingselectronen in een metaal werd bestudeerd. Bij de meeste experimenten speelden de banen van de electronen door het metaal een belangrijke rol, bijvoorbeeld wanneer verstrooiingsprocessen werden bestudeerd of de reflectie van electronen aan een oppervlak of aan een grensvlak. Puntcontacten bleken zeer geschikt te zijn om begin- en eindpunt van de banen van de electronen vast te leggen en om de energie te variëren waarmee de electronen in het metaal werden geïnjecteerd. Een magneetveld werd gebruikt om de banen van de electronen te beïnvloeden door middel van de Lorentz kracht. Bij sommige experimenten werd gebruik gemaakt van de wisselwerking tussen het aangelegde magneetveld en het magnetisch moment van de electronen.

Experimenten gebaseerd op transversale focussering van electronen werden gedaan met behulp van zeer zuivere Ag éénkristallen. Twee puntcontacten werden op het oppervlak van het kristal gezet, op een afstand kleiner dan de vrije weglengte van elkaar. De electronen werden geïnjecteerd door het ene puntcontact en door het aangelegde magneetveld werden ze gefocusseerd op het tweede puntcontact, dat de electronen detecteerde. Voor toenemende energie van de geïnjecteerde electronen nam het focusseringssignaal af als de vrije weglengte van de electronen voor fonon-emissie kleiner werd dan de afstand tussen de puntcontacten. Op deze manier werd de energie-afhankelijkheid van de electron-fonon wisselwerking in Ag gemeten. Door verschillende banen van de electronen tussen de twee puntcontacten te bestuderen, werd de anisotropie van de electron-fonon wisselwerking bepaald. Als de electronen werden geïnjecteerd met een grote energie was het focusseringssignaal niet nul; dit signaal is afkomstig van electronen die hun energie kwijt raken zeer dicht bij het puntcontact waar ze worden geïnjecteerd. In dit regime bevat het focusseringssignaal ook informatie over de electron-fonon wisselwerking, alhoewel de interpretatie minder eenvoudig is als bij lage energie. Voor grote waardes van de injectiestroom werd een asymmetrie waargenomen in het focusseringssignaal voor positieve en negatieve waardes van de stroom. Een berekening toont aan dat dit effect wordt veroorzaakt door de invloed van het magneetveld van de injectiestroom op de banen van de electronen.

Aan een grensvlak van een normaal metaal en een supergeleider kan een inkomend electron in het normale metaal geretroreflecteerd worden in de vorm van een gat terwijl een Cooper paar in de supergeleider wordt geïnjecteerd (Andreev reflectie). Als het gat terugkeert door het puntcontact waardoor het electron geïnjecteerd werd, wordt een "excess" stroom waargenomen. De excess stroom werd gemeten van een puntcontact op een dun Ag éénkristal waar op de achterkant een Pb laag was opgedampt. De banen van de electronen en gaten werden beïnvloed door middel van een magneetveld. De excess stroom voor grote velden kan verklaard worden door aan te nemen dat de electronen en gaten in

het Ag éénkristal worden verstrooid over kleine hoeken, bijvoorbeeld door dislocaties De structuur in de excess stroom voor kleine velden wordt nog niet geheel begrepen, de lengteschaal die hiermee correspondeert, impliceert dat rekening gehouden moet worden met het golfkarakter van de electronen Ook werd de excess stroom gemeten van puntcontacten op opgedampte Ag-Pb dubbellagen Hier was de laagdikte van dezelfde orde van grootte als de coherentielengte van de supergeleider De excess stroom vertoonde kenmerken die konden worden toegeschreven aan de geleidelijke toename van de supergeleidende paarpotentiaal bij het grensvlak ("proximity" effect) Een kwantitatieve vergelijking met de resultaten van numerieke berekeningen van de kans op Andreev reflectie bij een dergelijk grensvlak was niet mogelijk In de experimenten speelde de beperkte vrije weglengte van de electronen en de gaten een belangrijke rol terwijl in de theorie met dit effect geen rekening was gehouden Aan de andere kant is het door de beperkte vrije weglengte in principe mogelijk om de plaatsafhankelijkheid van de paarpotentiaal bij het grensvlak af te leiden uit de gemeten excess stroom

Het derde onderwerp betreft twee effecten die te maken hebben met het feit dat in een ferromagnetisch metaal de electronen met verschillende spin niet equivalent zijn Als een magneetveld wordt aangelegd, schuiven de energieniveaus van de spin-op en de spin-neer electronen in verschillende richtingen Als de toestandsdichtheden bij het Fermi-niveau van de twee spinbanden niet gelijk zijn, is een netto verschuiving van het Fermi-niveau het resultaat Deze verschuiving werd gemeten in de vorm van een verandering van de contactpotentiaal van een opgedampte Ni laag in een magneetveld De interpretatie van het resultaat wordt bemoeilijkt doordat de volumeverandering van een ferromagnetisch metaal in een magneetveld ook een verschuiving van het Fermi-niveau tot gevolg heeft Het tweede effect heeft te maken met de transporteigenschappen van de geleidingselectronen In een ferromagnetisch metaal wordt de stroom niet in gelijke mate gedragen door de electronen van beide spinrichtingen omdat het geleidingsvermogen van beide verschillend is Bij een grensvlak van een ferromagnetisch en een paramagnetisch metaal vindt een herverdeling van de stroom plaats Dit proces gaat vergezeld van een verschil in de electrochemische potentiaal van de spin-op en de spin-neer electronen Met dit theoretische model kunnen de resultaten van recente metingen gedaan door anderen direct begrepen worden

Curriculum vitae

Peter Cornelis van Son
geboren 6 juli 1959 te Dordrecht

sept. 1971 - mei 1977

Opleiding atheneum B aan het Titus Brandsma College te Dordrecht.

sept. 1977 - okt. 1982

Studie technische natuurkunde aan de Technische Hogeschool te Delft. Het afstudeerwerk lag op het gebied van de niet-evenwichts supergeleiding en werd verricht onder leiding van prof. dr. J. E. Mooij en dr. T. M. Klapwijk.

jan. 1983 - aug. 1987

Promotieonderzoek aan de Katholieke Universiteit te Nijmegen, van jan. 1983 tot mei 1983 in dienst van de KU en van mei 1983 tot mei 1987 in dienst van de Stichting FOM. Het onderzoek, waarvan de resultaten in dit proefschrift staan beschreven, werd verricht op de afdeling Vaste Stof II onder leiding van prof. dr. P. Wyder en prof. dr. H. van Kempen. Daarnaast werd, in het kader van de onderwijstaak, de begeleiding verzorgd bij verschillende practica.

okt. 1987

In dienst treding bij de Rijksuniversiteit Groningen op een post-doc positie in de groep van prof. dr. T. M. Klapwijk.

STELLINGEN

behorende bij het proefschrift

"Point contacts and the ways of electrons in metals"

("Puntcontacten en de wegen van electronen in metalen")

van P.C. van Son

- 1 -

De ruimtelijke vorm van het metaaloppervlak zoals dat gezien wordt door de geleidingselectronen kan bepaald worden door de diffractie-effecten te bestuderen die optreden als de electronen in een focusseringsexperiment aan een (gestapt) oppervlak reflecteren.

H.F.C. Hoevers, doctoraalscriptie, K.U. Nijmegen (1987).

- 2 -

Andreev reflectie van electronen aan een grensvlak van een normaal metaal en een supergeleider vertoont veel overeenkomsten met de fase conjugatie van licht door middel van "degenerate four-wave mixing" in een optisch niet-lineair medium.

- 3 -

Het is mogelijk onderscheid te maken tussen triplet- en singlet-supergeleiding door de richting van de spin te bestuderen van het electron en van het gat bij Andreev reflectie. Spin-selectieve injectie en detectie van electronen en gaten is mogelijk met een puntcontact van een (half-) metallische ferromagneet.

In een aangelegd magneetveld raken ladingsdragers met verschillende Hall hoeken uit evenwicht als de stroom langs een rand van het materiaal loopt. Dit effect kan direct gemeten worden in de vorm van een spanningsverschil tussen twee geschikt gekozen, verschillende spanningsprobes.

- 5 -

De waarneming van de Coulomb blokkade in tunneljuncties in de vorm van puntcontacten kan verklaard worden door de aanwezige parasitaire capaciteit niet in rekening te brengen.

L.E.C. van de Leemput en anderen, te publiceren.

- 6 -

Bij de analyse van het oriëntatie-effect in de CH_3I+Rb reactie door Stolte en anderen is ten onrechte de afhankelijkheid van de reactiviteit van het rotatieniveau van het molecuul verwaarloosd.

S. Stolte, K.K. Chakravorty, R.B. Bernstein, en D.H. Parker, Chem. Phys. 71, 353 (1982).
Henk Jalink, proefschrift, K.U. Nijmegen (1987).

- 7 -

Gij zult in het zweet uws aanschijns geen Si-MOSFETs fabriceren.

E.H. Snow, A.S. Grove, B.E. Deal, en C.T. Sah, J. Appl. Phys. 36, 1664 (1965).

Een wetenschappelijk artikel dat uit slechts twee zinnen bestaat, heeft alleen waarde als onderwerp van een stelling bij een proefschrift.

A. Widom, Phys. Lett. 90A, 474 (1982).

- 9 -

De poging tot integratie van geestelijk gehandicapten in de maatschappij door het oprichten van gezinsvervangende tehuizen is vaak niet erg succesvol omdat de tehuizen door de omgeving gezien worden als alternatieve gekkenhuizen in plaats van als ééngezins-woningen met een enigszins afwijkende bevolking.

- 10 -

De opdracht die vaak voor in een proefschrift te vinden is, dient in de regel niet letterlijk opgevat te worden als een omschrijving van het beoogde lezerspubliek.

- 11 -

De uitzondering bevestigt de regel.

Stelling 10 en opdracht van dit proefschrift.